Holocene Geomagnetic Secular Variation in Queensland

by Catherine Constable.

A thesis submitted to the Australian National University in fulfilment of the requirements for the degree of Master of Science.

December, 1982.

ERRATA

Page		Correction
(iii)	line 20	Magnetization
1	para 3 line 3	Maars (a type of volcanic crater lake)
2	para 2 line 7	ϕ the longitude, a the radius of and r...
3	para 2 line 1	insert "appear to" before "drift"
9	line 3	Denham (1973) first suggested using complex MEM time series analysis.
11	line 1	Irving (1957) not Verosub (1977).
14	lines 14,-7	comparatively
18	line 6	delete "G and"
	para 4 last line	after coring (a hole is drilled in the core tube above the level of the Kullenberg piston after loading the tube, so that air may enter the anchor chamber via the x line for the abort procedure).
20	line -8	Magnetization
25	line 12	$Q = \frac{Jn}{\chi H}$
28	Add to caption:	Crosses are the deepest points in each lake. Dots indicate coring sites and core numbers for Lake Barrine. Lake Eacham core sites are not available.
90	line 11	aberrant
101	line -7	occurred
102	line 19	occurred
112		Inclination axis labels should be -60, -30, 0, 30 not -90, -60, 30, 0
113		Inclination axis labels should be -90, -60, -30, 0
115	Figure caption	archaeomagnetic
122	line 15	consensus
123		Direction of arrows on the circle and the ellipse should be anticlockwise not clockwise.

Errata

Page		Correction
136	line 7	disappointing
137		E is missing from BARRINE in (b), (c) and (d).
138	Figure caption	comparative
139	line 6	suppressed
139		delete para 2.
142	line 10	change "second" to "earlier"
153	Creer, K.M. (1959)	A.C. demagnetization.....

Addition to references:

Irving, E (1957), Origin of the palaeomagnetism of the Torridonian Sandstones of north-west Scotland; Phil. Trans. Roy. Soc. London Ser.A, 250, 100-110.

None of this work has previously been submitted to any other institution. The research is my own work except where otherwise acknowledged.

C. G. Constable

Catherine Constable

ABSTRACT

Mackereth cores from Lakes Barrine and Eacham on the Atherton Tableland, N. Queensland have been examined to provide a geomagnetic secular variation record. Radiocarbon dating of the L. Eacham sequence shows that it spans the last 5 700 calendar years. The time scale for the L. Barrine record is less well constrained than that for Eacham, but it appears to cover the time period 1 600 to 16 200 years before present.

As well as directional measurements on all cores, relative palaeointensity estimates have been obtained for one core from each lake. These are in good agreement with archaeointensity measurements from south-eastern Australia.

Time series analysis using the periodogram and maximum entropy methods has been carried out on declination, inclination and complex equivalent directional data. The resulting periodicities show poor agreement between lakes. Motion of the geomagnetic vector has been predominantly clockwise over the time period spanned but two periods of anticlockwise motion have occurred from about 5 500 to 4 000 years B.P. and from 10 500 to 8 800 years B.P. The records are compatible with the secular variation being generated by westward drift of non-dipole sources of the geomagnetic field.

ACKNOWLEDGMENTS.

The author would like to thank the following people for assistance with this work.

From the Research School of Earth Sciences, A.N.U.:

Dr M. McElhinny, for initiating and supervising the project.

Dr P. McFadden, for finding time to help with the writing despite his own commitments.

Mrs J. Cowley, for help with draughting.

Mr D. Edwards, for assistance in the palaeomagnetic laboratory.

Mr S. Constable, for typing, draughting, proof reading and unsolicited crtitical comment.

From the Research School of Pacific Studies, A.N.U.:

Prof D. Walker, for assistance with field work, providing laboratory facilities, making the L. Eacham cores available and helpful discussion.

Mr J. Neale, for assistance in the field and laboratory.

Mr J. Head and others from the ^{14}C laboratory, for providing the radiocarbon dates.

From elsewhere:

Dr R. Thompson (Edinburgh University), for useful assistance.

Dr R.M. Clark (Monash University), for helpful discussion on statistical aspects.

This project was funded by the Research School of Earth Sciences, A.N.U.

The author was in receipt of an A.N.U. postgraduate award between October 1981 and December 1982 .

CONTENTS.

1 INTRODUCTION.

Studies of the secular variation of the geomagnetic field yield information about the time constants associated with changes in the geomagnetic dynamo. A comprehensive model of the secular variation requires it to be well defined both spatially and temporally.

Recent lake sediments can be a valuable tool for this purpose. Historical records for the field only span at most the last few hundred years. Archaeomagnetic data provide information going further back in time as do palaeomagnetic measurements on lava flows. However, both these methods only provide data at discrete points in time and space which places an inherent limitation on the amount of information available. Lake sediments on the other hand may provide continuous records of the field over time spans of thousands of years. Lakes typically have sedimentation rates of about 1m/ky which is about an order of magnitude higher than that occuring in most deep sea sediments. This allows close sampling in time, so that features in the secular variation with periodicities from about 10^2 to 10^4 years can be resolved.

Quiet depositional environments are necessary if the sediment is to preserve a record of the field in its post-depositional remanent magnetization (PDRM). Volcanic crater lakes are particularly suitable as they frequently have no inflow or outlet streams and remain relatively isolated from fluctuations in the local water table.

The present study is of sediments from two Australian maars, Lakes Barrine and Eacham on the Atherton Tableland in northern Queensland. Previous work in Australia has been carried out on three south-west Victorian maars by Barton and McElhinny (1981). They have obtained from these a secular variation curve for south-eastern Australia which is in good agreement with archaeomagnetic data obtained from the same area (Barton and Barbetti, 1982). The Queensland lakes should provide some indication of how wide an area is affected by the sources dominating these secular variation records.

1.1 The Geomagnetic Field.

Measurements of the declination of the Earth's magnetic field were first made in China in the 8th century AD. Although the compass arrived in Europe in the 12th century, declination was not discovered there until the latter part of the 15th century. As a result of the use of the compass in navigation quite a large number of measurements were made so that by the end of the 17th century secular variation had been documented by Halley.

The first mathematical treatment of geomagnetic field measurements was performed by Gauss in 1839. He used spherical harmonics to represent the magnetic potential V at a point on the Earth as a sum of terms with radial dependence

$$V(r,\theta,\phi) = \frac{a}{\mu_o} \sum_{n=1}^{\infty} \sum_{m=0}^{n} P_n^m(\theta)[\{(g_e)_n^m(\frac{r}{a})^n + (g_i)_n^m(\frac{a}{r})^{n+1}\}\cos(m\phi) + \{(h_e)_n^m(\frac{r}{a})^n + (h_i)_n^m(\frac{a}{r})^{n+1}\}\sin(m\phi)]$$

where θ is the colatitude, ϕ the longitude, r the distance from the centre of the Earth, $P_n^m(\theta)$ the Schmidt polynomial of degree n order m, and g_e, h_e, g_i, h_i are the Gauss coefficients of external (e) and internal (i) origin.

Terms with a positive power of r represent external sources, mostly arising from ionospheric currents. Gauss' analysis showed that the dominant contribution to the field is of internal origin. This is attributed to hydromagnetic sources in the Earth's core and crustal remanent magnetization sources. The field of core origin is believed to be described by harmonics up to n=8 and crustal sources by terms greater than n=12 (Cain, 1975).

At present the first order approximation to the Earth's magnetic field is a geocentric dipole inclined at 11.5° to the Earth's axis of rotation. Residual non-zero terms in the spherical harmonic expansion are representative of the non-dipole field which is about 10% of the total.

1.1.1 Secular Variation.

Both the dipole and non-dipole fields vary with time and this secular variation is represented on magnetic element maps by isopors or lines of equal annual change. Regions at which the secular change is most rapid are called isoporic foci.

The non-dipole field and the secular variation drift westwards with time. Bullard et al. (1950) compared the 1907.5 and 1945 geomagnetic fields and calculated that the non-dipole field was drifting west at an average rate of $.18 \pm .015^{o}y^{-1}$ and that the secular variation had an average drift rate of $0.32 \pm .067^{o}y^{-1}$. An analysis of worldwide historical records and archaeomagnetic data from 0-2000 AD (Yukutake, 1967) indicated that westward drift has been a persisting feature of the secular variation during the last 700 years and also that non-dipole parts of the Earth's field can exist for several hundred years without substantial change. Yukutake and Tachinaka (1969) observed that the non-dipole field appeared to possess two types of regional anomalies, some standing at the same locality and others drifting westwards. They suggested that a drifting field superimposed on a standing field could account for the different drift rates of the non-dipole field and the secular variation. Spherical harmonic analysis using the field separated into standing and drifting parts revealed the two parts to be of approximately the same intensity. The drifting field is mainly represented by low harmonics whereas the standing field is more complicated.

In comparison with the non-dipole field, motion of the dipole axis is very slow. Bullard et al. (1950) observed that there was no evidence of change in the dipole component of the field since 1880. Barraclough (1974) performed spherical harmonic analysis on historical data available over the time span 1600 to 1910 and concluded that the northern geomagnetic pole had drifted westwards at a rate of $0.11^{o}y^{-1}$ and southwards at $.03^{o}y^{-1}$ between 1650 and 1850.

On the basis of archaeomagnetic data Kawai et al. (1965) postulated an anticlockwise motion of the dipole axis with a mean rotation rate of $0.2^{o}y^{-1}$ in a 1000 km radius about the north geographic pole. Kawai and Hirooka (1967) invoked a quasi-hypotrochoidal motion of the dipole in order to reconcile the movement indicated by worldwide archaeomagnetic

data from the past 2000 years with the present day clockwise motion.

Now that more archaeomagnetic data are available it is evidently desirable to use some form of smoothing to average out contributions from the non-dipole field. Barbetti (1977) used 100 year means of VGP (virtual geomagnetic pole) data for a number of regions on the Earth (divided according to availability of data) and suggested that 500 year means might be necessary to eliminate the regional non-dipole signals. Champion (1980) has applied this technique in detail and Merrill and McElhinny (1983) have extended his analysis to include new data from Hawaii. The 100 year means are illustrated in Figure 1.1. Merrill and McElhinny (1983) are of the opinion that these may well represent successive positions of the north geomagnetic pole over the last 2000 years.

1.1.2 The Geocentric Axial Dipole Hypothesis.

It is an axiom of palaeomagnetic research that, if taken over sufficient time, the average of the secular variation of the geomagnetic field will be zero and the true mean pole will average to the geographic pole. The palaeomagnetic directions at a site would then be those given by a magnetic dipole at the centre of the earth aligned with the earth's axis of rotation, i.e.

$$D = 0 \quad \text{and} \quad \tan I = 2\tan\lambda$$

where D is the declination, I the inclination and λ the latitude of the site.

Analysis of the time averaged field for global data over the past 5 m.y. shows that these data do average to the geographic pole (McElhinny, 1973). Wilson (1970) suggested that this is only a first order approximation, and that in the approximation to second order the axial dipole is offset northwards from the centre of the earth by several hundred kilometres. Subsequent work by McElhinny (1973) and Wilson and McElhinny (1974) showed that there is a time variation to this second order approximation. The geocentric axial dipole hypothesis is valid to first and second order for the past 2 m.y., while between 2 and 7 m.y. a small offset distance along the axis is required for the dipole.

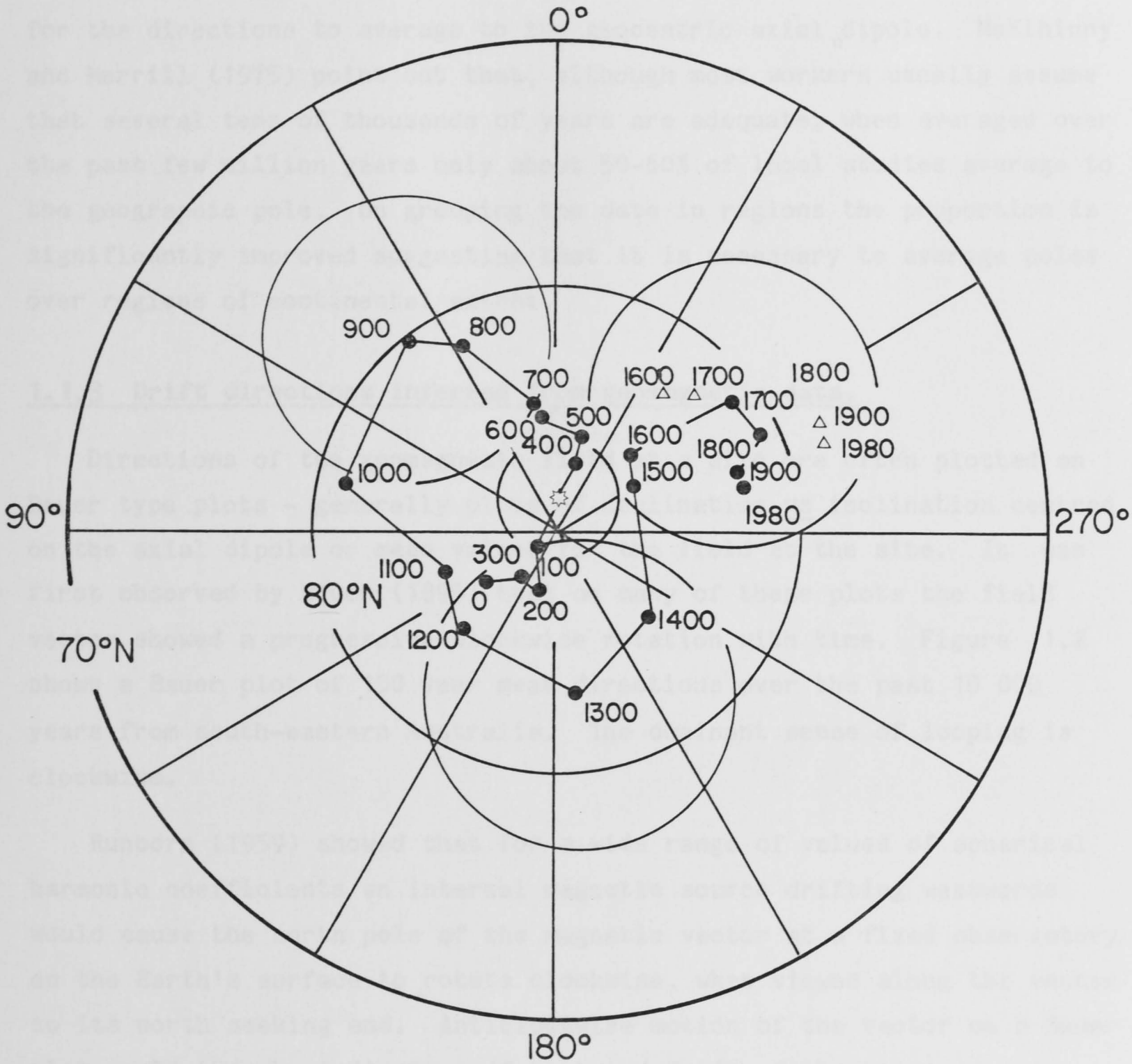

Figure 1.1 Location of the north geomagnetic pole over the past 2 000 years, as estimated from 100 year means of VGP data. Circles indicate 95% confidence limits about the 1700, 1300 and 900 year means. Triangles show poles obtained from the spherical harmonic analysis of Barraclough (1974). * indicates the mean VGP position over the past 2 000 years.

It is by no means obvious what should be regarded as sufficient time for the directions to average to the geocentric axial dipole. McElhinny and Merrill (1975) point out that, although most workers usually assume that several tens of thousands of years are adequate, when averaged over the past few million years only about 50-60% of local studies average to the geographic pole. On grouping the data in regions the proportion is significantly improved suggesting that it is necessary to average poles over regions of continental extent.

1.1.3 Drift directions inferred from geomagnetic data.

Directions of the geomagnetic field at a site are often plotted on Bauer type plots - generally plots of declination vs inclination centred on the axial dipole or mean values for the field at the site. It was first observed by Bauer (1895) that on many of these plots the field vector showed a progressive clockwise rotation with time. Figure 1.2 shows a Bauer plot of 100 year mean directions over the past 10 000 years from south-eastern Australia. The dominant sense of looping is clockwise.

Runcorn (1959) showed that for a wide range of values of spherical harmonic coefficients an internal magnetic source drifting westwards would cause the north pole of the magnetic vector at a fixed observatory on the Earth's surface to rotate clockwise, when viewed along the vector to its north seeking end. Anticlockwise motion of the vector on a Bauer plot would then be indicative of eastward drift of the source causing it. This is known as Runcorn's rule. The vector motions of Figure 1.2 thus indicate that they are caused by predominantly westwards drifting sources. It is an important result in that it allows the determination of rates and direction of drift from data at a single site.

Skiles (1970) has amplified this work and suggested that, since the motion of the surface field vector is not due to a single harmonic but to the combined effect of all the harmonics, the conditions required to violate Runcorn's rule would imply a very specialised source configuration.

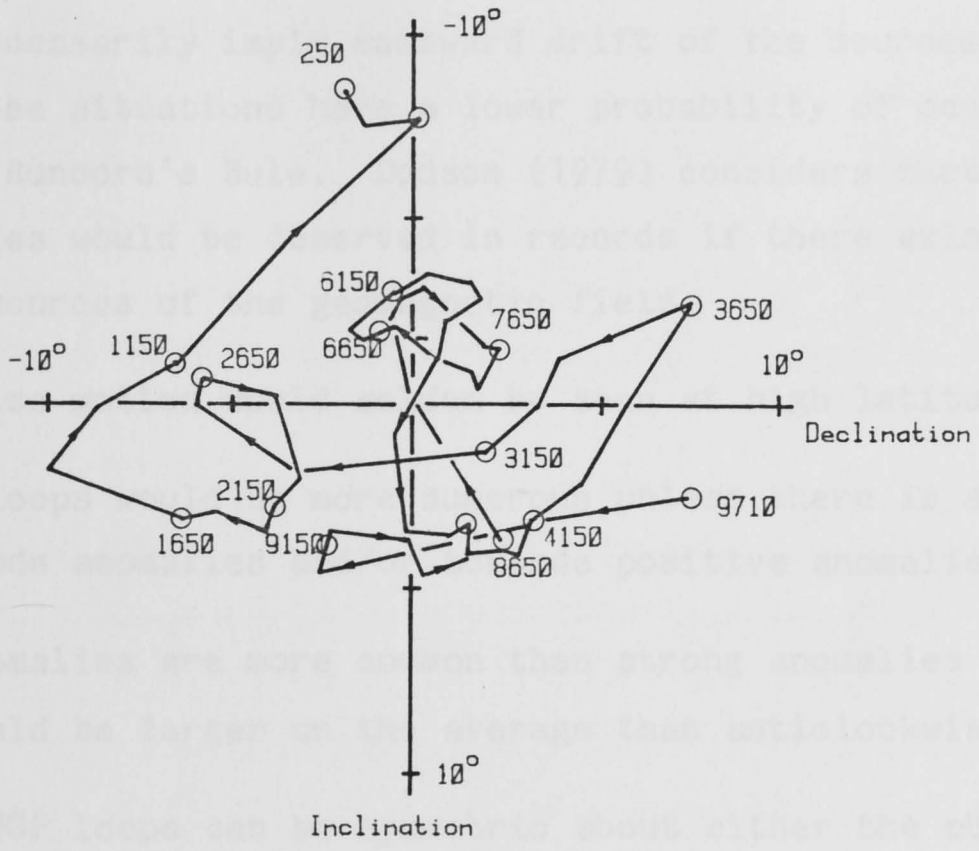

Figure 1.2 Bauer plot of 100 year mean directions over the past 10 000 years from L. Keilambete, S.E. Australia (after Barton and McElhinny, 1981).

Dodson (1979) has shown that an eccentric dipole source opposing the axial dipole and drifting westwards could result in anticlockwise precession of the field vector, when the source is located at higher latitudes than the observer. Similarly an eastward drifting source could result in clockwise precession. Thus the presence of anticlockwise precessing field vector paths in some secular variation records does not necessarily imply eastward drift of the sources causing them. However, these situations have a lower probability of occurring than those obeying Runcorn's Rule. Dodson (1979) considers that the following asymmetries would be observed in records if there existed no eastward drift of sources of the geomagnetic field.

(1) Anticlockwise motion would seldom be seen at high latitudes.

(2) Clockwise loops would be more numerous unless there is a bias towards high latitude anomalies and/or towards positive anomalies.

(3) If weak anomalies are more common than strong anomalies clockwise loops would be larger on the average than anticlockwise loops.

(4) Clockwise VGP loops can be symmetric about either the observer's meridian or anti-meridian, but anticlockwise loops can only be symmetric about the meridian.

(5) Anticlockwise motion would always be accompanied by a decrease in the total field intensity but clockwise motion could be accompanied by either a decrease or an increase in intensity.

At present there are insufficient data to test these conditions adequately. Continuous records of secular variation from a large number of sites would be necessary in order to do so.

1.1.4 The Geomagnetic Spectrum.

Cox and Doell (1964) observed that variations in the geomagnetic field appear to occur over a continuous spectrum rather than at discrete periods. By using a Fourier transform to convert the data from the time domain into the frequency domain it is possible to obtain information about the dominant frequencies present in secular variation records. Many of the periods of interest are of almost the same length as the records themselves and Burg's (1967) maximum entropy method (MEM) is widely used in geomagnetism in attempts to improve the resolution at the

long period end of the spectrum.

Currie (1968, 1973) has performed several analyses of observatory records of the field. Denham (1975) first suggested using time series analysis on lake sediment records. Barton (1982) has performed an analysis of observatory, lake sediment, archaeomagnetic and deep sea core data from ten different locations. This has provided a first order estimate of the global power spectrum (Figure 1.3). The major feature of this spectrum is an apparent dip at around 10^2 years. This may well be due to the change from analysis of historical to lacustrine records (Barton, 1982). Lacustrine records are likely to suffer from power attenuation as a result of both sedimentological processes and the stacking techniques used to obtain the secular variation curves. However, a number of authors have noted a concentration of power in the spectrum at periods of about 50 to 60 years preceding the apparent dip (e.g. Yukutake, 1973; Currie, 1973). Apart from this possible dip the other main feature of the spectrum is the broad maximum in power between 10^3 and 10^5 years. This includes the continuum of periods generally attributed to westward drift of the field, but is not necessarily exclusively caused by westward drift.

1.2 Recent Lake Sediments.

1.2.1 Postdepositional Remanent Magnetization (PDRM).

The derivation of a geomagnetic field record from sediments relies on their ability to preserve a faithful representation of the ambient field at or soon after deposition.

Verosub (1977) has discussed depositional and postdepositional processes in the magnetization of sediments. A depositional detrital remanent magnetization (depositional DRM) is one acquired by previously magnetized detrital grains which statistically align with the ambient field during deposition. This alignment may be disturbed to some extent by gravitational or current flow forces at the water-sediment interface causing systematic errors in the record of the field. A number of workers (e.g. Irving and Major, 1964; Kent, 1973; Løvlie, 1974, 1976) have performed experiments which show that sediments may acquire their magnetization after deposition. This is termed postdepositional

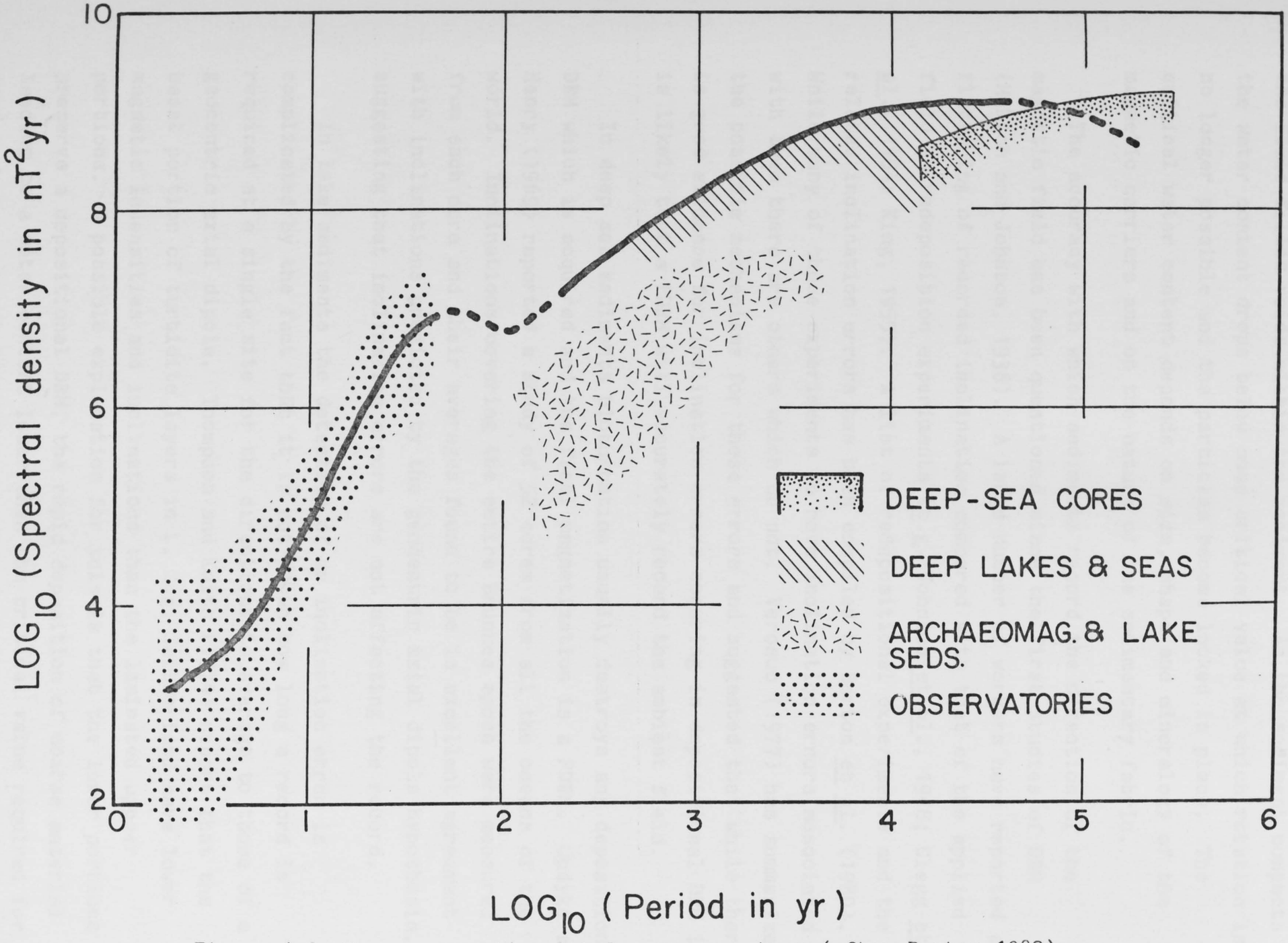

Figure 1.3 The geomagnetic global power spectrum (after Barton, 1982).

detrital remanent magnetization (PDRM). Verosub (1977) proposed a mechanism for this, based on magnetic particles being free to rotate in the fluid filled voids within the sediment. As the sediment compacts the water content drops below some critical value at which rotation is no longer possible and the particles become locked in place. The critical water content depends on size, shape and mineralogy of the magnetic carriers and on the nature of the sedimentary fabric.

The accuracy with which sediments record the direction of the magnetic field has been questioned since the first studies of DRM (McNish and Johnson, 1938). A large number of workers have reported a flattening of recorded inclination compared with that of the applied field in redeposition experiments (e.g. Johnson et al., 1948; Clegg et al., 1954; King, 1955). A list of redepositional experiments and the related inclination errors has been compiled by Barton et al. (1980). While many of these experiments do have inclination errors associated with them there are others which do not. Verosub (1977) has summarized the possible mechanisms for these errors and suggested that while there is good evidence for inclination errors occuring in depositional DRM it is likely that a PDRM will accurately record the ambient field.

In deep sea sediments bioturbation usually destroys any depositional DRM which is acquired and the final magnetization is a PDRM. Opdyke and Henry (1969) reported a study of 52 cores from all the oceans of the world. Inclinations covering the entire Brunhes epoch were measured from each core and their averages found to be in excellent agreement with inclinations predicted by the geocentric axial dipole hypothesis, suggesting that inclination errors are not affecting the record.

In lake sediments the detection of an inclination error is complicated by the fact that it is not known how long a record is required at a single site for the directions to average to those of a geocentric axial dipole. Thompson and Kelts (1974) report that the basal portion of turbidite layers in L. Zug, Switzerland have lower magnetic intensities and inclinations than the laminated uppper portions. A possible explanation for this is that the lower portions preserve a depositional DRM, the rapid deposition of coarse material leading to a water content lower than the critical value required for PDRM. The finer, more slowly deposited upper material could reflect a PDRM which accurately records the field direction (Verosub, 1977).

Varves from Sweden (Granar, 1958) and Iceland (Griffiths et al., 1955) show similar behaviour, with the silty summer layers having shallower inclination than the clayey winter layers. It is important to distinguish environments with a depositional DRM from those with PDRM, as those with a PDRM could be expected to preserve a more accurate record of the field.

Barton and McElhinny (1979), Barton et al. (1980), Hamano (1980) and Tucker (1979, 1980a, 1980b, 1981) have studied PDRM through redeposition experiments. Barton and McElhinny (1979) used very fine grained natural sedimentary material. This acquired a depositional DRM with no error in the field record and a time lag in remanence acquisition of less than two days. Postdepositional reorientation of particles did occur but was unimportant over periods of several months. Tucker (1981) on the other hand used synthetic sediments of known relative grain size. On the basis of his results he maintains that the time scale for acquisition of a PDRM will depend on the void size/magnetic grain size ratio in the sediment. Initially free grains may later be compacted with cement or gel formation taking place. More overprinting or smoothing of the geomagnetic signal will occur with a coarse than with a fine-grained fabric as there will be more grains free to move and the compaction period will be longer.

In general, depositional DRM and PDRM will probably both contribute to the magnetic remanence of lake sediments. Gravitational flattening of the inclination may occur with depositional DRM while with a PDRM there will be a smoothing of the geomagnetic signal over the time taken to acquire the PDRM.

After acquisition of its primary remanence the sediment and/or the remanence carrying minerals may undergo chemical change, resulting in the growth of a chemical remanent magnetization (CRM). Henshaw and Merrill (1980) discuss the effects of chemical change on magnetic remanence in marine sediments. Amplitude attenuation of directional swings as an increasing function of sediment depth has been reported in lake sediment secular variation records from south-eastern Australian crater lakes (Barton and McElhinny, 1981) and L. Windermere, England (Mackereth, 1971). This could be caused by a real trend in the geomagnetic field variation, but is quite possibly the result of long term particle remagnetization or the authigenic growth of magnetic

minerals.

1.2.2 Sampling and data processing.

The general techniques for sampling wet lake sediment have been summarized by Lund and Bannerjee (1979). Sediment cores are obtained from a lake using either a gravity or a piston corer. The usual procedure is then to sample the sediment at discrete intervals (generally 2-5 cm) down the length of the core and use alternating field (AF) cleaning to obtain palaeomagnetic directions for these specimens. Dodson *et al.* (1974, 1977) have used an open access cryogenic magnetometer to obtain continuous records from unopened cores.

Replicate cores are necessary to establish the validity of lake sediment records of secular variation, both within lakes and from other sites. The noise level in the data is generally high so core levels within a lake are matched using sedimentary or magnetic stratigraphy and data from equivalent horizons are stacked and then smoothed to provide a secular variation curve. Barton and McElhinny (1981) have used 100 year block means of the interquartile range of the data, while Clark and Thompson (1978) have suggested a more sophisticated algorithm using spline functions for smoothing. Chronological control is usually provided by radiocarbon dating of organic material in the sediment.

1.2.3 Worldwide and S.E. Australian Studies.

Mackereth (1971) first discovered long period declination variations in L. Windermere, England. Substantiation of the accurate recording properties of the sediment was provided by comparison with historical records of the geomagnetic field. Extensive work has since been carried out on lakes of varying sediment type in both Britain and Europe. These include L. Windermere, Loch Lomond and Llyn Geirionydd in the U.K. (Mackereth, 1971; Thompson, 1975; Turner and Thompson, 1981), a group of five Finnish lakes (Stober and Thompson, 1977), Polish, Swiss and Greek sites (Creer *et al.*, 1979, 1980, 1981) and sediment cores from the Black Sea (Creer, 1974).

Inclination variations are small and irregular compared with those of the declination but like the declination have been shown to be reproducible between different cores and lakes (see for example Turner and Thompson, 1981). Neither inclination nor declination swings are periodic and there is attenuation in their amplitude with time. Motion of the geomagnetic vector has been predominantly clockwise over the past 10 000 years with a period of anticlockwise motion from 1100 to 600B.P. Thompson and Turner (1979) have produced a master curve for Britain and western Europe in which the main features of the secular variation have been dated by the radiocarbon method.

Lund and Bannerjee (1979) have discussed the secular variation records from N. American lake sediments. The records are superficially similar to the European ones, showing large swings in declination and comparitively small inclination variations. Features have been shown to be reproducible within lakes but as yet no master curve has been attempted.

Barton and McElhinny (1981) have performed studies on Lakes Bullenmerri, Keilambete and Gnotuk, three volcanic crater lakes in south-eastern Australia. Detailed within lake magnetic stratigraphies allowed the construction of composite secular variation curves for each lake. Each of the three sequences has a comprehensive radiocarbon chronology associated with it, enabling a comparison to be made between the time scaled records. These are in good agreement suggesting that they do provide an estimate of the geomagnetic secular variation during the past 10 000 years.

In contrast to the northern hemisphere data these show pronounced swings in inclination with comparitively flat declination. Mean directions over the 10 000 years spanned at the three sites coincide with their geocentric axial dipole field directions. It is of interest to note that they also average to the geocentric axial dipole over the last 2 000 years (Barton and Barbetti, 1982). This is considerably shorter than the averaging time generally accepted as required for data at a single site (see section 1.2.3).

Records from the three lakes have been stacked and smoothed to provide a master curve for the south-eastern Australian region. Like the European records these show amplitude attenuation in the directional swings as an increasing funcion of age. Barton and McElhinny (1981) attribute this to long time scale remagnetization processes in the sediment rather than to a real feature of the geomagnetic field.

Barton and McElhinny (1981) have compared the British and S.E. Australian records and suggested that since the longer period variations have periods of the same order then the dominant source mechanisms should be similar in character. Comparison of VGP paths from the two sites shows no direct correlation, which precludes a common dipole wobble component at the two sites. The secular variation is thus attributed to independent non-dipole source mechanisms of a similar nature at the two sites. Westward drift of these sources is indicated by the predominantly clockwise sense of looping of the magnetic vectors and VGP paths in both regions.

2 SAMPLING AND MEASURING METHODS.

The following basic procedure was used. A set of cores was obtained from two North Queensland crater lakes, Lakes Barrine and Eacham. After whole core measurements of declination and horizontal remanence had been performed a subset of these was then selected for detailed study. These were cut open, a descriptive and photographic log of the core made and the sediment then subsampled at close intervals to provide material for secular variation studies.

Natural remanent magnetizations and magnetizations after AF cleaning were then measured for all the specimens. The data obtained were transferred to a UNIVAC 1100/82 series computer for processing.

2.1 Coring and Sampling Techniques.

2.1.1 Collection of cores.

Mackereth (1958) developed a pneumatic coring device for recovering continuous 6m cores of soft sediment in water depths of up to 100m. Barton and Burden (1979) made a number of modifications to the Mackereth design in order to make a corer capable of operating as a convertible 6/12m system.

The corer which was used in the Atherton Tableland maars is illustrated in Figure 2.1. This is the one developed by Barton and Burden with the minor modification of an additional independent air line to the buoyancy chamber to prevent this from filling with air and causing lift-off during coring.

The fundamentals of operation are as follows.

(1) Lower corer to lake floor with all air lines depressurized and the plunger valve open. The main piston should be at the top of its stroke.

◂ Seals

KP- Kullenberg piston
A, X, C, F - control taps for anchoring, abort, coring and buoyancy chamber airlines

TP - top plug

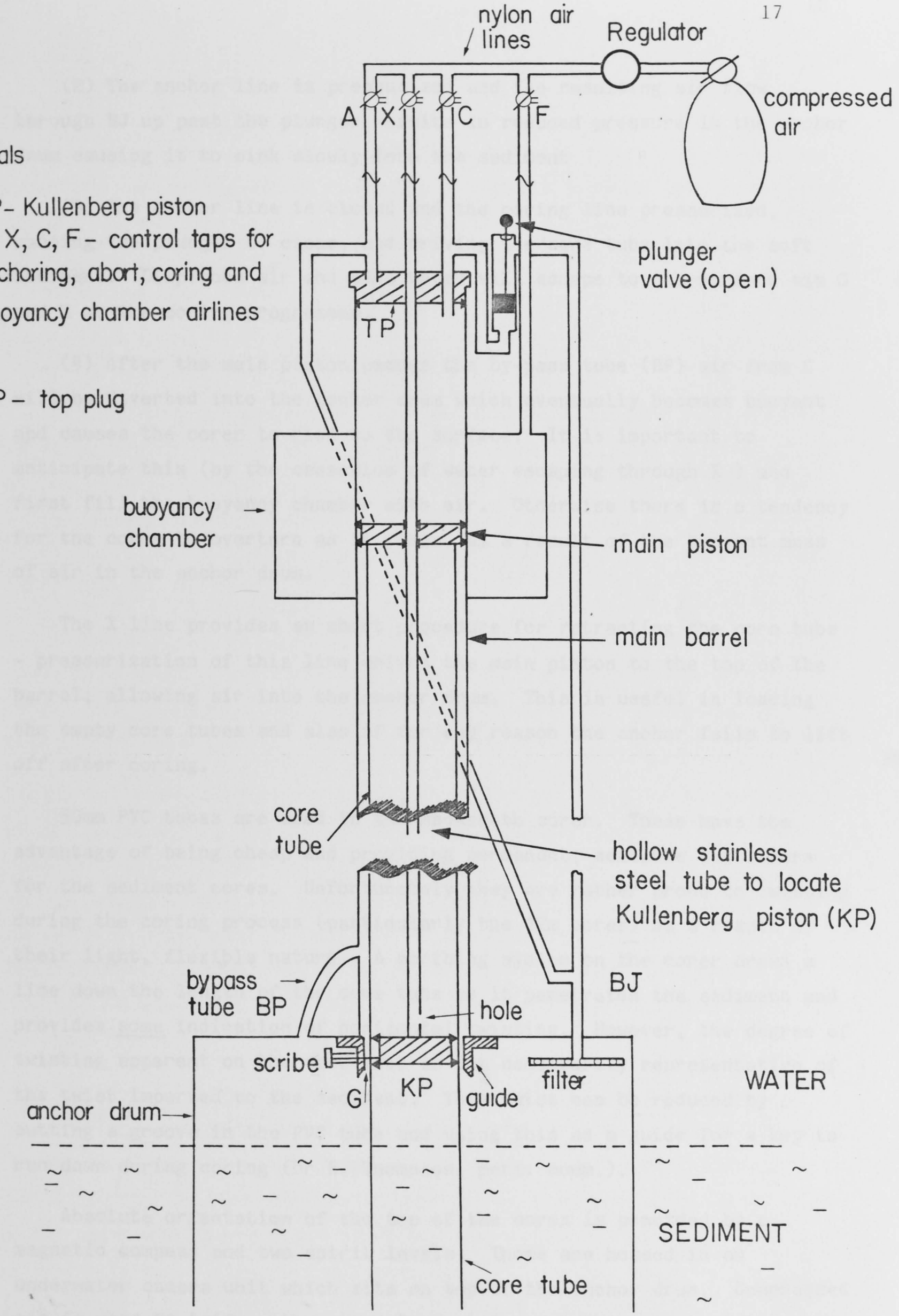

Figure 2.1 Schematic representation of the Mackereth corer.

(2) The anchor line is pressurized and the resulting air flow through BJ up past the plunger results in reduced pressure in the anchor drum causing it to sink slowly into the sediment

(3) The anchor line is closed and the coring line pressurized, causing the plunger to close, and driving the core tube into the soft sediment. Displaced air and some water will escape to the surface via G and X as the coring progresses.

(4) After the main piston passes the by-pass tube (BP) air from C will be diverted into the anchor drum which eventually becomes buoyant and causes the corer to rise to the surface. It is important to anticipate this (by the cessation of water escaping through X) and first fill the buoyancy chamber with air. Otherwise there is a tendency for the corer to overturn as it rises, as a result of the buoyant mass of air in the anchor drum.

The X line provides an abort procedure for retracting the core tube - pressurization of this line drives the main piston to the top of the barrel, allowing air into the anchor drum. This is useful in loading the empty core tubes and also if for any reason the anchor fails to lift off after coring.

50mm PVC tubes are used in the Mackereth corer. These have the advantage of being cheap and providing permanent, sealable containers for the sediment cores. Unfortunately they are rather prone to twisting during the coring process (particularly the 12m cores) as a result of their light, flexible nature. A scribing system on the corer draws a line down the length of the core tube as it penetrates the sediment and provides some indication of horizontal twisting. However, the degree of twisting apparent on the core tube is not necessarily representative of the twist imparted to the sediment. This twist can be reduced by cutting a groove in the PVC tube and using this as a guide for a key to run down during coring (Dr R. Thompson, pers. comm.).

Absolute orientation of the top of the cores is provided by a magnetic compass and two spirit levels. These are housed in an underwater camera unit which sits on top of the anchor drum. Compressed air is used to trigger the camera and photograph the orientation of the compass. This system is described in detail by Barton and Burden (1979).

Seven cores were obtained from L. Barrine in September 1979 using the 12m corer. Four additional 6m cores from L. Eacham were used in this study. These were collected by the department of Biogeography and Geomorphology of the Research School of Pacific Studies, ANU during their 1977 and 1978 field seasons. Despite the long storage time before opening, these cores appeared remarkably well preserved and to have undergone no significant chemical alteration.

2.1.2 Selection of cores for subsampling.

All the cores obtained were sectioned into 3m lengths and measured on an automated version of the Digico fluxgate long core spinner magnetometer (Molyneux et al., 1972; Barton, 1978). The fluxgate was 7cm in diameter and its response curve had a half peak width of 4.4cm. Declination and horizontal remanence were measured at 1cm intervals down the length of the cores.

A number of cores from each lake were then selected for subsampling (five from Barrine and four from Eacham) on the basis of correlativity of intensity between cores, length of the record and smoothness of the declination profiles.

Three of the L. Barrine cores (B1,B3,B4) had excellent correlations on the basis of their horizontal natural remanent magnetizations (NRM). However, B3 and B4 were only 10m in length. B5 and B7 were both close to 12m long and although they were less easy to correlate with the other three, they were sampled in the hope of extending the record further back in time. Also B5 and B7 were comparitively undisturbed near the top of the cores unlike B1 and B4 which had very wet disturbed material in the top metre.

Thirteen L. Eacham cores were measured on the long core spinner. All the declination profiles showed large swings and scatter in the data in the top metre or so, suggesting that the sediment had been disturbed during coring or transportation. Four cores with excellent correlation below this were selected for subsampling.

Nearly all the cores showed trends in declination down their length. These were not in the same direction for all cores and are assumed to be due to twisting of the core tube during coring. Twisting of the 12m L. Barrine cores was particularly bad, resulting in poor absolute declination control. No absolute declination control existed for the L. Eacham cores as they had not originally been intended for palaeomagnetic work.

2.1.2 Subsampling Procedure.

The subsampling technique used was largely the same as that described by Barton (1978). Cores were opened by cutting two slots along the length of the PVC tubes and then finishing the cut with a stainless steel knife. Thin sheets of stainless steel were then pushed through one of the cuts to separate the two sections of the core. This avoided any pollen contamination which might occur using a wire or knife to separate the material. The core was sectioned in such a way as to allow two adjacent $5.3cm^3$ boxes to be used for sampling at 2.5cm intervals down the length of the core. This required about 60% of the core. The smaller section was used for palynological, X-ray diffraction and mechanical analyses.

A small modified drill press was used to align and press the perspex specimen boxes into the sediment. Air escaped via a small hole drilled in the bottom of the box which was later sealed with an adhesive label. After sampling the boxes were stored on aluminium trays in the refrigerator.

2.2 Subsample Measurements.

2.2.1 Natural Remanent Magnetisation.

Measurements of the direction and intensity of the natural remanent magnetization (NRM) were carried out on all the core subsamples. These were made on a 2-axis Super Conducting Technology (SCT) cryogenic magnetometer interfaced to an HP2100 series computer. The whole system is surrounded by large Parry coils which null the field at the sample access port of the magnetometer. The SCT magnetometer uses an RF-driven SQUID sensor of the type described by Goree and Fuller (1976). The high

sensitivity of this sensor makes it ideal for the measurement of even very weak sedimentary specimens which would require unduly long counting times on conventional spinner magnetometers. The magnetic moment sensitivity of the SCT magnetometer is about 2×10^{-9} emu.

2.2.2 Alternating Field Cleaning.

While the intensity and directions of the NRM of recent sediments may well yield useful information about the past geomagnetic field it is important to determine whether or not the remanence is primary. When dealing with wet lake sediment the only practical method of magnetic cleaning is by alternating field (AF) demagnetization.

Specimens are placed in an alternating magnetic field H (usually produced by a solenoid) which is decreased continuously to zero. Magnetic domains exposed to a peak AF field larger than their coercive forces will follow the field as it alternates. As H is gradually reduced to zero the domains will become locked in random orientations, provided that no dc field or even harmonics of the AF field are present. This is equivalent to cycling the specimen around successively smaller hysteresis loops as shown in Figure 2.2.

This method was first introduced by As and Zijderveld (1958), who demagnetized specimens successively along three orthogonal directions. The major disadvantage of this technique is that not all directions of the specimen are exposed to the same peak field. McFadden (1981) observes that the maximum value of the angle between the AF field and the coercive force of a magnetic domain is 54.7^{o}. Creer (1959) introduced the technique of tumbling the specimen within the AF field to help reduce this problem. Two axis tumbling systems are now in quite general use. A tumbling ratio of 11:16 is regarded as one of the most efficient in terms of exposure of all directions in the specimen to the AF field (McElhinny, 1966).

A problem associated with tumbling specimens during AF cleaning is that they may acquire a rotational remanent magnetization (RRM). Wilson and Lomax (1972) first reported this phenomenon, whereby a rotating specimen demagnetized in an AF field acquires a remanence antiparallel to the rotation vector when the rotation axis is perpendicular to the AF axis. Theoretical explanations for this have been propounded by Smith

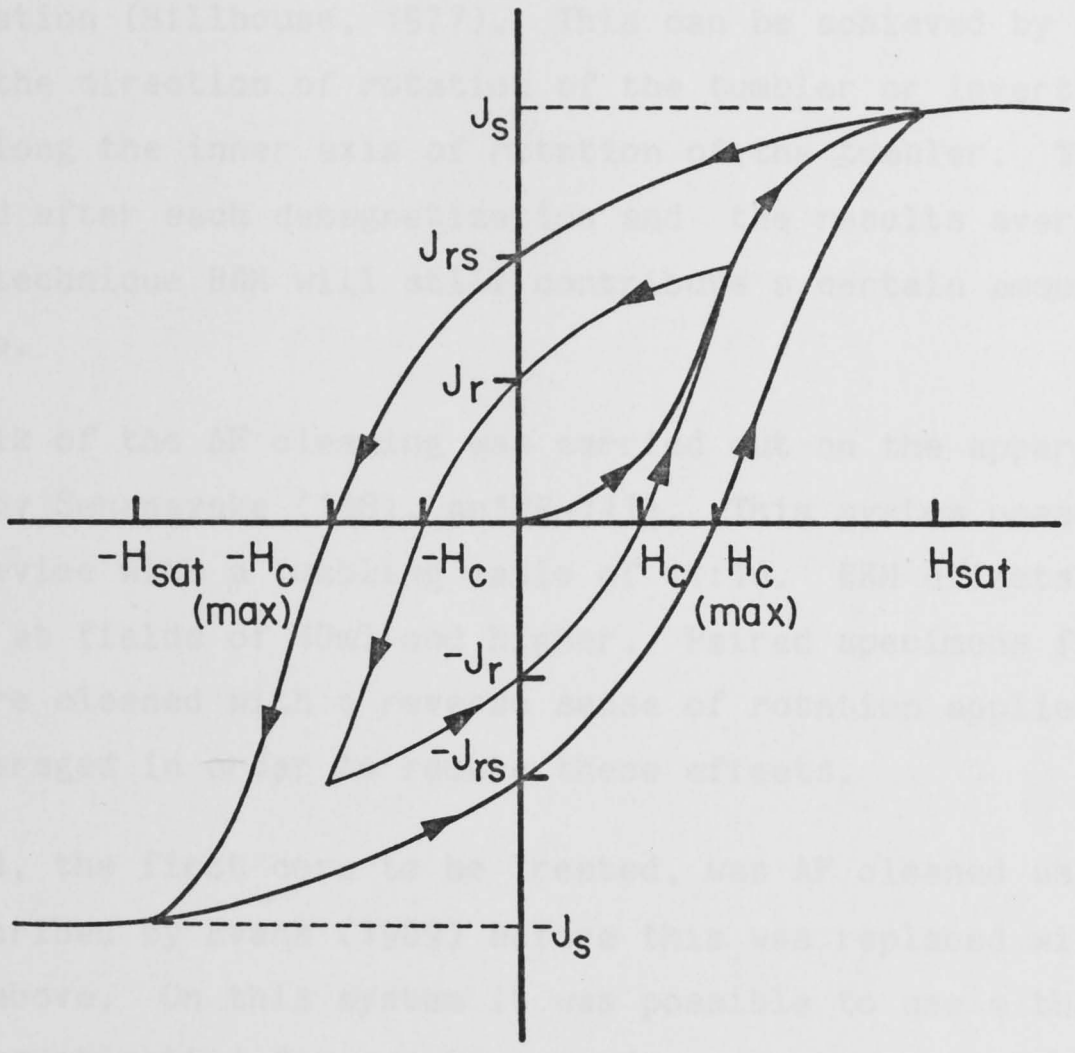

Figure 2.2 Cycling of a magnetic domain around successively smaller hysteresis loops. J_s is the saturation magnetization, J_r the remanent magnetization, H_c the coercive force.

and Merrill (1980) and Stephenson (1980). In practice the effects of RRM can be minimized by using a double demagnetizing procedure - reversing the sense of rotation of the specimen for the second demagnetization (Hillhouse, 1977). This can be achieved by either reversing the direction of rotation of the tumbler or inverting the specimen along the inner axis of rotation of the tumbler. The specimen is measured after each demagnetization and the results averaged. Even with this technique RRM will still contribute a certain amount of noise to the data.

The bulk of the AF cleaning was carried out on the apparatus described by Senanayake (1981, pp129-141). This system uses a 2-axis tumbling device with a tumbling ratio of 11:16. RRM effects were detectable at fields of 10mT and higher. Paired specimens from the same horizon were cleaned with a reverse sense of rotation applied and the results averaged in order to reduce these effects.

Core B1, the first core to be treated, was AF cleaned using the system described by Evans (1969) before this was replaced with the one described above. On this system it was possible to use a three axis static demagnetization for greater speed.

In general AF cleaning had slight effects on the directions of remanence, mostly just reducing the visible scatter in the data. Figure 2.3 shows the inclination data for core E80 before and after AF cleaning at 10mT. The changes are attributed to the removal of small viscous components, possibly acquired after sampling. The cleaned directions are assumed to represent those of the geomagnetic field at or soon after the deposition of the sediment. Chemical changes in the magnetic remanence carriers with time could however render this assumption invalid. The ultimate justification for regarding this as a geomagnetic record must be its reproducibility between sites.

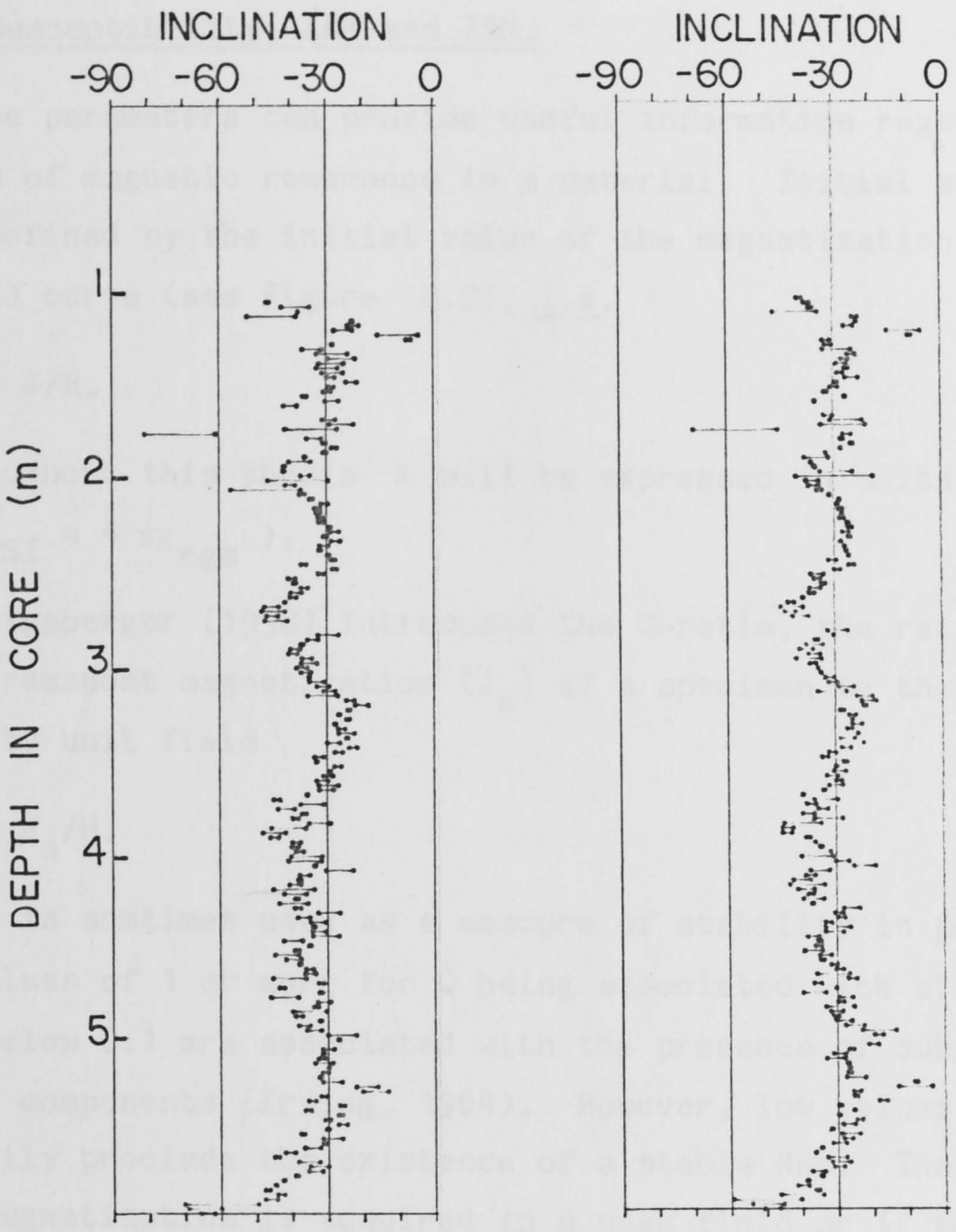

(a) E80 NRM (b) E80 AF

Figure 2.3 Effect of AF cleaning on core E80 inclination. Vertical lines join pairs of data at the same level. (a) before (mean inclination = -34.2), (b) after (mean = -30.9).

2.2.3 Susceptibility, ARM and IRM.

These parameters can provide useful information regarding the carriers of magnetic remanence in a material. Initial susceptibility, χ, is defined by the initial value of the magnetization (J) *vs* applied field (H) curve (see Figure 2.2), *i.e.*

$$\chi = J/H.$$

Throughout this thesis χ will be expressed in units of emu-cm^{-3} (in S.I. $\chi_{SI} = 4\pi\chi_{cgs}$).

Koenigsberger (1938) introduced the Q-ratio, the ratio of the natural remanent magnetization (J_n) of a specimen to the magnetization induced by unit field

$$Q = J_n/H.$$

This is somtimes used as a measure of stability in palaeomagnetic work, values of 1 or more for Q being associated with stable NRMs. Values below 0.1 are associated with the presence of substantial unstable components (Irving, 1964). However, low values do not necessarily preclude the existence of a stable NRM. They may arise if a stable magnetization is acquired in a weak field or if there has been viscous decay of the NRM without the build-up of unstable components.

Initial susceptibility measurements were made for all the subsamples on a Digico bulk susceptibility bridge. For each specimen the mean of 4 measurements was obtained which in general resulted in a standard deviation of less than 5%.

Anhysteretic remanent magnetizations (ARMs) were imparted in a dc bias field of .01mT with an AF cleaning field of 100mT, along the direction of the NRM. This treatment was performed on specimens from one core in each lake.

Saturation isothermal remanent magnetizations (SIRMs) were imparted in a dc field of 1T and measured on a Digico spinner magnetometer (Molyneux, 1971).

3 CORE DESCRIPTONS AND RADIOCARBON CHRONOLOGIES.

3.1 Site Description.

Lakes Barrine and Eacham are situated on the Atherton Tableland in North Queensland (see Figure 3.1). This is a small basaltic lava plateau with over 40 eruption points on it. At least six of these are maars and Barrine, Eacham and Euramoo contain lakes (de Keyser, 1972).

The latest volcanic phase in the area appears to have been the eruption of various scoria cones (Mt Quincan and the Seven Sisters). Euramoo's basal organic sediments have been dated at around 10 000B.P. (although the crater itself may be older) and sediment from another nearby site, Lynch's Crater, is estimated to span at least 60 000 years (Kershaw, 1974). Eacham and Barrine show more signs of weathering than Euramoo (Timms, 1976) and are probably intermediate in age between Euramoo and Lynch's Crater. Dating of the organic sediment from the bottom of 12m cores from L. Barrine has provided radiocarbon ages ranging from about 11 000 to 16 000 years before present.

Lakes Barrine and Eacham are deep and flat bottomed and each is surrounded by a crater rim of pyroclastics which has a low outer and high inner slope of on average about 30^{o} but as high as 75^{o} in some places (Timms, 1976). Figure 3.2 shows bathymetric maps and cross sections of each crater. It may be seen from these that the catchment of Eacham is considerably steeper than that of Barrine. Both lakes have a bay on the eastern side each of which is attributed to a mild subsidiary explosion (de Keyser and Lucas, 1968; Best, 1960). Various characteristics of the two lakes are tabulated below.

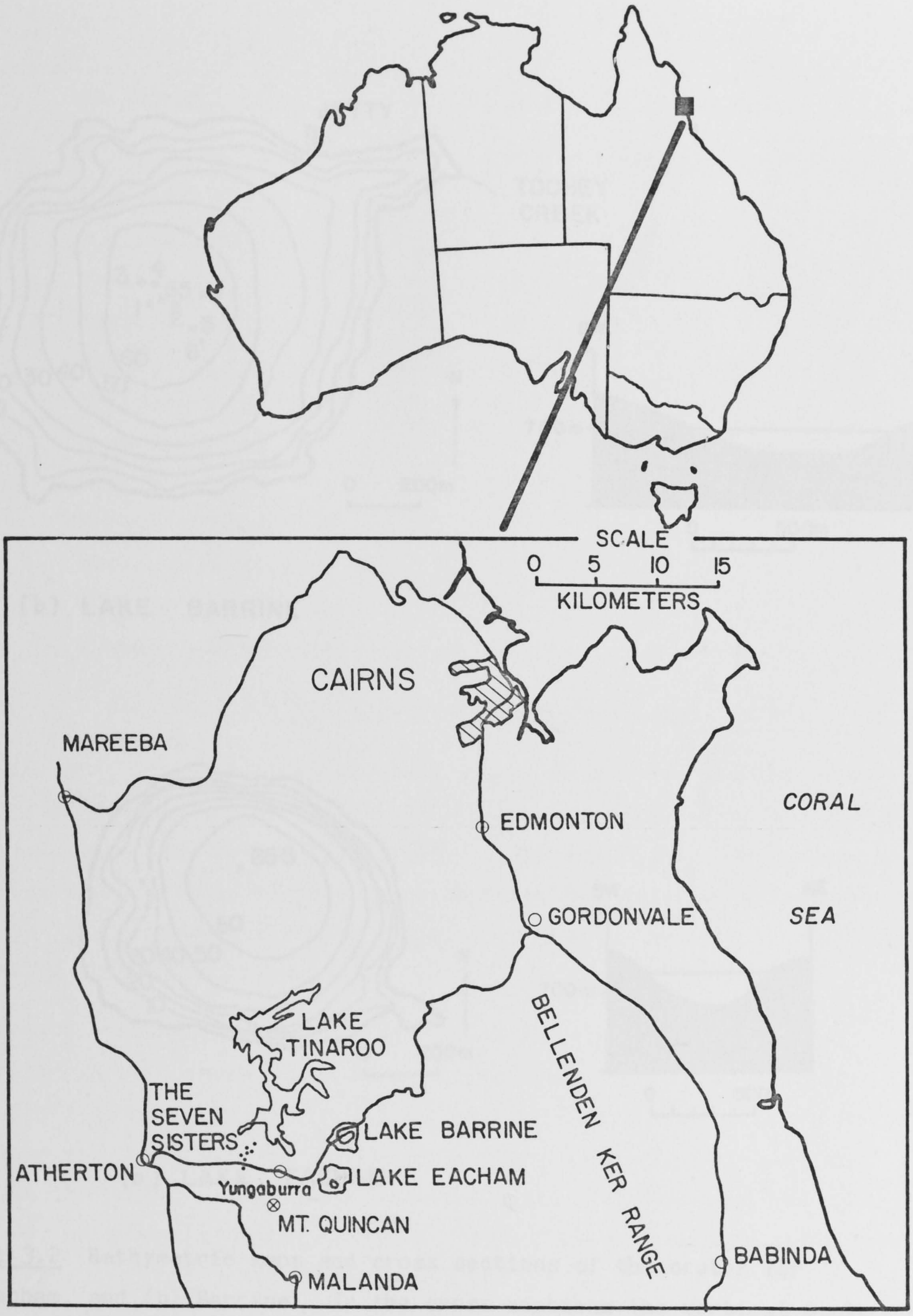

Figure 3.1 Location of Lakes Barrine and Eacham. Shaded areas surrounding the lakes indicate rainforest.

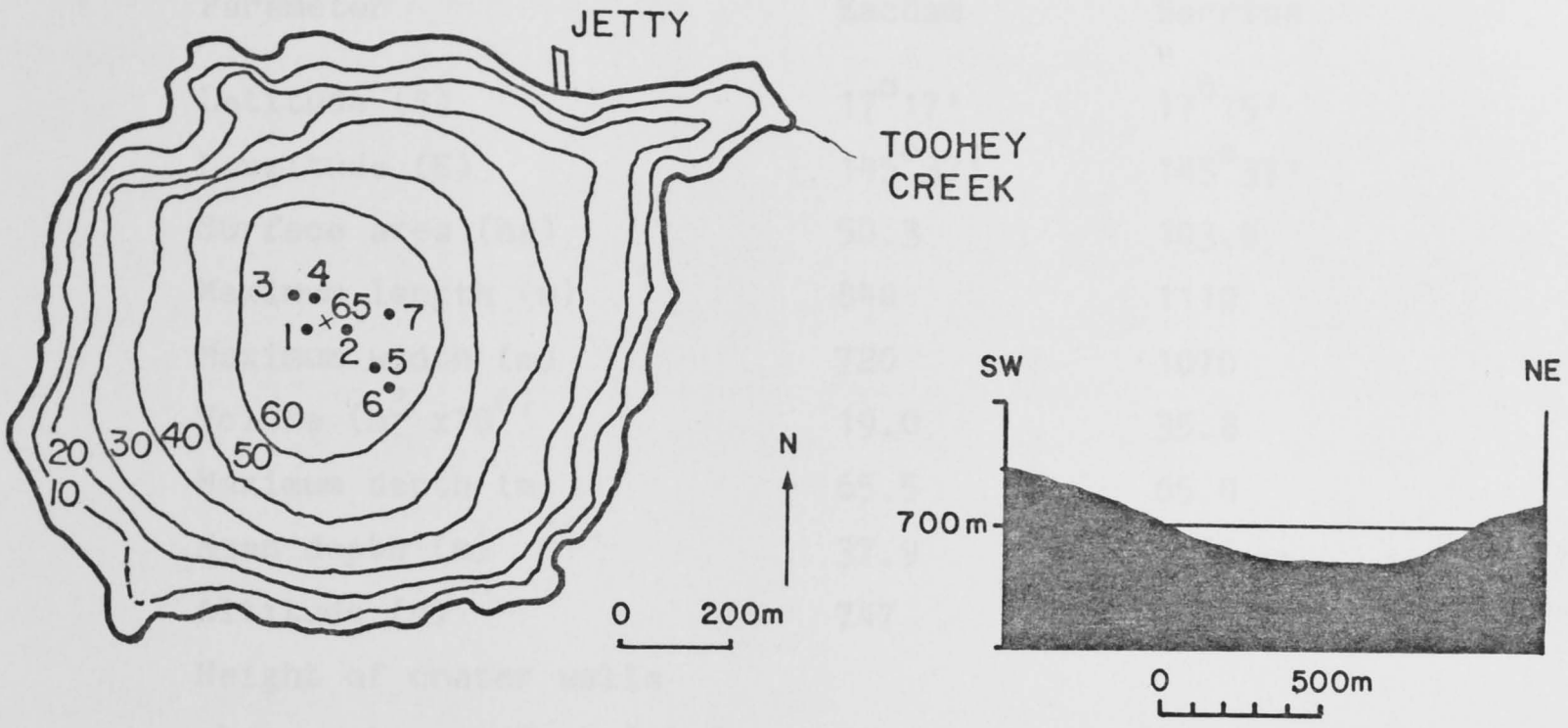

(b) LAKE BARRINE

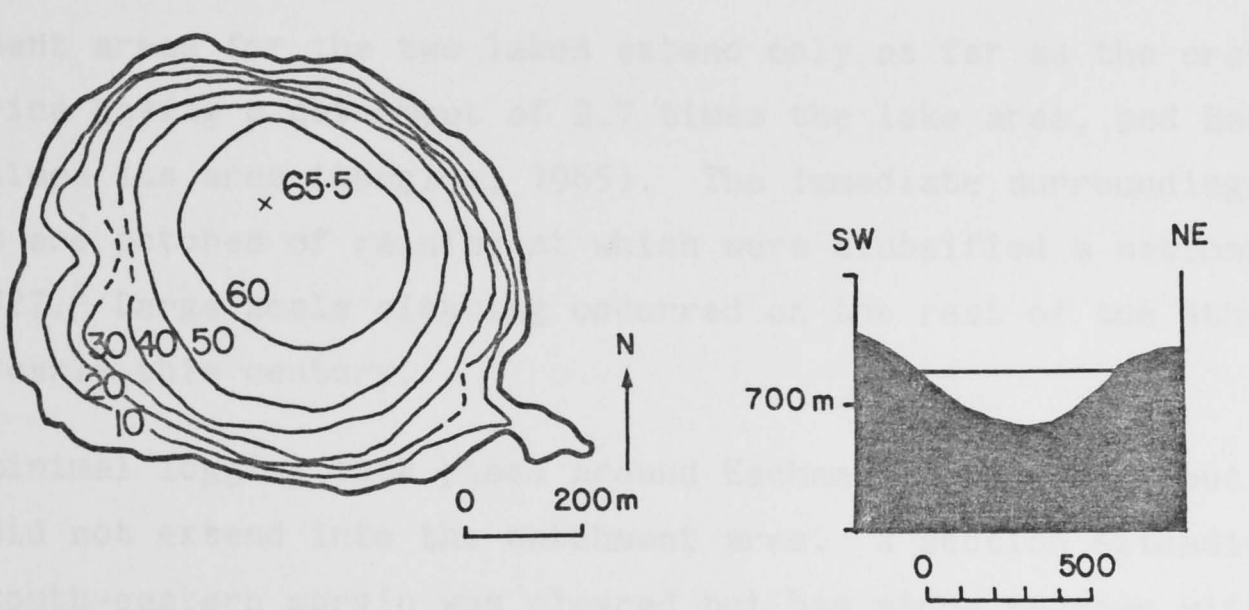

(a) LAKE EACHAM

Figure 3.2 Bathymetric maps and cross sections of the crater for (a) Eacham, and (b) Barrine. In the cross sections the vertical scale is exaggerated by a factor of 2.

Table 3.1

Parameter	Eacham	Barrine
Latitude (S)	17°17'	17°15'
Longitude (E)	145°37'	145°37'
Surface area (ha)	50.3	103.5
Maximum length (m)	840	1110
Maximum width (m)	720	1070
Volume (m^3 x10^6)	19.0	35.8
Maximum depth (m)	65.5	65.0
Mean depth (m)	37.9	34.6
Altitude (m)	747	725
Height of crater walls above water surface (m) *	30	27
Average diameter (m)	790	1100
Crater diameter (m)	900	1500

* Jardine (1925), all rest of above from Timms (1976).

Catchment areas for the two lakes extend only as far as the crater rims, Barrine having a catchment of 2.7 times the lake area, and Eacham only 1.2 times its area (Douglas, 1965). The immediate surroundings of both lakes are patches of rainforest which were classified a national park in 1927. Large scale clearing occurred on the rest of the Atherton Tableland early this century.

Some minimal logging took place around Eacham in the 1920s, but probably did not extend into the catchment area. A section extending from the south-eastern margin was cleared but has since regrown with acacia and a small cleared area exists, which is visited by tourists, between the road and the lake. An area on the north-eastern side of Barrine, next to the jetty, has been cleared and various buildings there inhabited since early this century. Prior to the arrival of Caucasians there was effectively no interference with the ecology of the lakes as the Aborigines believed the former volcanic vents to be inhabited by totemic beings (Kershaw, 1973, p309).

The tableland has a warm tropical mountain climate with dry cool winters and warm wet summers. During the wet season rainfall can cause the level of Eacham to rise by up to three or four metres as there is no outflow stream. Douglas (1965) suggests that the main water loss from Eacham is by seepage through basaltic material on the eastern edge of the crater. Barrine on the other hand is drained by Toohey Creek and thus maintains a relatively constant level. The bathymetric map of Barrine indicates that there is a sublacustrine channel on the eastern side of the lake and according to Timms (1976) "this must be a relic of a former inflow; perhaps the upper reach of Toohey Creek once flowed into the lake."

3.2 Core Descriptions.

After opening, but before sampling, a photographic and a descriptive log was made of each core. Many of the cores had air gaps in them as a result of pressure equilibration occurring after the cores were brought to the lake surface.

3.2.1 L. Barrine.

The core log for B1 is shown in Figure 3.3 alongside the horizontal intensity of magnetization. This is fairly typical of all the L. Barrine cores, the sediment being roughly divided into four main zones as follows.

0-3m Finely laminated, organic silty clay containing a few bands of amorphous dark material. The laminations are predominantly dark brown and greenish in colour. At present the cause of the laminations is unknown, although it is conceivable that they are seasonal, caused by the contrast in conditions between the wet summers and dry winters.

3-7.5m Obscurely banded, mostly dark brown silty clay with occasional bands containing fine laminae.

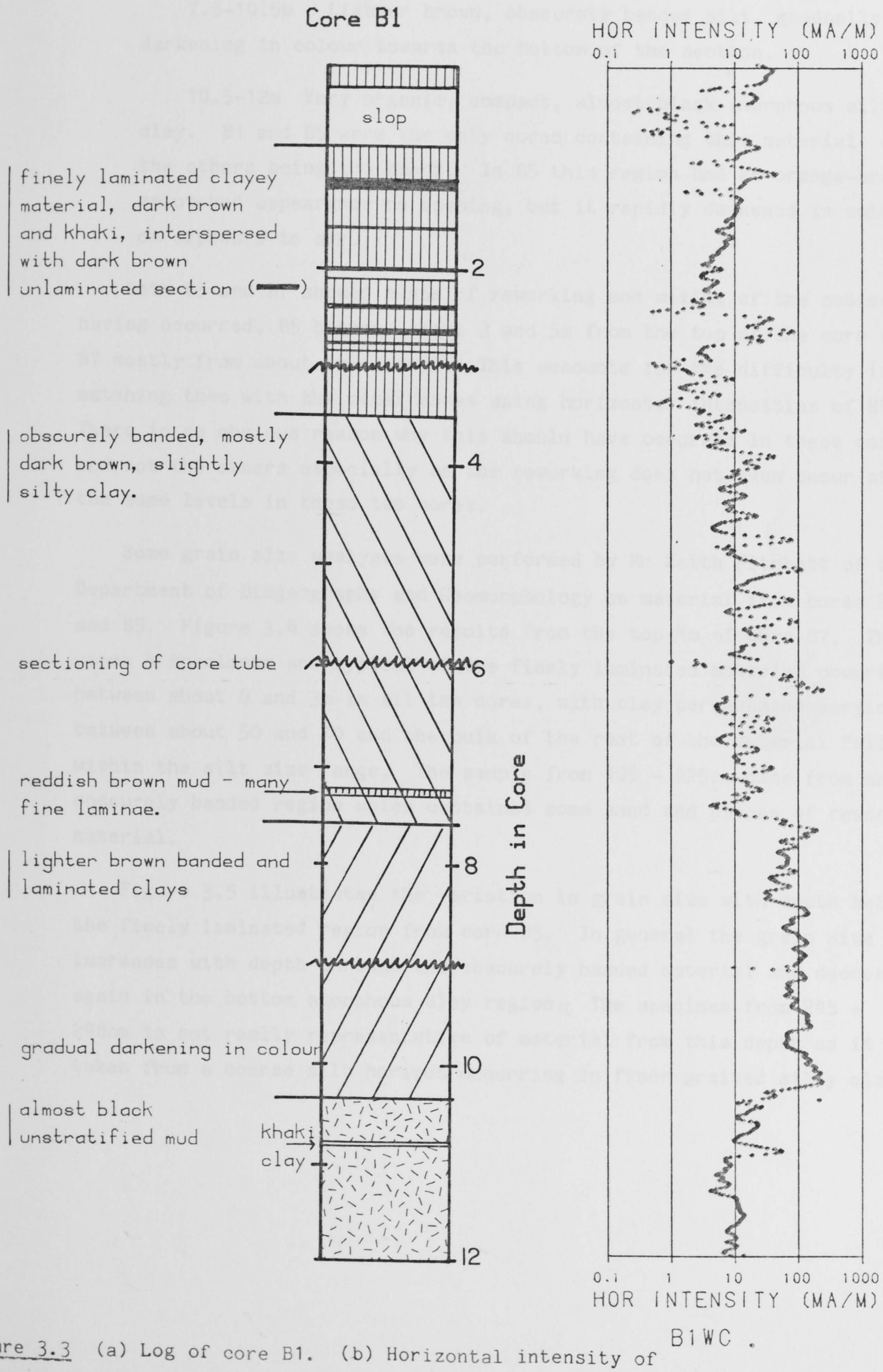

Figure 3.3 (a) Log of core B1. (b) Horizontal intensity of magnetization for core B1.

7.5-10.5m Lighter brown, obscurely banded silt, gradually darkening in colour towards the bottom of the section.

10.5-12m Very organic, compact, almost black amorphous silty clay. B1 and B5 were the only cores containing this material, all the others being too short. In B5 this region had an orange-brown splotched appearance on opening, but it rapidly darkened in colour on exposure to air.

Both B5 and B7 showed signs of reworking and mixing of the sediment having occurred, B5 between about 3 and 5m from the top of the core and B7 mostly from about 6m onwards. This accounts for the difficulty in matching them with the other cores using horizontal intensities of NRM. There is no obvious reason why this should have occurred in these cores and not the others especially as the reworking does not even occur at the same levels in these two cores.

Some grain size analyses were performed by Mr Keith Fitchett of the Department of Biogeography and Geomorphology on material from cores B7 and B5. Figure 3.4 shows the results from the top 4m of core B7. The upper 4 specimens are typical of the finely laminated material occuring between about 0 and 3m in all the cores, with clay percentages varying between about 50 and 70 and the bulk of the rest of the material falling within the silt size range. The sample from 405 - 425cm came from an obscurely banded region which contained some sand and pieces of reworked material.

Figure 3.5 illustrates the variation in grain size with depth below the finely laminated region from core B5. In general the grain size increases with depth through the obscurely banded material and decreases again in the bottom amorphous clay region. The specimen from 245 - 248cm is not really representative of material from this depth as it was taken from a coarse silt horizon occurring in finer grained silty clay.

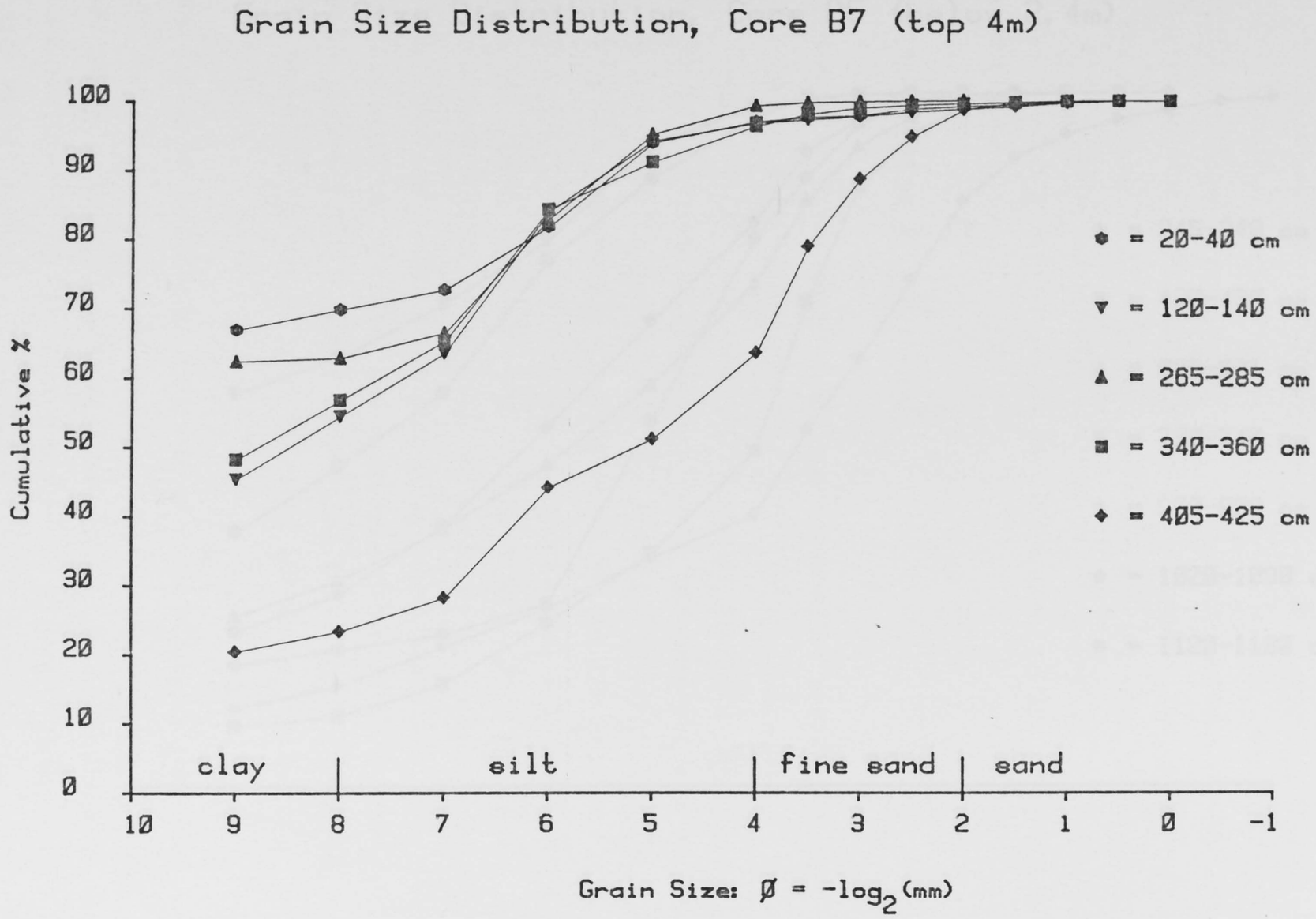

Figure 3.4

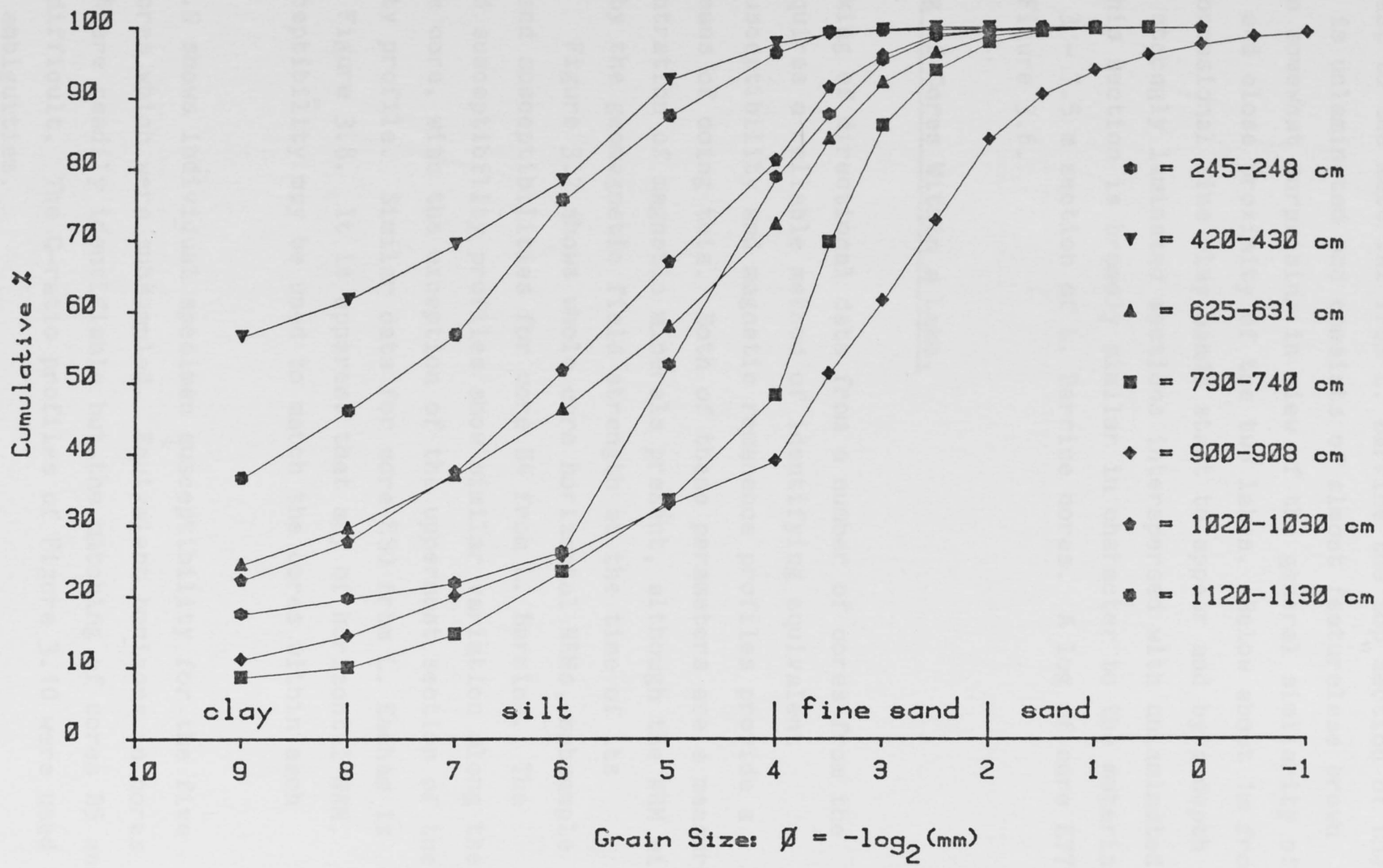
Grain Size Distribution, Core B5 (below 2.4m)
Cumulative %
100
90
80
70
60
50
40
30
20
10
0
clay
silt
fine sand
sand
10
9
8
7
6
5
4
3
2
1
0
-1
Grain Size: Ø = -log2(mm)
= 245-248 cm
= 420-430 cm
= 625-631 cm
= 730-740 cm
= 900-908 cm
= 1020-1030 cm
= 1120-1130 cm

Figure 3.5

3.2.2 L. Eacham.

In contrast to the material from L. Barrine the top section of the Eacham cores is unlaminated and consists of almost featureless brown mud. This is somewhat surprising in view of the general similarity of environments and close proximity of the two lakes. Below about 1m from the surface occasional fine clay bands start to appear and by a depth of 2m there are strongly laminated sections interspersed with unlaminated material. This section is broadly similar in character to the material found in the 3 - 7.5 m section of L. Barrine cores. A log of core E77 is shown in Figure 3.6.

3.3 Matching of Cores Within a Lake.

The stacking of directional data from a number of cores from the same lake requires a reliable method of identifying equivalent horizons. Susceptibility and magnetic remanence profiles provide a convenient means of doing this. Both of these parameters are a measure of the concentration of magnetic minerals present, although the NRM will be affected by the geomagnetic field strength at the time of its acquisition. Figure 3.7 shows whole core horizontal NRMs, subsample NRMs, ARMs, and susceptibilities for core B4 from L. Barrine. The remanence and susceptibility profiles show similar variation along the length of the core, with the exception of the uppermost section of the susceptibility profile. Similar data for core E80 from L. Eacham is exhibited in Figure 3.8. It is apparent that any of horizontal NRM, NRMs and susceptibility may be used to match the cores within each lake.

Figure 3.9 shows individual specimen susceptibility for the five L. Barrine cores which were subsampled. Equivalent horizons in cores B1, B3 and B4 are readily identifiable but the matching of cores B5 and B7 was more difficult. The Q-ratio profiles of Figure 3.10 were used to resolve some ambiguities.

The horizontal whole core NRMs and declinations for L. Eacham used to select which cores to open are shown in Figures 3.11 and 3.12. As can be seen from the scattered declination profiles the top sections of very sloppy sediment had been disturbed during transportation or whole core spinner measurements. Below this disturbed material the intensity

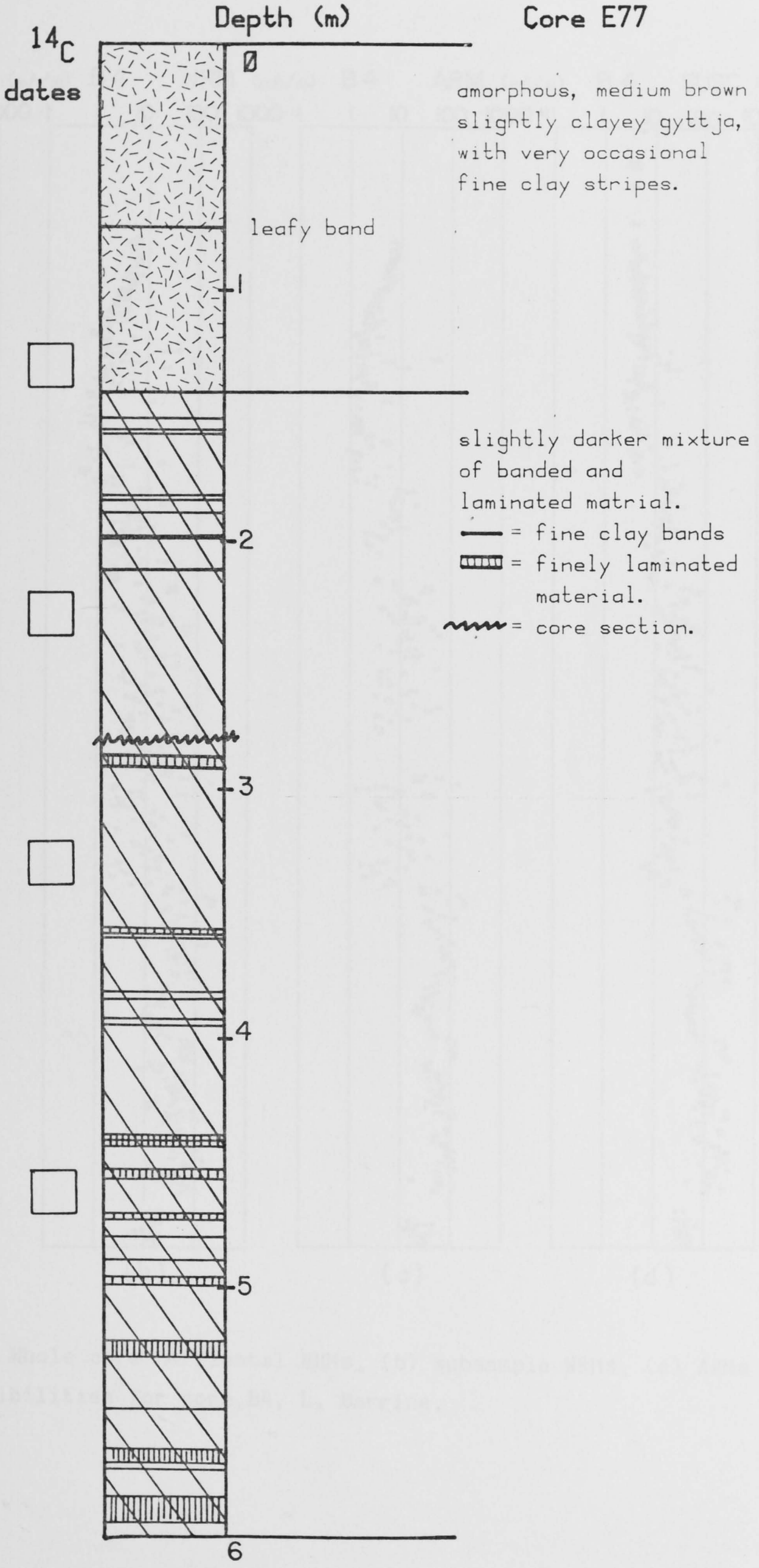

Figure 3.6 Log of core E77.

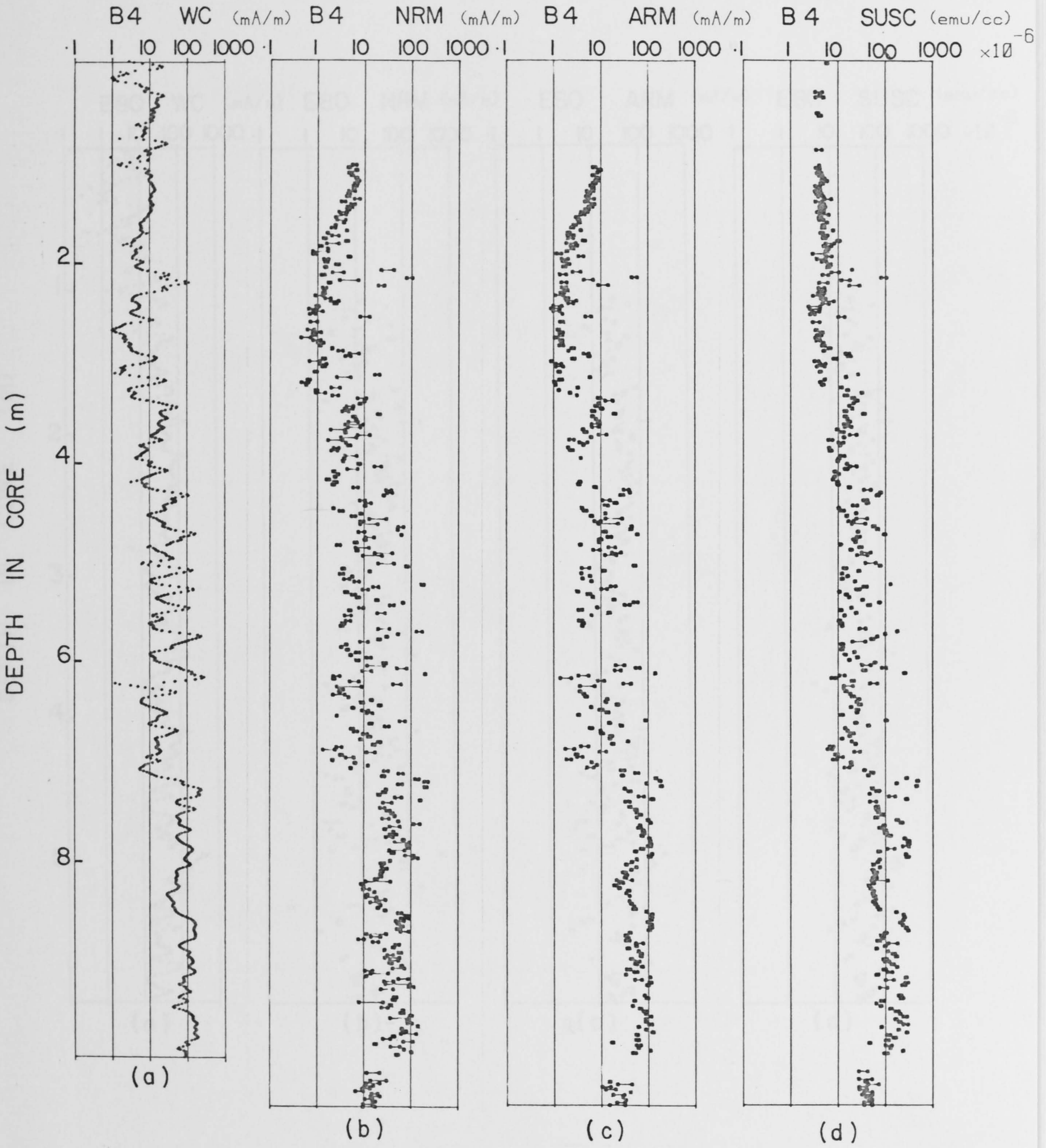

Figure 3.7 (a) Whole core horizontal NRMs, (b) subsample NRMs, (c) ARMs and (d) susceptibilities for core B4, L. Barrine.

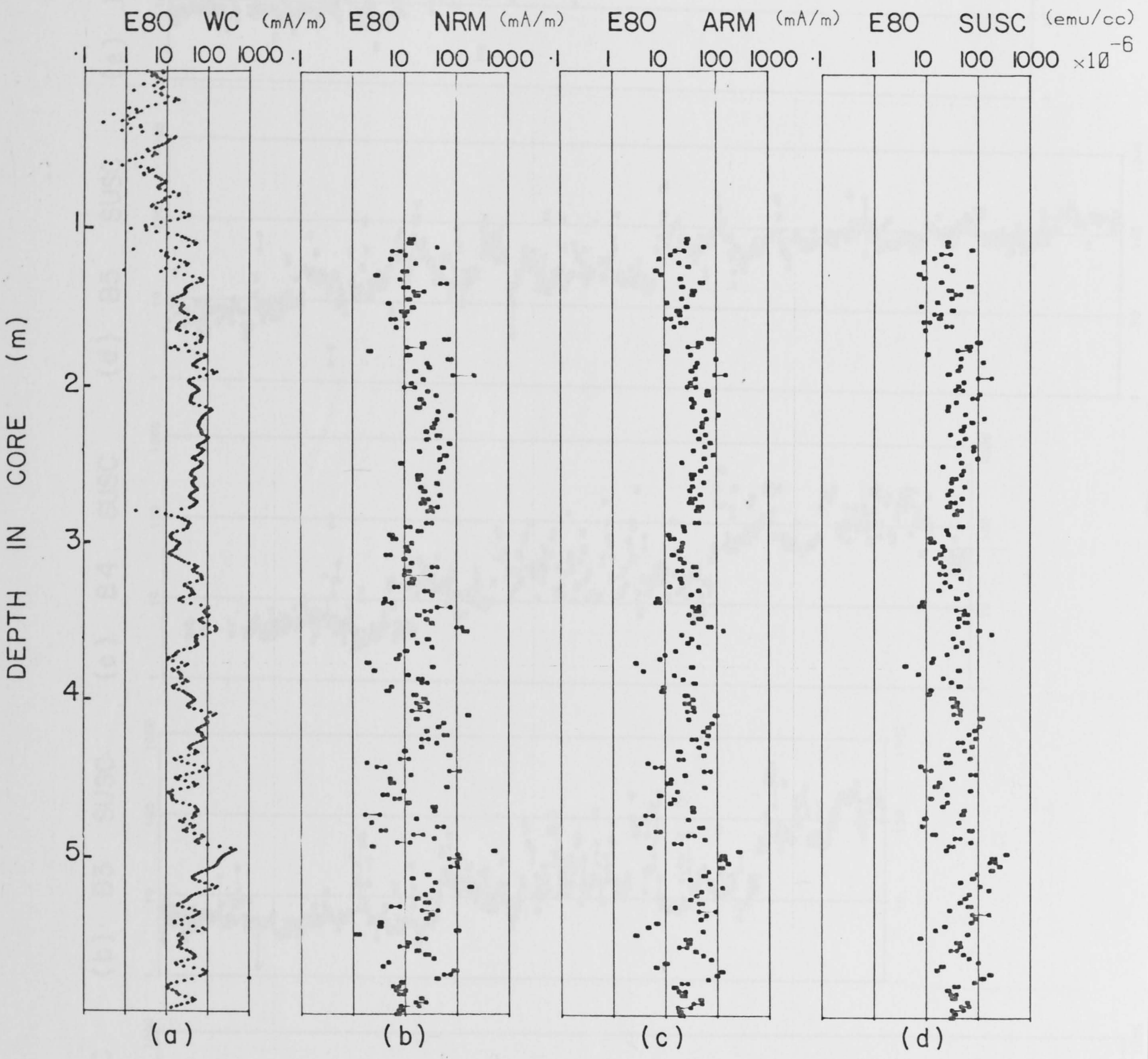

Figure 3.8 (a) Whole core horizontal NRMs, (b) subsample NRMs, (c) ARMs and (d) susceptibilities for core E80, L. Eacham.

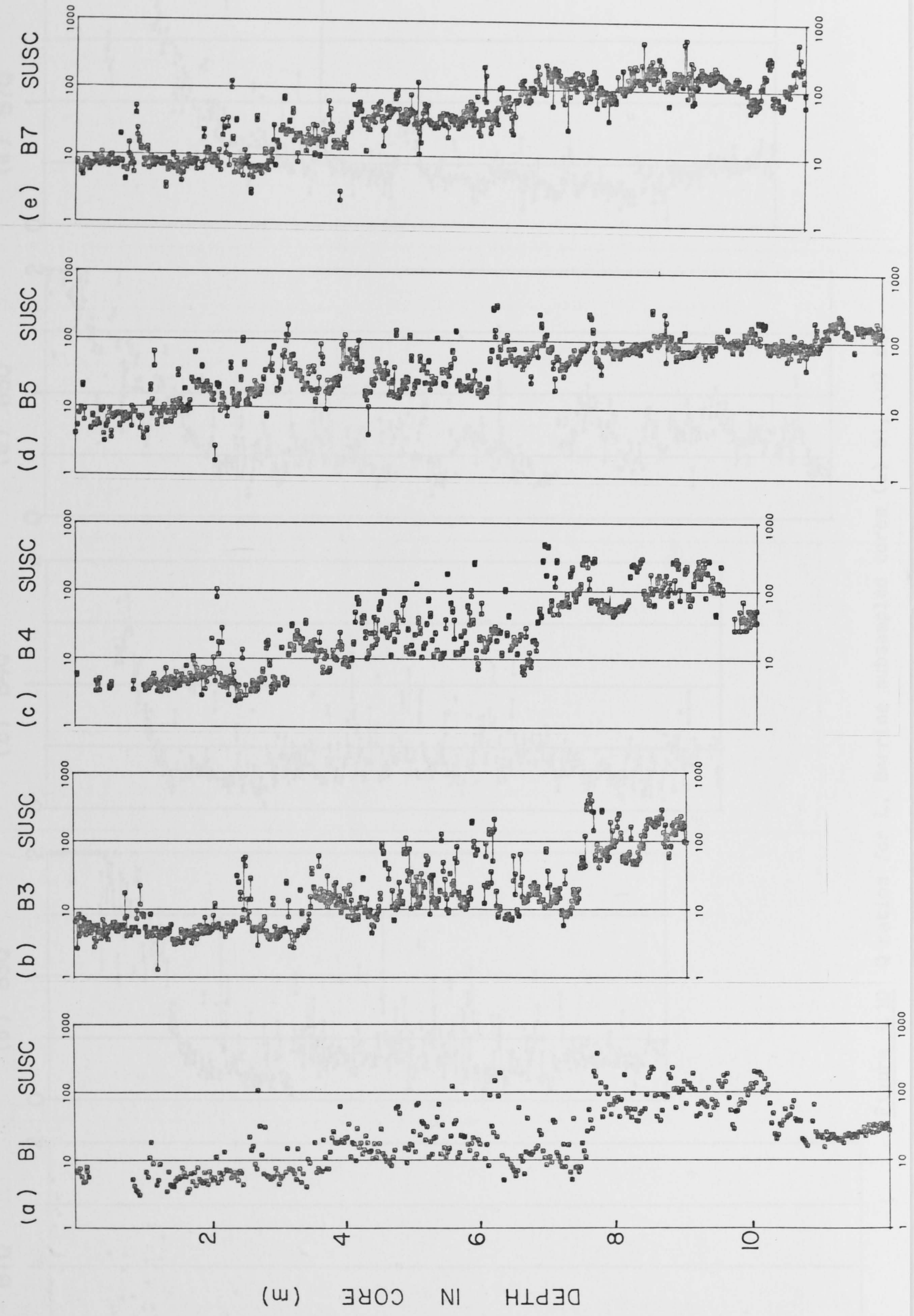

Figure 3.9 Individual specimen susceptibilities for cores (a) B1, (b) B3, (c) B4, (d) B5 and (e) B7 from L. Barrine. Units are emu/cc x 10^{-6}.

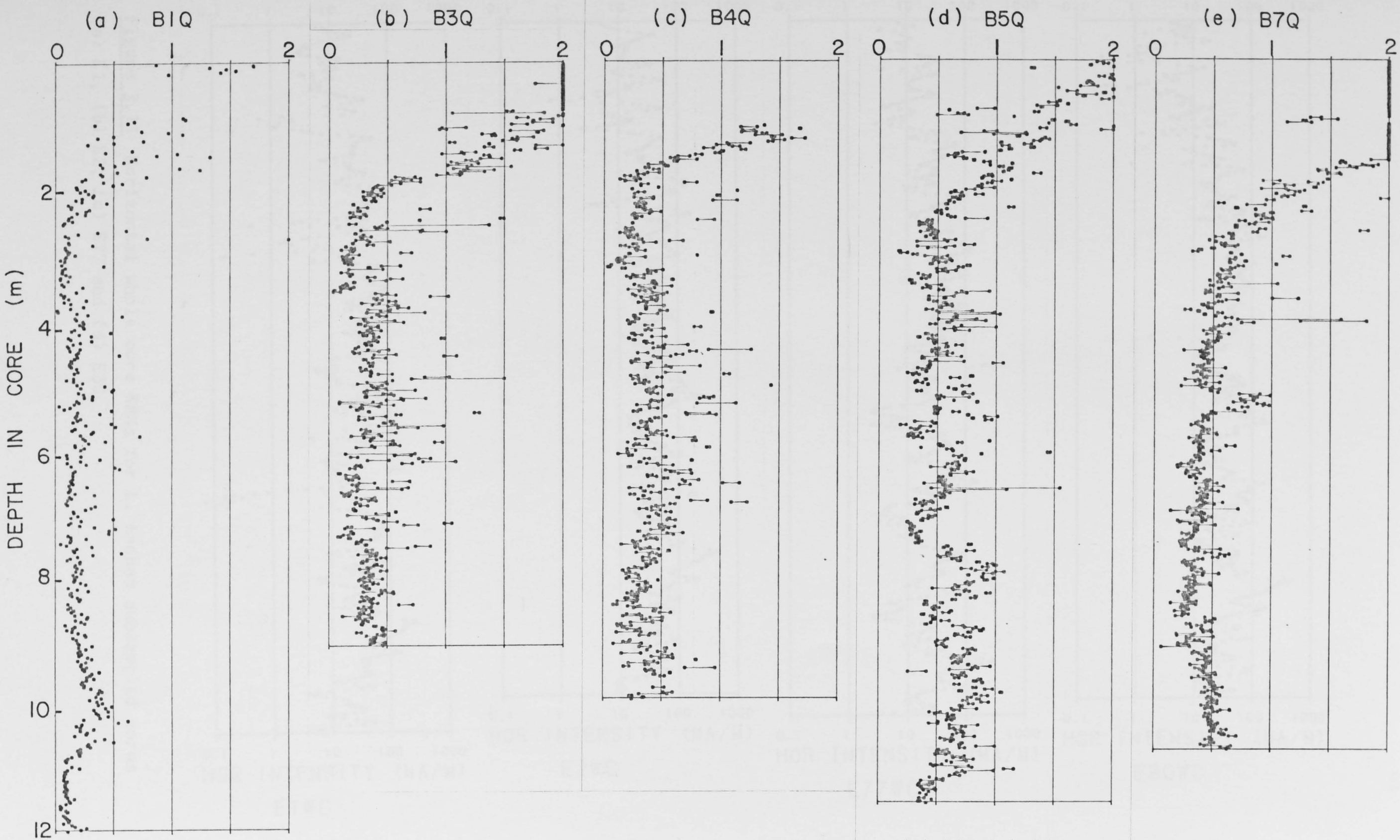

Figure 3.10 Q ratios for L. Barrine subsampled cores (a) B1, (b) B3,

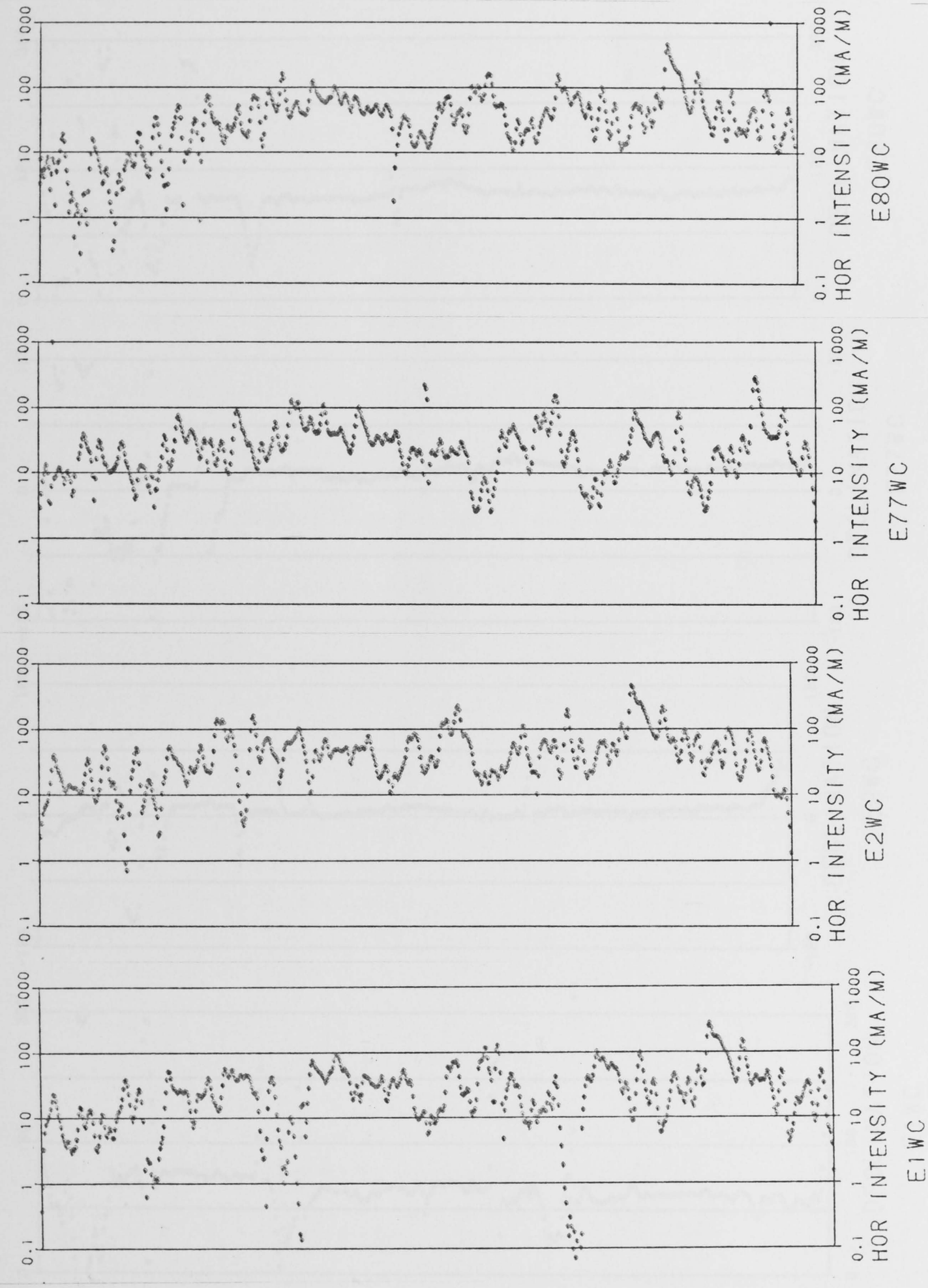

Figure 3.11 Horizontal whole core NRMs for L. Eacham subsampled cores (a) E1, (b) E2, (c) E77 and (d) E80.

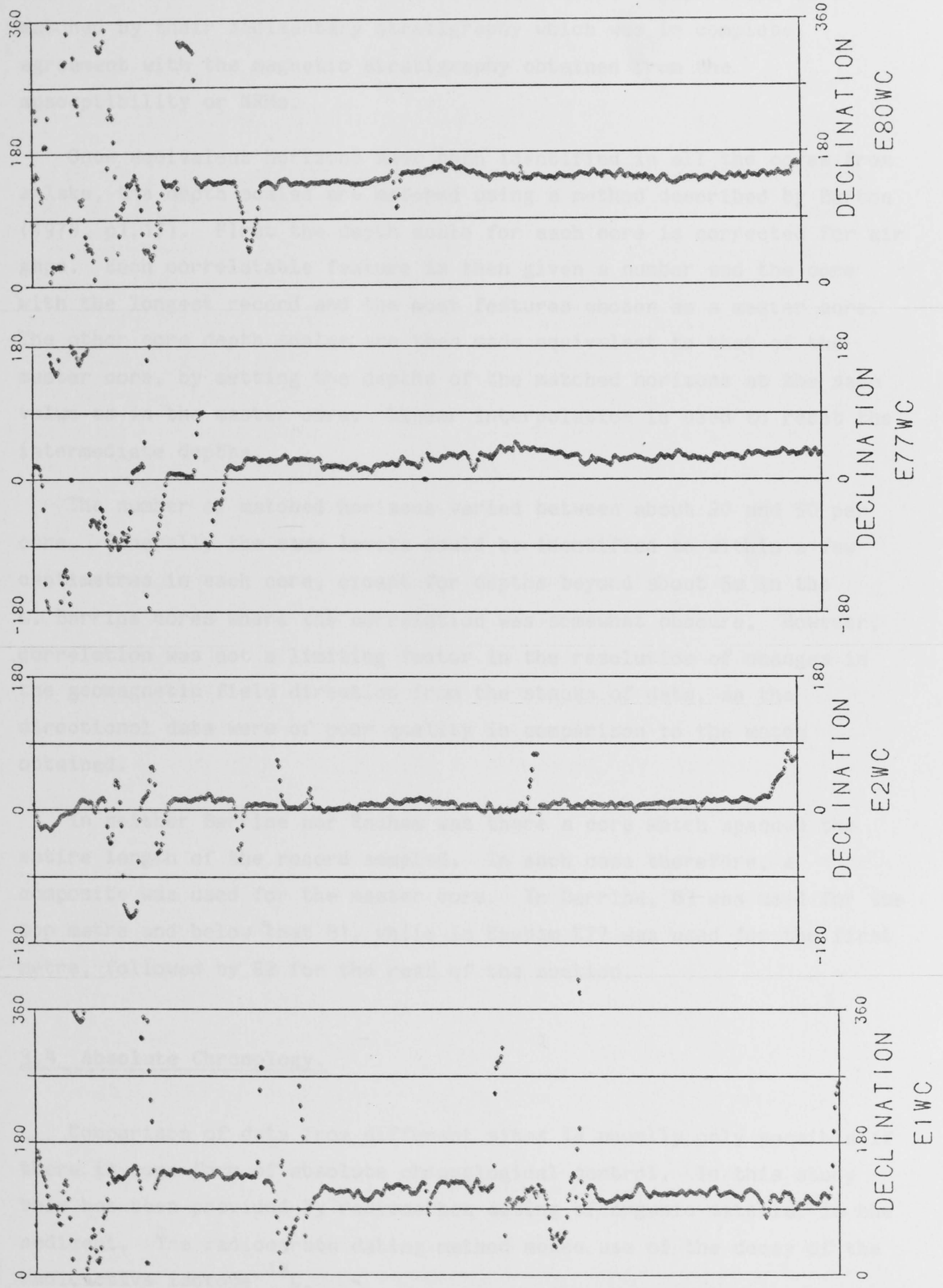

Figure 3.12 Whole core declinations for L. Eacham subsampled cores.

shows an excellent correlation between the cores. These cores were matched by their sedimentary stratigraphy which was in complete agreement with the magnetic stratigraphy obtained from the susceptibility or NRMs.

Once equivalent horizons have been identified in all the cores from a lake, the depth scales are matched using a method described by Barton (1978, p1.17). First the depth scale for each core is corrected for air gaps. Each correlatable feature is then given a number and the core with the longest record and the most features chosen as a master core. The other core depth scales are then made equivalent to that of the master core, by setting the depths of the matched horizons at the same value as in the master core. Linear interpolation is used to reset the intermediate depths.

The number of matched horizons varied between about 20 and 50 per core. Generally the same levels could be identified to within a few centimetres in each core, except for depths beyond about 8m in the L. Barrine cores where the correlation was somewhat obscure. However, correlation was not a limiting factor in the resolution of changes in the geomagnetic field direction from the stacks of data, as the directional data were of poor quality in comparison to the match obtained.

In neither Barrine nor Eacham was there a core which spanned the entire length of the record sampled. In each case therefore, a composite was used for the master core. In Barrine, B3 was used for the top metre and below that B1, while in Eacham E77 was used for the first metre, followed by E2 for the rest of the section.

3.4 Absolute Chronology.

Comparison of data from different sites is usually only possible if there is some form of absolute chronological control. In this study this has been provided by radiocarbon dating of organic material in the sediment. The radiocarbon dating method makes use of the decay of the radioactive isotope ^{14}C,

$$^{14}C \longrightarrow {}^{14}N + \beta^-$$

which has a half life ($t_{1/2}$) of 5730 years. Living materials absorb and incorporate atmospheric CO_2 along with its trace level of radiogenic ^{14}C. Measurement of the residual ^{14}C concentration of old organic material thus allows an estimate to be made of the age of the material.

Traditionally the amount of radiogenic carbon present in a sample has been determined indirectly by using a scintillation counter to detect the number of β^- particles emitted over a given time period. As noted by Oeschger et al. (1970), there are significant advantages in using a method which counts the ^{14}C directly using an ultra-sensitive mass spectrometric technique rather than the above radiometric method. The isotopic ratio $^{14}C/^{12}C$ in a contemporary sample is 1.2×10^{-12} implying a concentration of 6×10^{7} ^{14}C atoms per milligram of carbon. The fractional disintegration of ^{14}C is 1.4×10^{-8}/hour so that for routine indirect measurements of age several grams of C are required. A direct method of counting ^{14}C with even a collection efficiency of 10^{-3} will clearly require orders of magnitude smaller sample sizes than the radiometric technique. As a consequence much finer scale chronologies will be accessible for materials such as lake sediments, as well as the potential to date further back in time than with the conventional technique. Polach and Chappell (1979) have outlined the fundamentals of accelerator dating and its potential advantages over the radiometric technique.

The bulk of the ^{14}C dating described here was carried out by members of the Australian National University (A.N.U.) Radiocarbon Dating Laboratory using the conventional indirect counting technique. A 15-20cm section of core material generally provided sufficient organic carbon to obtain a date. The samples were pretreated with an acid wash to remove inorganic carbonate.

Three dates of much smaller sample size were obtained on material from a frozen finger type core (Rymer and Neale, 1979), which is designed to sample the water-sediment interface of lake deposits with a minimum of disturbance. The sample preparation for this material was carried out at the A.N.U. laboratory and the actual dating performed by Dr W. Wölfli on the tandem accelerator dating facility at the Eidgenössische Technische Hochschule (E.T.H.) in Zürich. The development of this dating facility is described by Suter et al. (1981a,

1981b) and Wölfli et al. (1982).

3.4.1 Calibration.

Conventional radiocarbon dates are calculated using $t_{1/2}$ = 5568 years as opposed to the presently accepted value of 5730 years. This, and the fact that the concentration of ^{14}C in the atmosphere (and hence the initial activity of the samples) has fluctuated in the past, means that conventional dates must be calibrated in order to correspond to calendar years.

A number of calibration curves have been proposed (e.g. Suess, 1970; Ralph et al., 1973; Damon et al., 1972; Switsur, 1973; Clark, 1975) based on the comparison of radiocarbon and dendrochronological ages. These mostly differ in the degree of smoothing applied to the original data and the assignment of accuracies to the calibrated dates. Too little smoothing will result in lots of kinks and wiggles which are not justified by the accuracy of the basic data, whereas too much can hide genuine kinks of archaeological or geophysical importance.

Clark's (1975) curve has been used here. The procedure used to derive this curve is based on convolution smoothing (Clark, 1977) with a cross validation technique used to determine the optimal degree of smoothness. Clark's curve is intermediate in its degree of smoothness and has the advantage of providing 95% confidence limits for the calibrated dates. Differences between the other calibration curves mentioned and Clark's are generally small except in the assignment of accuracies to the calibrated dates. Some of the other curves grossly overestimate the accuracy of the results.

There is no calibration available for radiocarbon ages older than 6 500 years, so in order to avoid a discontinuity in the time scale the technique described by McElhinny and Senanayake (1982) has been used. It has been assumed that radiocarbon and calendar ages are equivalent again at 10 000 years before present and linear interpolation of age used to calibrate ages lying in the 6 500 to 10 000 year interval.

Radiocarbon ages are written as years b.p. (before present) and calibrated radiocarbon or calendar ages are written as years B.P. Present day is taken as 1950 A.D. Both calibrated and uncalibrated results are given so that comparisons may be made with other published work on either scale.

3.4.2 Lake Eacham Results.

A total of 11 samples from the L. Eacham cores were dated. These are listed in Table 3.2 along with their calibrated values. To facilitate obtaining a time scale for the secular variation records these were transposed to equivalent depths in the master core using the matching procedure described above. The uncalibrated dates are plotted in Figure 3.13(a) where the bars show 1 standard error as determined from the counting statistics, and the calibrated dates are in Figure 3.13(b) where the bars represent the 95% confidence intervals given by Clark's calibration method.

A least squares linear regression was then used to calculate a best fitting straight line to each of the above sets of dates as a function of depth in core. Although there are errors associated with the individual age data these have not been used to weight the fit. These errors only indicate the uncertainty associated with determining firstly, the age of the carbon in the sediment, and secondly, the fit to the calibration curve, and not the uncertainty in the age of sediment formation. Additional error will be introduced as a result of the sedimentary process e.g.

(1) an unknown time will elapse between the death of the organic matter containing the carbon and its incorporation into the lake sediment, and

(2) any reworking of the sedimentary material which occurs will result in a mixing of carbon of varying age. Thus there is no reason to believe any one date is more accurate than any other.

Table 3.2 Lake Eacham Radiocarbon Dates

Depth in Master Core (cm)	Core	Age ±1 std error	Calibrated Age ±95% confidence limit
41.5-61.5	E1	320±100	270±270
99.5-117.1	E77	1230±70	1180±170
106.0-127.6	E80	1540±90	1500±200
109.0-126.8	E2	1470±100	1440±220
199.5-214.9	E77	1690±150	1640±310
279.3-302.5	E77	2720±80	2940±250
371.9-393.7	E2	3020±80	3260±280
411.8-420.6	E77	3660±80	4070±310
563.0-584.0	E1	4996±80	5780±230
578.5-598.5	E2	4480±100	5200±290
578.6-601.4	E80	4640±80	5400±250

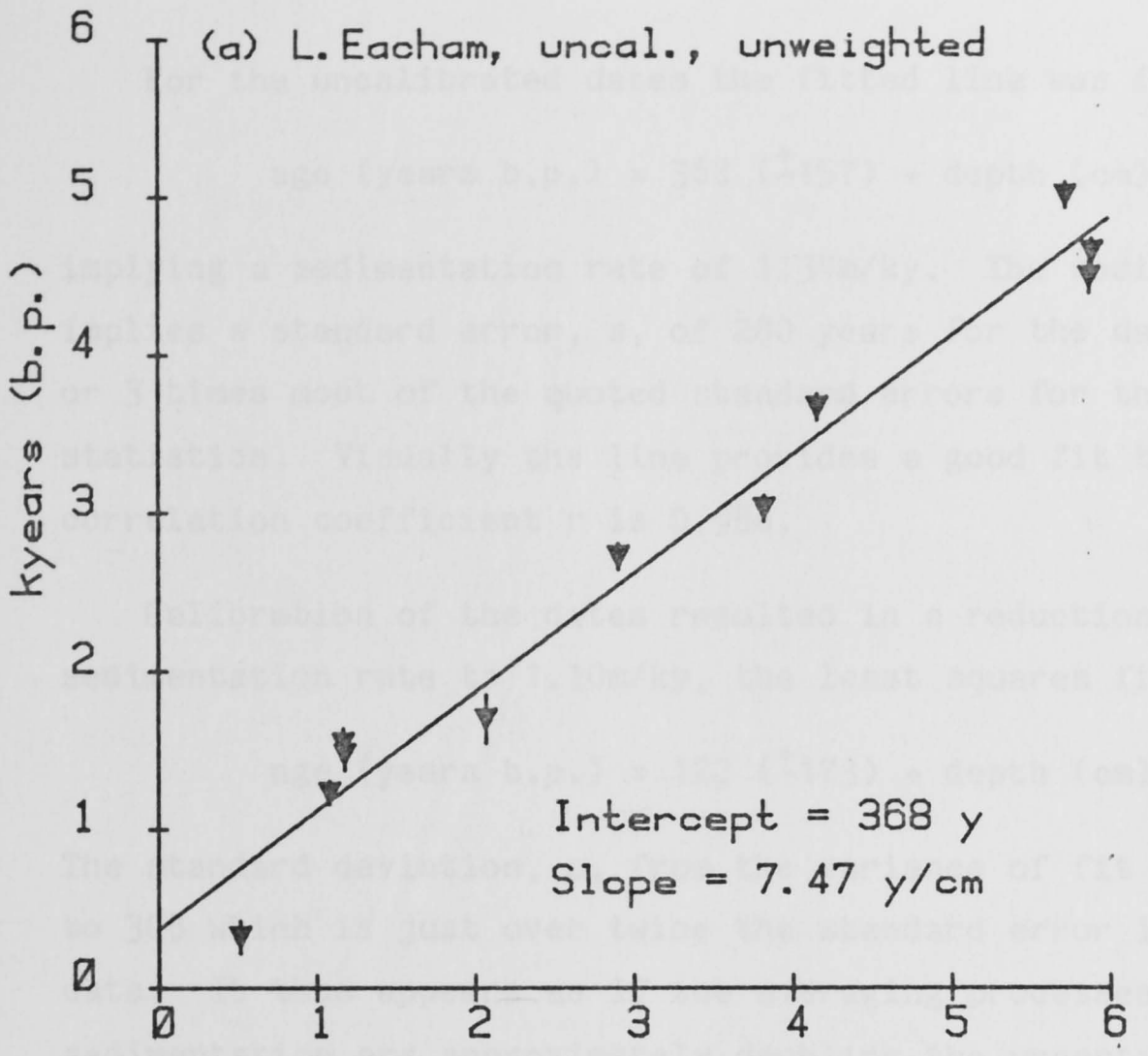

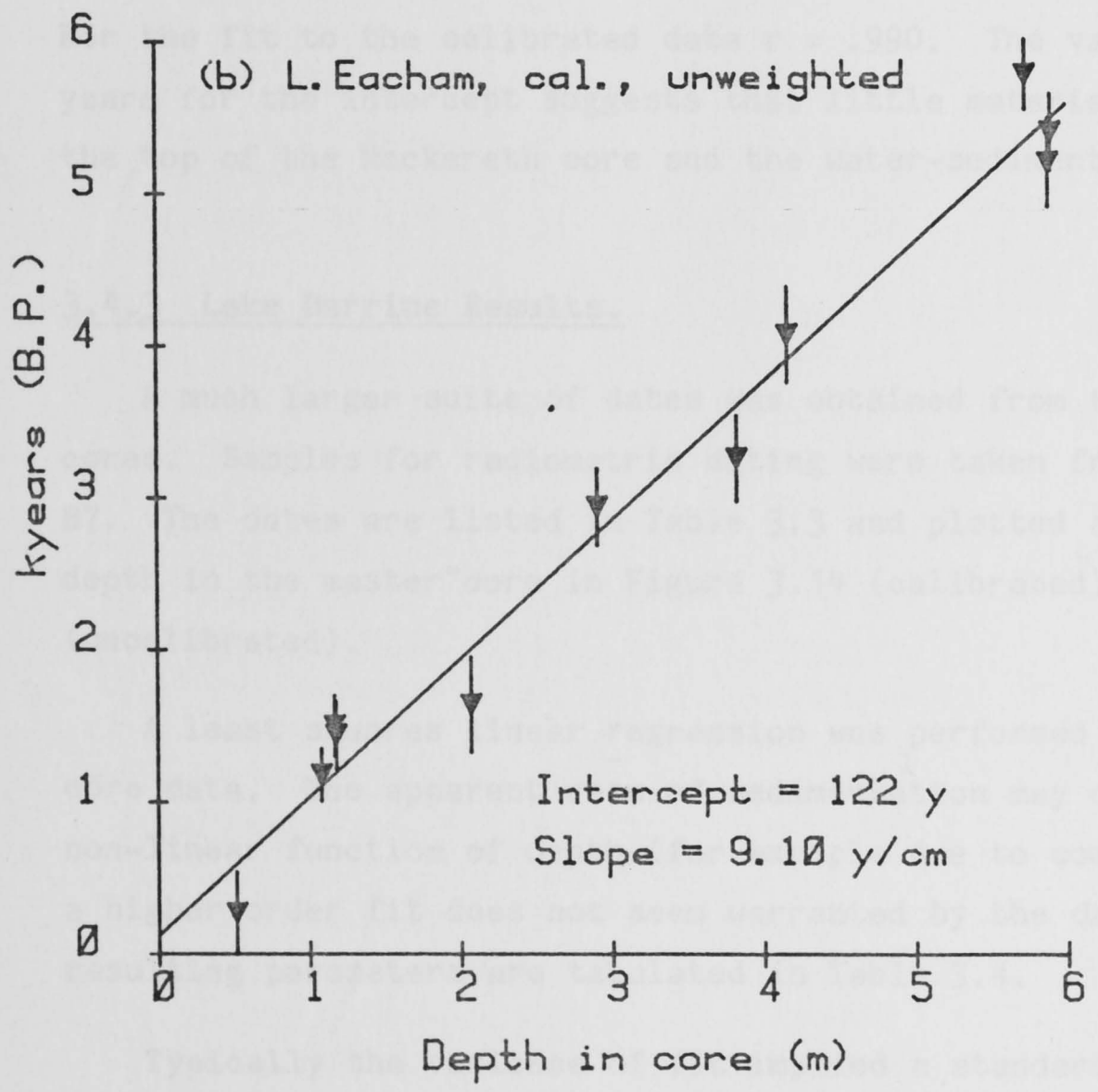

Figure 3.13 (a) Uncalibrated L. Eacham radiocarbon dates transposed to equivalent depths in the master core. (b) Calibrated L. Eacham radiocarbon dates transposed to equivalent depths in the master core.

For the uncalibrated dates the fitted line was found to be

$$\text{age (years b.p.)} = 368\ (\pm 157) + \text{depth (cm)} \times 7.47\ (\pm .425)$$

implying a sedimentation rate of 1.34m/ky. The residual variance implies a standard error, s, of 280 years for the data, which is about 2 or 3 times most of the quoted standard errors for the counting statistics. Visually the line provides a good fit to the data and the correlation coefficient r is 0.986.

Calibration of the dates resulted in a reduction of the apparent sedimentation rate to 1.10m/ky, the least squares fit being

$$\text{age (years b.p.)} = 122\ (\pm 173) + \text{depth (cm)} \times 9.10\ (\pm .467).$$

The standard deviation, s, from the variance of fit increased slightly to 308 which is just over twice the standard error in the calibrated data. It thus appears as if the averaging processes occuring during sedimentation are approximately doubling the uncertainty in the age. For the fit to the calibrated data r = .990. The value of 122 $\pm$ 173 years for the intercept suggests that little material is missing between the top of the Mackereth core and the water-sediment interface.

3.4.3 Lake Barrine Results.

A much larger suite of dates was obtained from the L. Barrine cores. Samples for radiometric dating were taken from cores B3, B4, B5, B7. The dates are listed in Table 3.3 and plotted as a function of depth in the master core in Figure 3.14 (calibrated) and Figure 3.15 (uncalibrated).

A least squares linear regression was performed on the individual core data. The apparent rate of sedimentation may conceivably be a non-linear function of depth (for example due to compaction effects) but a higher order fit does not seem warranted by the data quality. The resulting parameters are tabulated in Table 3.4.

Typically the variance of fit implied a standard error, s, 5 to 10 times the average radiocarbon standard errors for each core. A large contribution to this must be the high scatter in data deep in the core. Mixing of carbon of different ages appears to have taken place here, and the apparent age of the sediment does not increase monotonically with

Table 3.3 Lake Barrine Radiocarbon Dates

Depth in Master Core (cm)	Core	Age ±1 std error	Calibrated Age ±95% confidence limit
16.0-36.0	B3	2220±100	2240±290
190.8-210.7	B3	3380±160	3730±410
609.5-627.3	B3	9090±110	9310±250
652.5-660.8	B3	14250±170	
660.8-675.5	B3	9540±110	9650±250
689.3-725.5	B3	10740±130	
810.0-828.8	B3	16650±500	
937.0-957.0	B3	13920±530	
145.9-165.9	B4	3070±100	3320±290
219.7-239.2	B4	4060±100	4630±340
299.9-321.2	B4	6640±150	7470±320
342.0-362.0	B4	5050±90	5840±230
427.0-447.0	B4	6020±100	6840±280
461.5-482.9	B4	7250±120	7930±270
596.8-610.8	B4	8640±110	8980±250
610.8-645.2	B4	9380±120	9530±270
657.5-682.5	B4	10250±130	
698.3-726.1	B4	10160±120	
838.8-860.2	B4	13050±470	
995.5-1015.5	B4	13650±200	
90.5-100.5	B5	3770±150	4240±460
154.5-163.3	B5	4900±135	5680±300
209.0-220.8	B5	5840±90	6690±250
227.2-240.9	B5	6250±100	7120±230
341.9-360.2	B5	7200±110	7890±250
483.3-504.5	B5	7520±110	8130±250
547.5-567.3	B5	8790±140	9090±300
583.1-598.0	B5	12750±300	
710.7-727.2	B5	10640±270	
768.0-811.8	B5	12040±330	
995.0-1015.0	B5	13320±240	
1083.1-1101.0	B5	11420±490	
85.5-100.8	B7	2620±140	2770±380
117.0-128.5	B7	2670±150	2830±420
234.1-243.3	B7	3810±130	4290±410
254.6-265.9	B7	3380±270	3730±710
338.9-361.4	B7	4600±130	5330±340
427.0-437.8	B7	5840±120	6700±290
579.4-589.5	B7	9630±140	9720±300
636.5-662.8	B7	12440±180	
662.8-690.3	B7	11400±170	
787.7-807.0	B7	12260±320	
985.2-1006.4	B7	11390±260	

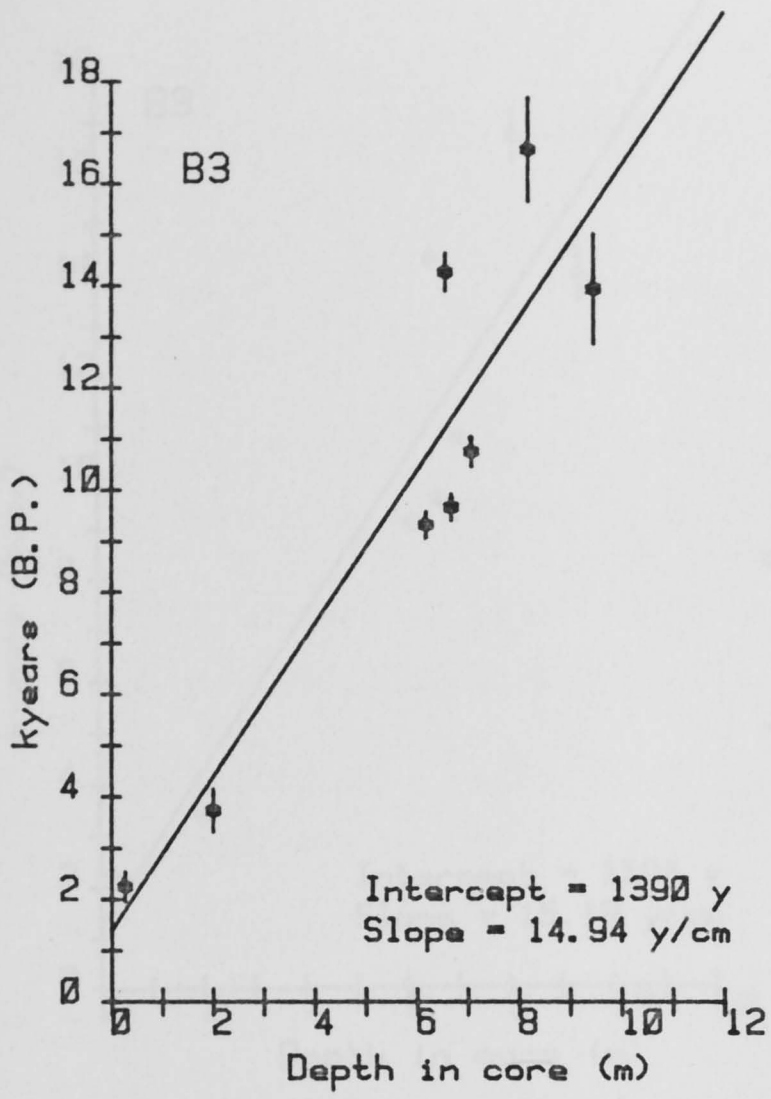

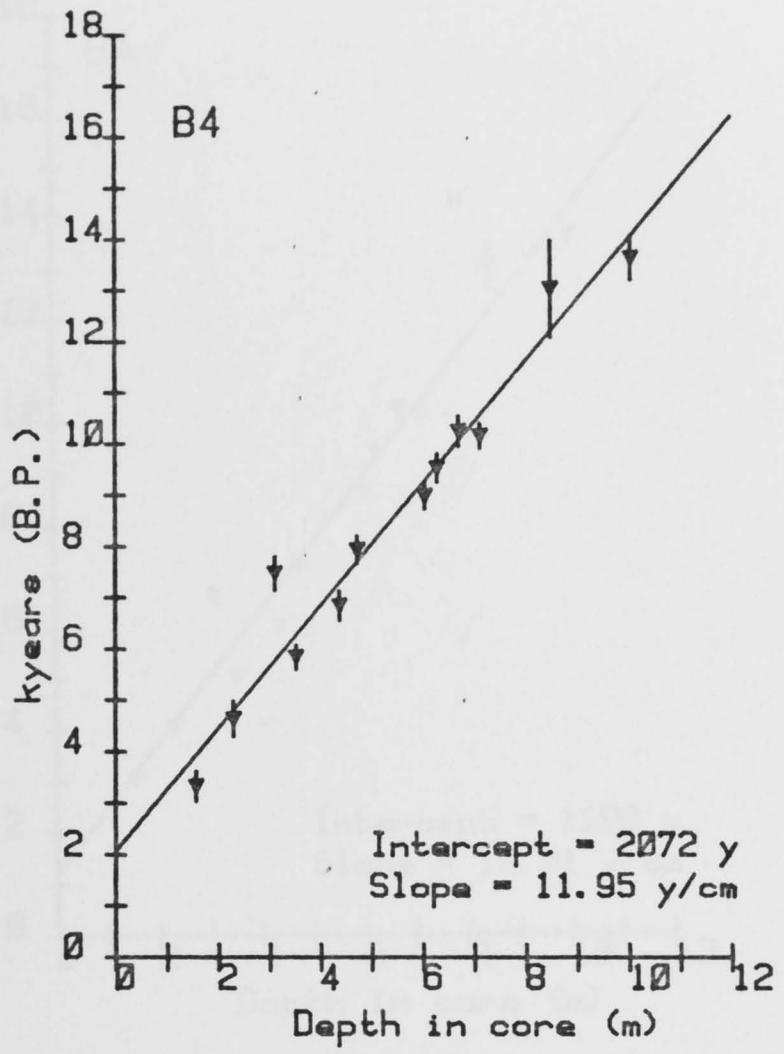

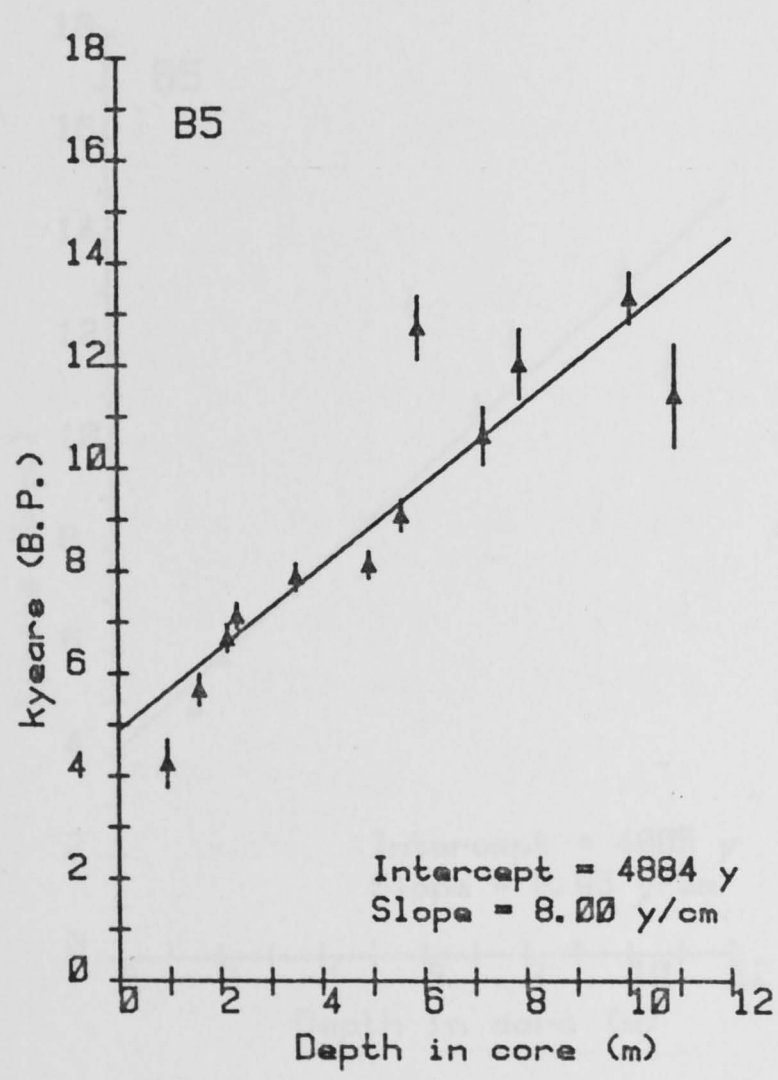

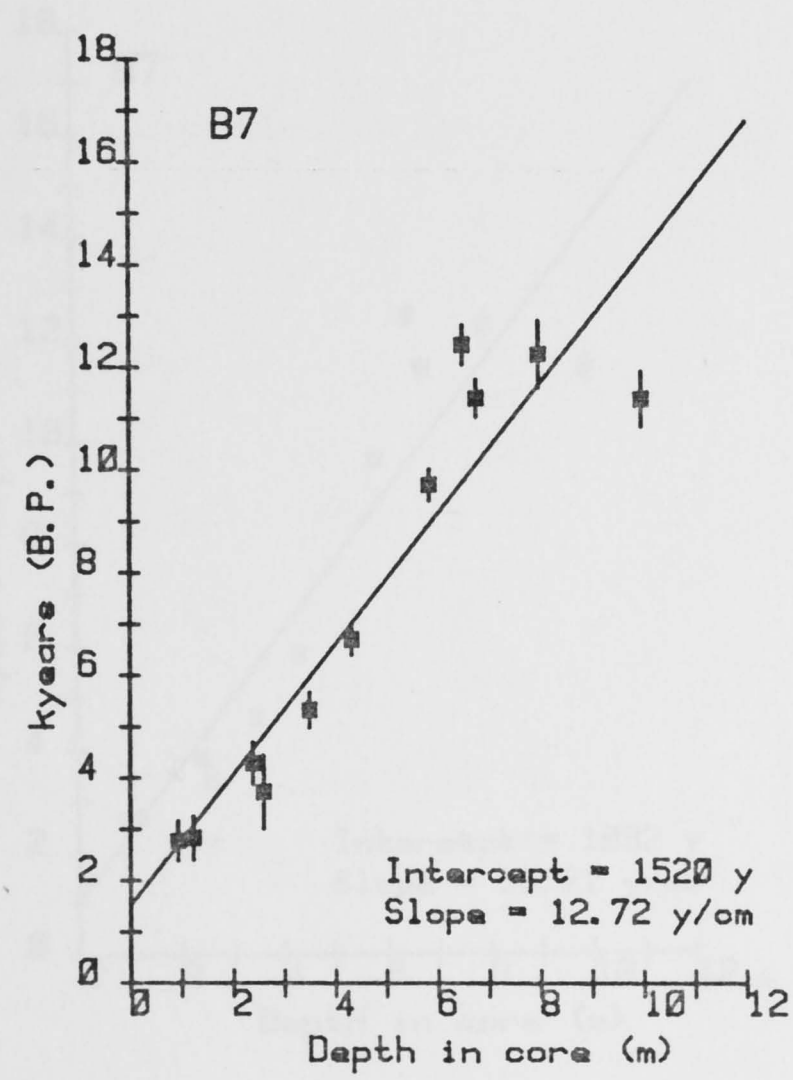

Figure 3.14 Calibrated radiocarbon dates as a function of depth in master core for L. Barrine cores B3, B4, B5 and B7. Vertical bars indicate 95% confidence limits on the ages obtained from Clark's (1975) calibration scheme. The linear regressions are unweighted.

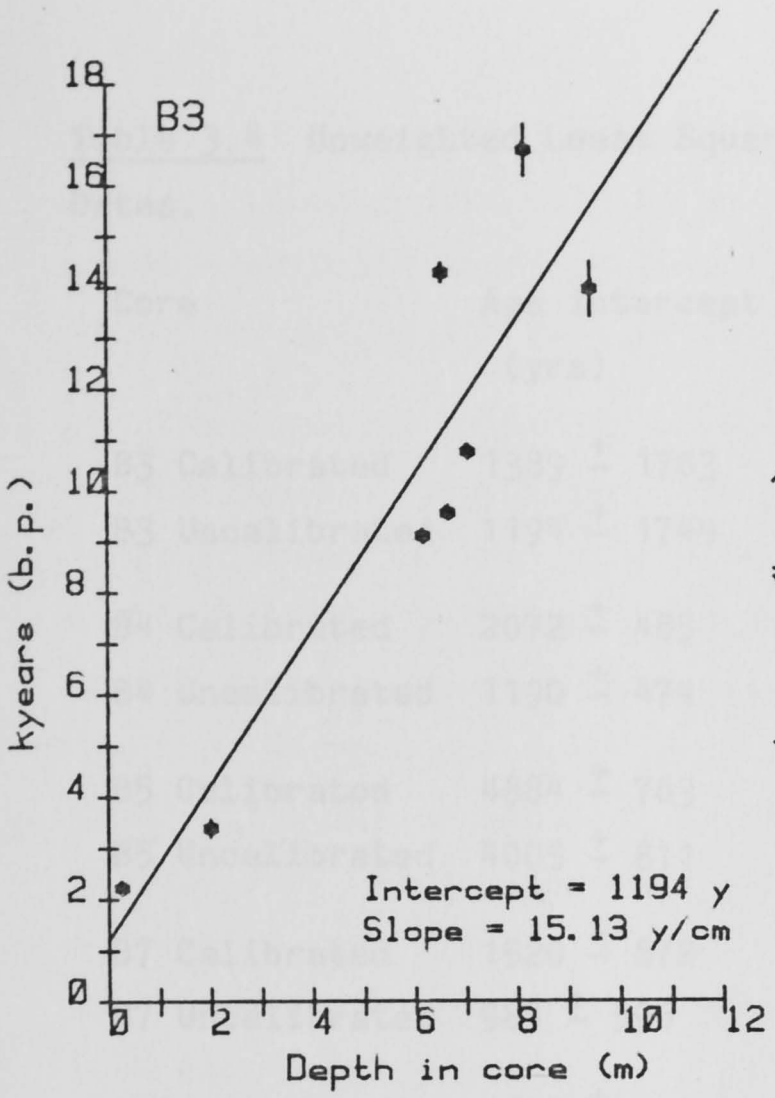

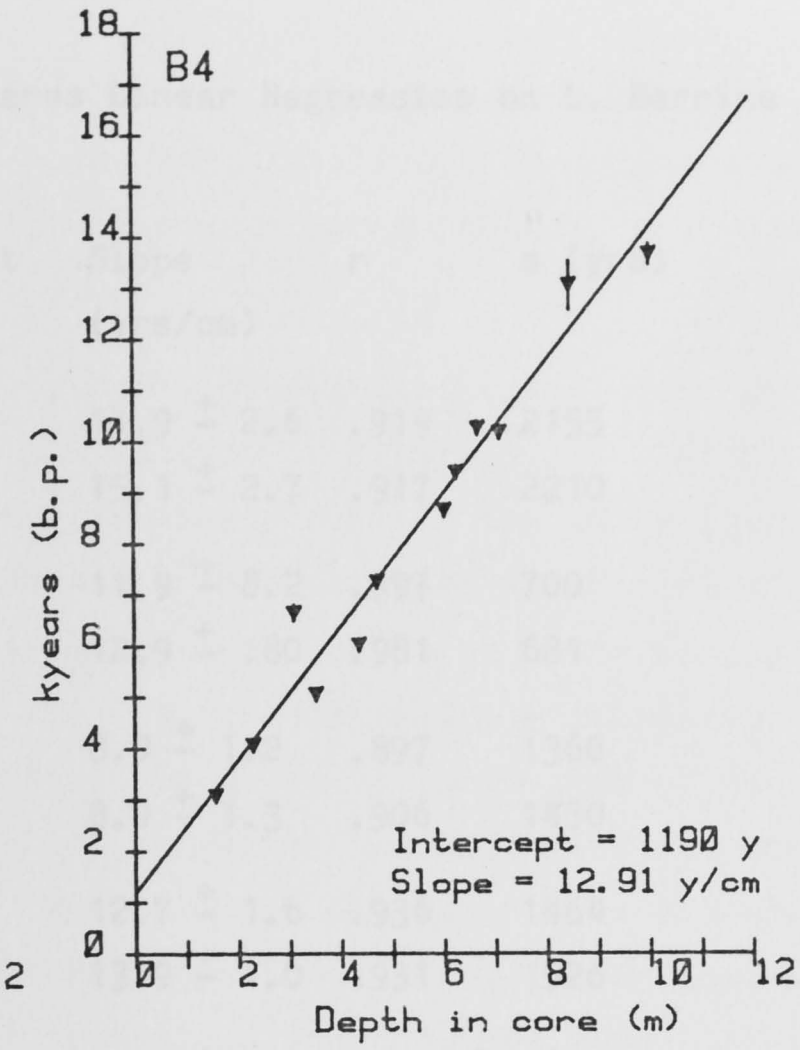

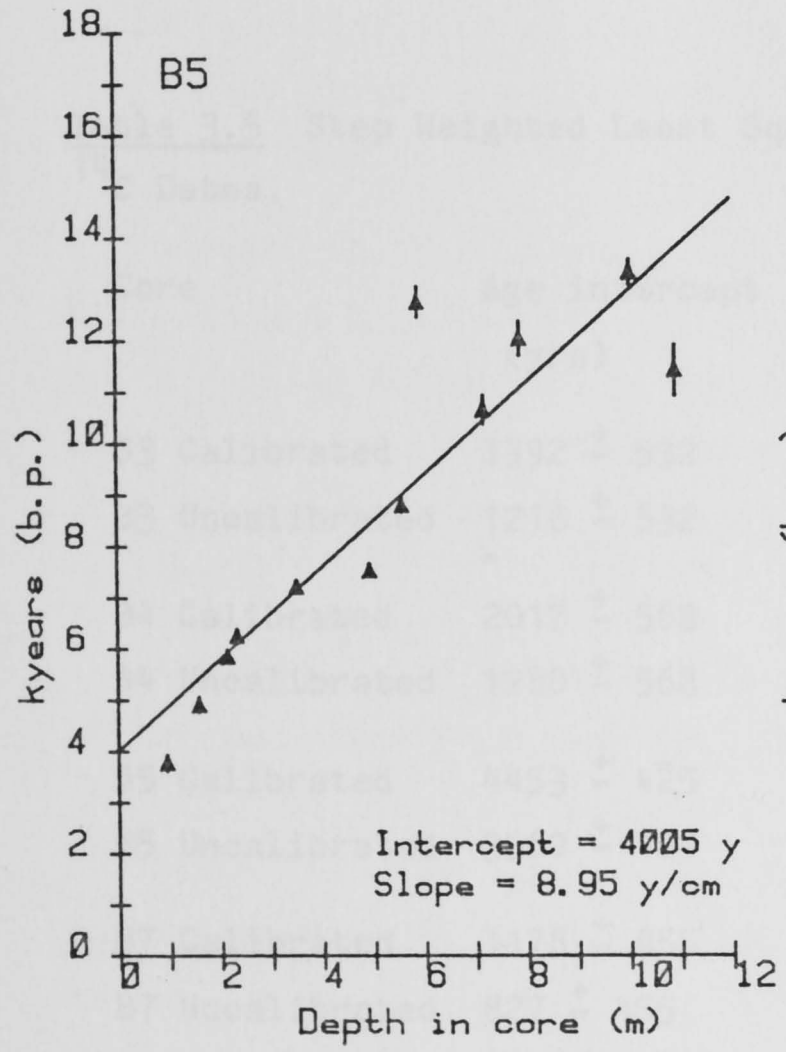

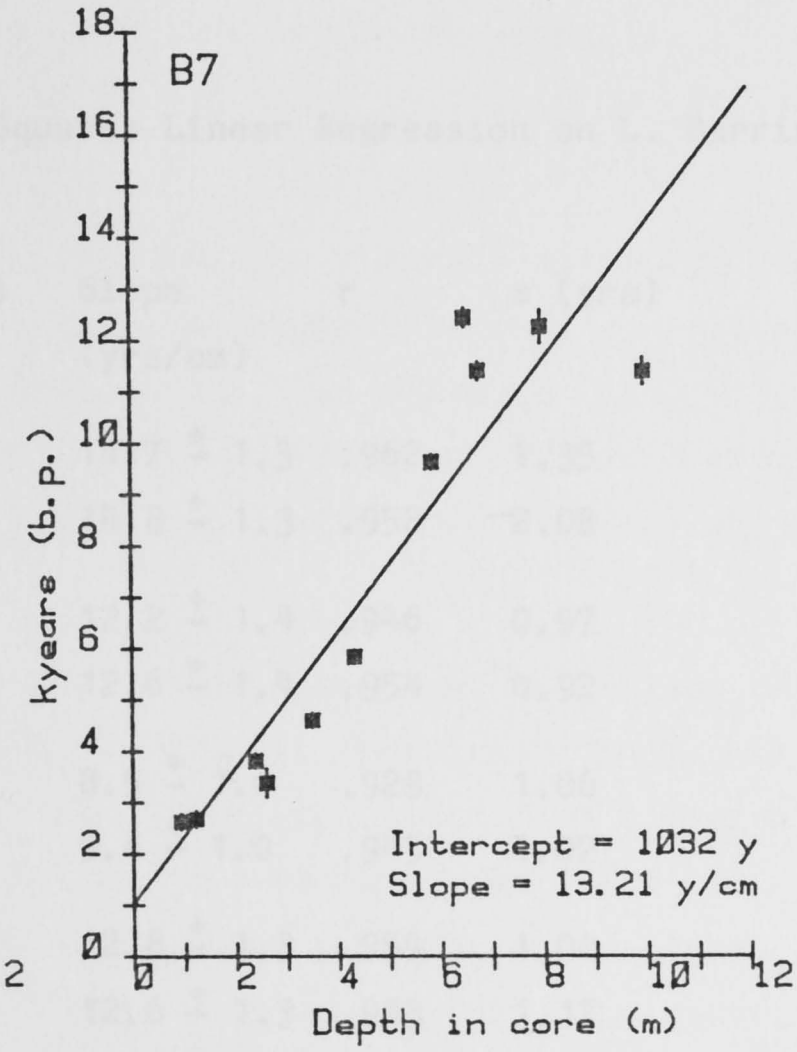

Figure 3.15 Uncalibrated radiocarbon dates for L. Barrine cores B3, B4, B5 and B7. Vertical bars indicate 1 standard error in the ^{14}C age. Linear regressions are unweighted.

Table 3.4 Unweighted Least Squares Linear Regression on L. Barrine ^{14}C Dates.

Core	Age intercept (yrs)	Slope (yrs/cm)	r	s (yrs)
B3 Calibrated	1389 ± 1703	14.9 ± 2.6	.919	2155
B3 Uncalibrated	1194 ± 1749	15.1 ± 2.7	.917	2210
B4 Calibrated	2072 ± 485	11.9 ± 8.2	.997	700
B4 Uncalibrated	1190 ± 474	12.9 ± .80	.981	681
B5 Calibrated	4884 ± 763	8.0 ± 1.2	.897	1360
B5 Uncalibrated	4005 ± 811	8.9 ± 1.3	.906	1450
B7 Calibrated	1520 ± 872	12.7 ± 1.6	.936	1464
B7 Uncalibrated	984 ± 596	13.9 ± 1.0	.931	1526
All data Cal.	2648 ± 513	11.5 ± .86	.903	1600
All data Uncal.	1992 ± 522	12.2 ± .87	.909	1634

Table 3.5 Step Weighted Least Squares Linear Regression on L. Barrine ^{14}C Dates.

Core	Age intercept (yrs)	Slope (yrs/cm)	r	s (yrs)
B3 Calibrated	1392 ± 532	14.7 ± 1.3	.962	1.35
B3 Uncalibrated	1218 ± 532	14.8 ± 1.3	.958	2.08
B4 Calibrated	2017 ± 568	12.2 ± 1.4	.946	0.97
B4 Uncalibrated	1280 ± 568	12.6 ± 1.4	.954	0.92
B5 Calibrated	4453 ± 425	8.5 ± 1.0	.928	1.06
B5 Uncalibrated	3560 ± 424	9.4 ± 1.0	.943	1.02
B7 Calibrated	1178 ± 455	12.8 ± 1.3	.959	1.00
B7 Uncalibrated	827 ± 455	12.6 ± 1.3	.943	1.17
All data Cal.	2323 ± 240	11.9 ± 0.6	.905	1.46
All data Uncal.	1751 ± 240	12.1 ± 0.6	.914	1.41
All-B5 Cal.	1359 ± 291	13.4 ± .73	.950	1.11
All-B5 Uncal.	929 ± 291	13.4 ± .73	.943	1.18

depth. In determining a suitable time scale for the sedimentary process it is obviously desirable to use some weighting function in the linear regression which ascribes less importance to the scattered data beyond about 6m than to the more recent data.

The absolute values of the residuals for the individual core fits to the calibrated, unweighted data are plotted in Figure 3.16. There is a large increase in the value of the residuals for all the cores starting at about 5.8m. Although the standard errors assigned in the radiocarbon dating process increase with age, weighting the fit by these errors does not much improve the quality of the fit nor decrease the structure apparent in the residual plot. Based on a visual inspection of the residuals it was decided that a step weighting function with the step at a depth of 5.8m was reasonable. The standard deviation from the mean of the residuals on either side of the step was calculated. For depths less than 5.8m this was s_{lo} = 637 years and greater than 5.8m s_{hi} = 1696 years.

A new least squares regression was then performed using $(s_{lo})^{-2}$ and $(s_{hi})^{-2}$ to weight the fit according to the depth in the core. Table 3.5 lists the results for the new fits.

Because the fit is now a weighted one, the standard deviation of the fit s should be close to 1 if the assigned standard errors s_{lo} and s_{hi} are a good approximation to the true errors. As shown in Table 3.5, this is now the case. The fitted line to all the data with the above step weighting is shown in Figure 3.17 along with the resulting weighted residuals.

A further problem arose with these data concerning the effect on the fit of the dates from core B5. It can be seen from Figure 3.17 that in the upper 6m these are systematically older than dates from comparable depths in the other cores. The fit to core B5 data results in an intercept which is about 2ky older than those from the other cores, and an implied sedimentation rate which is anomalously high. The material from this section in core B5 did show signs of some reworking of the sediment having occured. It is therefore possible that in the part of the lake where B5 came from, there has been mixing of ancient carbon with contemporaneous material at the time of formation of the sediment. If this is the case then the assigned time scale will be distorted by

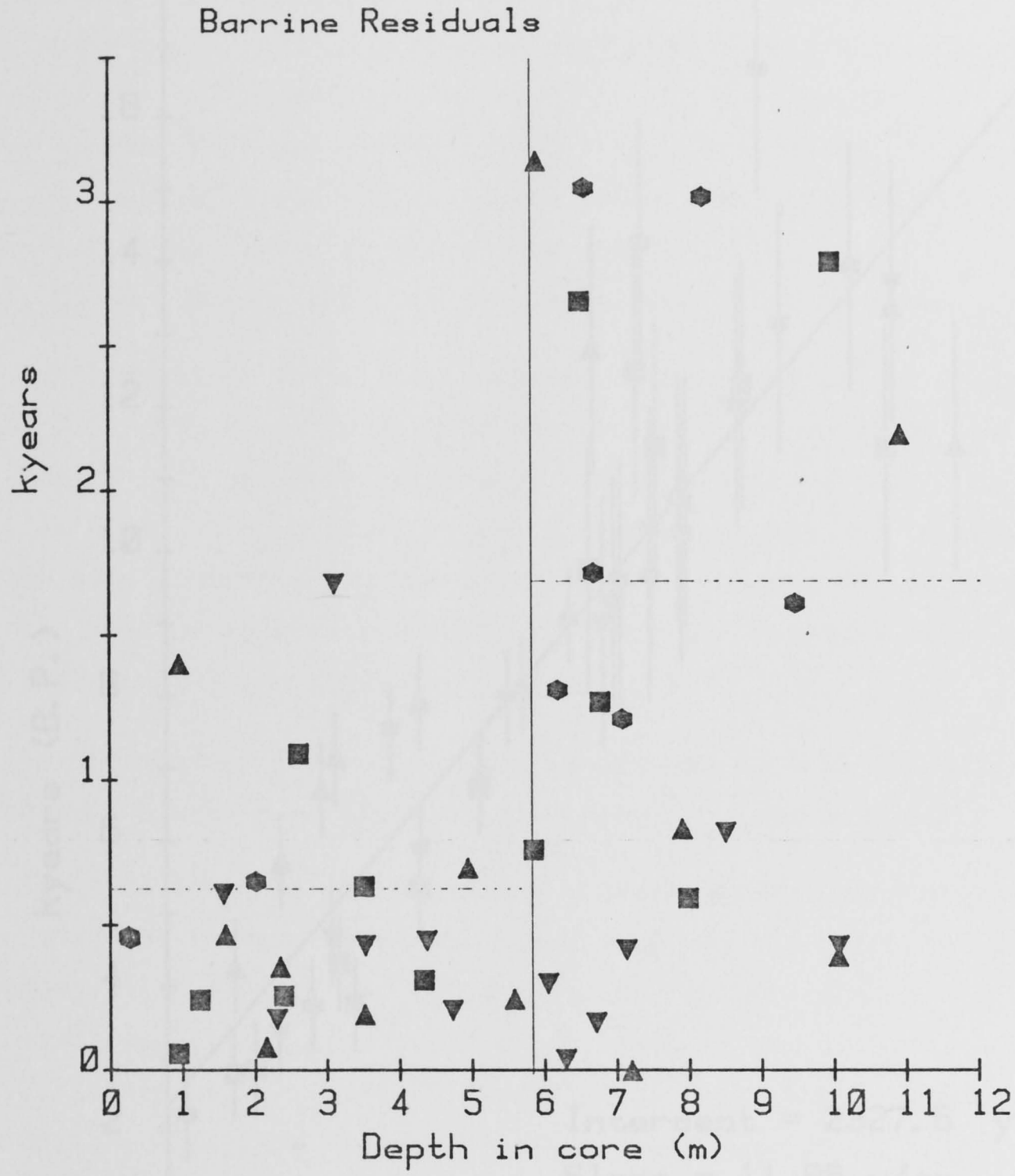

Figure 3.16 Absolute values of the residuals for the unweighted individual core fits to the calibrated data. Coding of symbols is as for Figure 3.15.

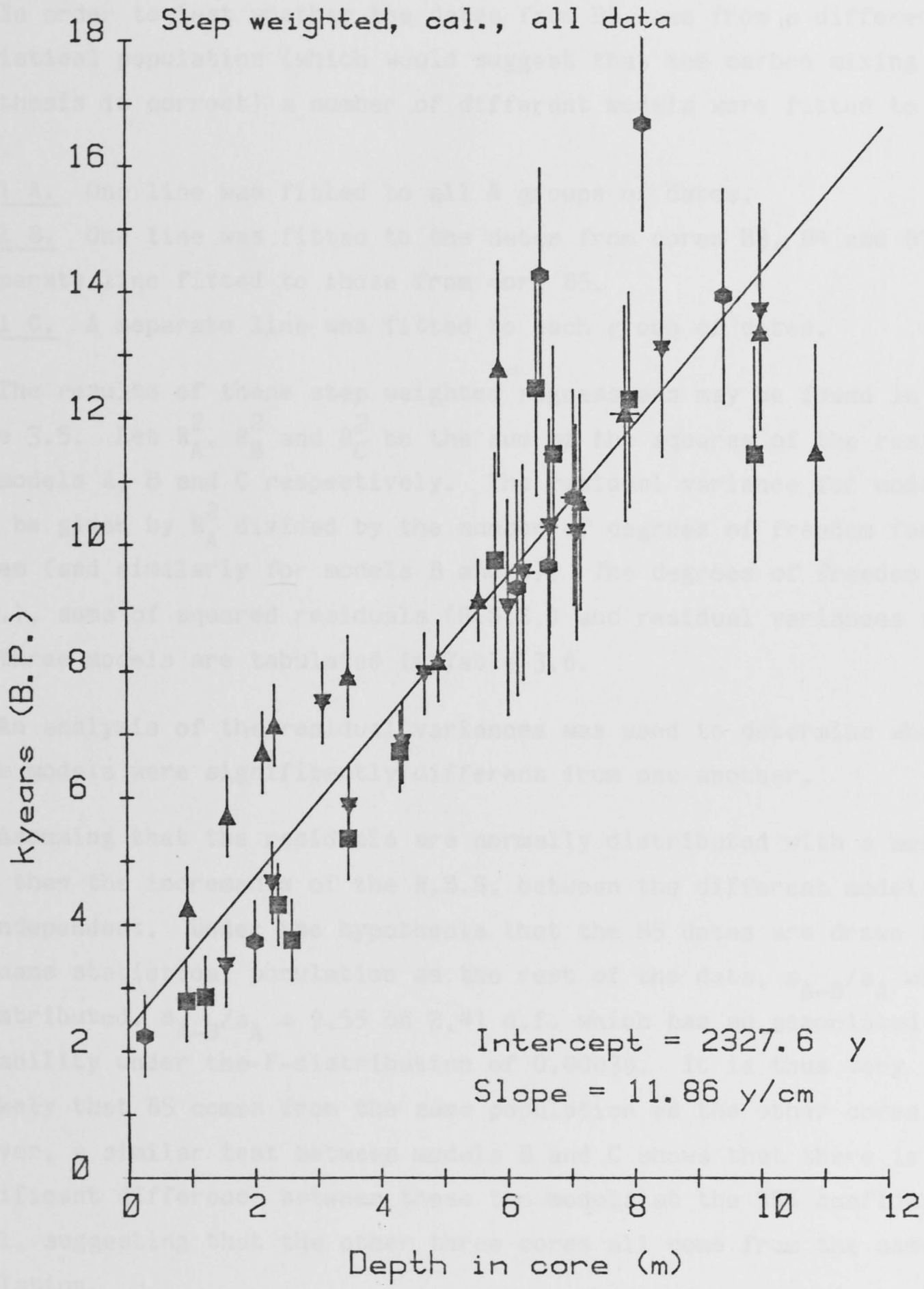

Figure 3.17 Step weighted linear regression on all the L. Barrine data. Vertical bars indicate the errors assigned in the step weighting procedure. Coding of symbols is as for Figure 3.15.

the influence of these dates.

In order to test whether the dates from B5 come from a different statistical population (which would suggest that the carbon mixing hypothesis is correct) a number of different models were fitted to the data.

Model A. One line was fitted to all 4 groups of dates.

Model B. One line was fitted to the dates from cores B3, B4 and B7 and a separate line fitted to those from core B5.

Model C. A separate line was fitted to each group of dates.

The results of these step weighted regressions may be found in Table 3.5. Let R_A^2, R_B^2 and R_C^2 be the sum of the squares of the residuals for models A, B and C respectively. The residual variance for model A will be given by R_A^2 divided by the number of degrees of freedom for the system (and similarly for models B and C). The degrees of freedom (d.f.), sums of squared residuals (R.S.S.) and residual variances for the three models are tabulated in Table 3.6.

An analysis of the residual variances was used to determine whether these models were significantly different from one another.

Assuming that the residuals are normally distributed with a mean of zero then the increments of the R.S.S. between the different models will be independent. Under the hypothesis that the B5 dates are drawn from the same statistical population as the rest of the data, s_{A-B}/s_A will be F-distributed. $s_{A-B}/s_A = 9.55$ on 2,41 d.f. which has an associated probability under the F-distribution of 0.00039. It is thus very unlikely that B5 comes from the same population as the other cores. However, a similar test between models B and C shows that there is no significant difference between these two models at the 95% confidence level, suggesting that the other three cores all come from the same population.

The evidence of physical disturbance in the upper section of core B5 and the likelihood that it comes from a different statistical population justifies excluding that data from the determination of the time scale. The final fits were based on the step-weighted data from cores B3, B4 and B7, and are illustrated in Figures 3.18 (calibrated) and 3.19 (uncalibrated). They were

Table 3.6 Variance Analysis of Barrine Radiocarbon Models.

Model	d.f.	$(R_i)^2$	System Variance
A	41	$R_A^2 = 87.993$	$s_A^2 = 2.144$
B	39	$R_B^2 = 47.03$	$s_B^2 = 1.206$
C	35	$R_C^2 = 40.710$	$s_C^2 = 1.631$
(A-B)	2	$R_A^2 - R_B^2 = 40.958$	$s_{A-B}^2 = 20.479$
(B-C)	4	$R_B^2 - R_C^2 = 6.752$	$s_{B-C}^2 = 1.688$

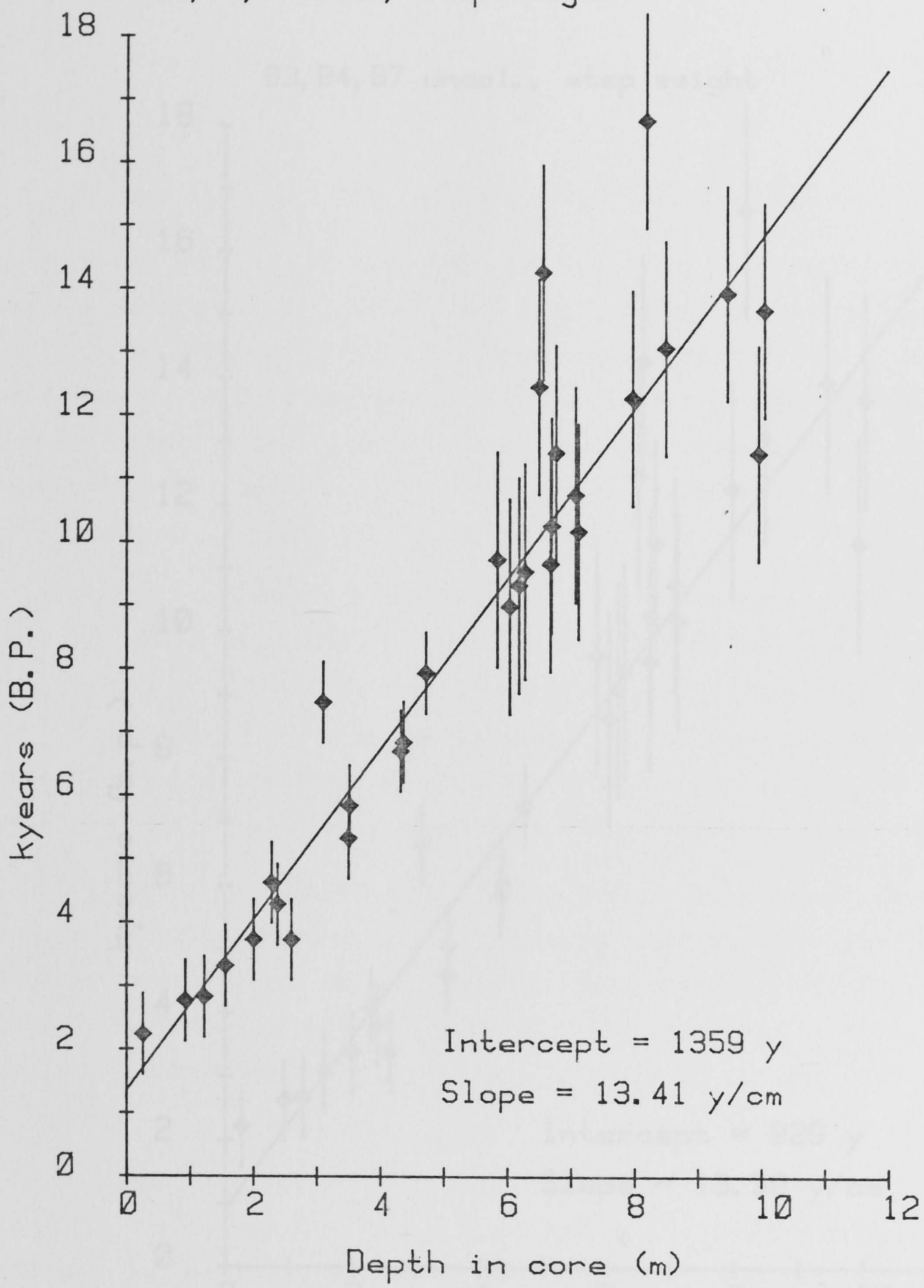

Figure 3.18 Final fit to the calibrated dates from cores B3, B4 and B7.

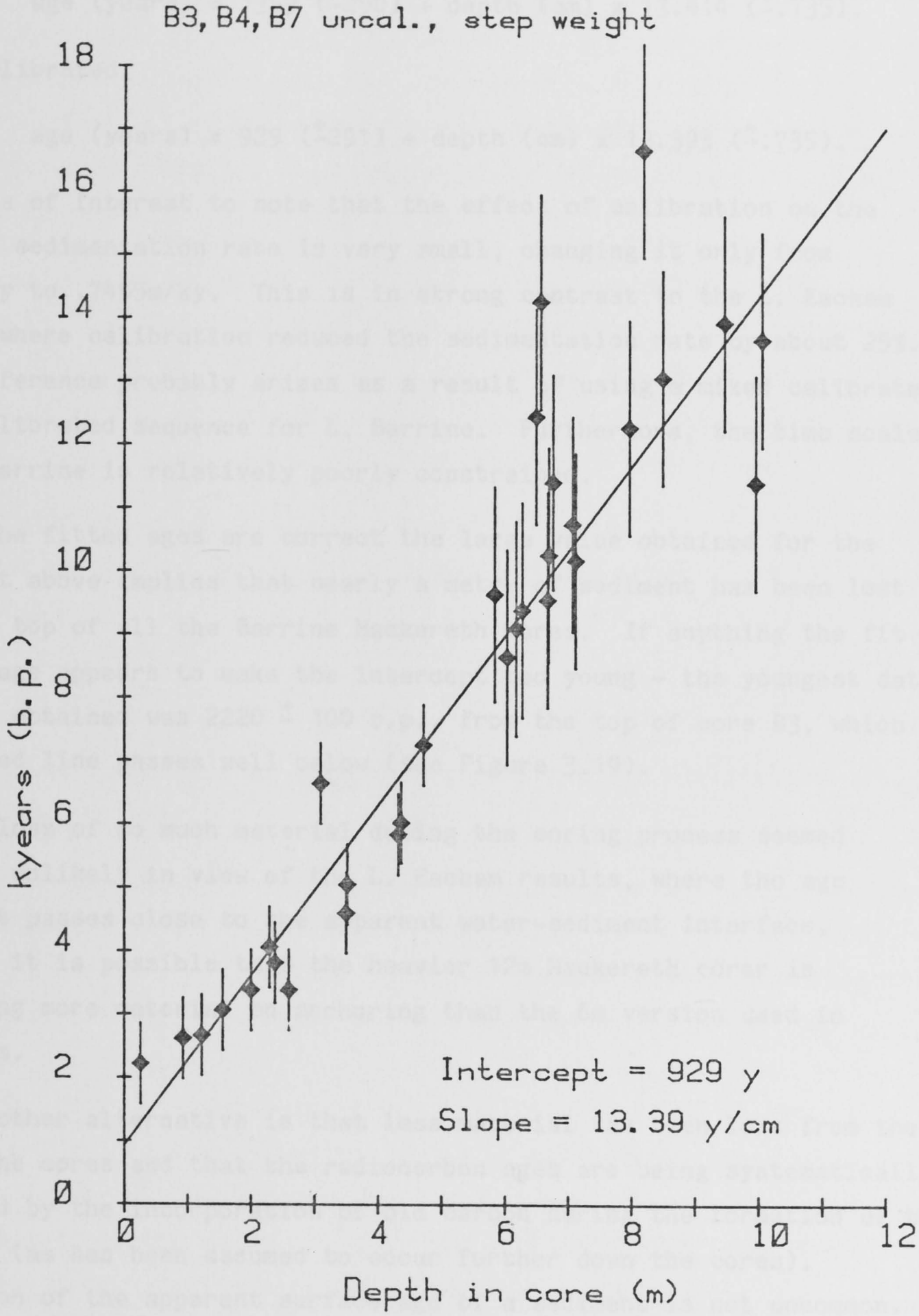

Figure 3.19 Final fit to the uncalibrated dates from cores B3, B4 and B7.

(1) Calibrated;

$$\text{age (years)} = 1359\ (\pm 290) + \text{depth (cm)} \times 13.414\ (\pm .735).$$

(2) Uncalibrated;

$$\text{age (years)} = 929\ (\pm 291) + \text{depth (cm)} \times 13.393\ (\pm .735).$$

It is of interest to note that the effect of calibration on the apparent sedimentation rate is very small, changing it only from .7467m/ky to .7455m/ky. This is in strong contrast to the L. Eacham records where calibration reduced the sedimentation rate by about 25%. This difference probably arises as a result of using a mixed calibrated and uncalibrated sequence for L. Barrine. Furthermore, the time scale for L. Barrine is relatively poorly constrained.

If the fitted ages are correct the large value obtained for the intercept above implies that nearly a metre of sediment has been lost from the top of all the Barrine Mackereth cores. If anything the fit to the ^{14}C age appears to make the intercept too young - the youngest date actually obtained was 2220 $\pm$ 100 b.p., from the top of core B3, which the fitted line passes well below (see Figure 3.19).

The loss of so much material during the coring process seemed somewhat unlikely in view of the L. Eacham results, where the age intercept passes close to the apparent water-sediment interface. However, it is possible that the heavier 12m Mackereth corer is displacing more material on anchoring than the 6m version used in L. Eacham.

The other alternative is that less material has been lost from the top of the cores and that the radiocarbon ages are being systematically depressed by the incorporation of old carbon during the formation of the sediment (as has been assumed to occur further down the cores). Depression of the apparent surface age of a sediment is not uncommon. Davis (1969) reports an apparent surface age of 730 b.p. for Rogers Lake, Connecticut, Kendall (1969) 400 b.p. for Lake Victoria, East Africa and Barton and Barbetti (1982) report an age depression of 450 radiocarbon years for sediment from L. Keilambete, S.E. Australia.

A number of frozen-finger cores were obtained from L. Barrine by Prof. D. Walker and Dr L. Rymer of the Department of Biogeography and Geomorphology, R.S.Pac.S., A.N.U. In the frozen finger coring technique the unconsolidated material near the water-sediment interface is frozen to form a solid envelope around the outside of a metal core tube. In this way samples can be recovered from the water-sediment interface which is generally too wet to sample with the Mackereth corer. The frozen finger core can be up to 1.5m in length.

A group of small samples from frozen finger number B11,79,F were collected by Prof. D. Walker and dated on the E.T.H. linear accelerator dating facility by Dr W. Wölfli in an attempt to establish whether the apparent age of the surface of the sediment is depressed. Preliminary dates from these samples were available and are listed below.

Depth below w/s interface (cm)	Uncalibrated Age (b.p.) $\pm$ 1 std error
0-3.2	225 $\pm$ 120
47.8-51.0	865 $\pm$ 130
51.0-55.0	1075 $\pm$ 90

Each sample was selected to be a five year sample if the laminations were seasonal in origin.

There is undoubtedly some depression of the true age since one would expect the bomb spike to affect the radiocarbon age of the uppermost material in the sediment, making it appear younger than it actually is. It is possible that, because of the shallower inner slopes in the L. Barrine crater than in L. Eacham (see Figure 3.2), it takes some considerable time for sedimentary material to migrate to the bottom central part of the lake, down the sides of the crater. This could be tested by dating material from a series of frozen finger cores spanning the distance from the centre to the edge of the lake, to see if material at the same stratigraphic level is younger at the edges.

It is inferred from the above results that at the surface the ^{14}C age of the sediment is depressed by several hundred years compared with the true age. Further measurements on the frozen finger cores should define better the magnitude of this age depression. It seems likely, however, that there is still a substantial portion of the record missing from the top of the Mackereth cores, although probably closer to 0.5m than 1m.

4 RELATIVE PALAEOINTENSITY ESTIMATES.

There is as yet no technique by which absolute estimates of the palaeointensity of the geomagnetic field may be made from sedimentary material. However, in an ideal situation in which the type and quantity of magnetic minerals present in a sediment were constant, and the intensity of the remanence linearly related to the external field fixing it, the fluctuations in NRM down a sedimentary profile would reflect relative changes in the intensity of the geomagnetic field. In practice this situation never arises, but attempts to correct for variations in a sediment's magnetic content and remanence potential are made by normalizing the NRM by some other magnetic property. It is then in principle possible that the variations in this relative intensity might represent variations in the geomagnetic field intensity.

Isothermal remanent magnetization (IRM) was used first as a normalising parameter by E.A. Johnson et al. (1948). Other workers have used initial susceptibility (e.g. Harrison, 1966 and Nesbit, 1966) or SIRM (Nakajima and Kawai, 1973). H.P. Johnson et al. (1975) and Levi and Bannerjee (1976) suggest that ARM is a preferable normalizing parameter as it has a coercivity spectrum closer to that of the NRM than the susceptibility or IRM. IRM and initial susceptibility probably over-emphasise the role of multidomain (MD) and superparamagnetic (SP) particles respectively.

King et al. (1981) suggest that this normalization technique will only provide valid relative intensity estimates if the DRM mechanism, magnetic mineralogy and grain size are uniform over the length of the sedimentary column to which it is applied. As pointed out by these authors, there are two approaches to evaluating these relative intensities as estimates of the geomagnetic field intensity.

(1) A detailed rock magnetic examination may be performed to determine if the assumptions of a uniform DRM mechanism, magnetic mineralogy and grain size are reasonable. Demagnetization curves of NRM, ARM, and IRM, ARM and IRM acquisition curves, hysteresis parameters, J_s versus temperature curves and plots of ARM versus susceptibility are useful in identifying the mineralogy and domain state of the magnetic component. These measurements may be used to determine

whether the technique might in principle be useful in a given environment.

(2) ^{14}C dated lake sediment relative intensity estimates can be compared with Thellier method (Thellier and Thellier, 1959) absolute palaeointensity records from ^{14}C dated lava flows and archaeomagnetic studies. These comparisons are complicated by the existence of non-dipole field sources and dating problems.

A detailed rock magnetic examination of the type suggested by King et al. (1981) is really beyond the scope of this project. However, some information was available as a by-product of other measurements and is presented here in an attempt to assess the usefulness of the method.

4.1 AF Demagnetization of NRM and ARM.

One specimen every metre down cores E2 and B4 was selected for a pilot study and successively AF demagnetized at fields up to 45mT. An ARM was then imparted along the direction of the NRM (after cleaning at 10mT) in the hope of mimicking as closely as possible the conditions under which the NRM was acquired. A dc bias field of .01mT was selected because it imparted an ARM of similar magnitude to the NRM and hence the ARM should involve magnetic material with approximately the same coercivity spectrum as the NRM. The AF demagnetization curves for NRM and ARM for E2 are illustrated in Figures 4.1 and 4.2 respectively and the median demagnetizing fields (MDF) listed in Table 4.1.

The Eacham data are remarkably similar for material from the whole section. NRM intensities ranged from 113.4 mAm^{-1} down to 1.232 mAm^{-1} yet the normalized demagnetization curves are virtually indistinguishable. The MDFs for the NRMs are consistently slightly lower than for the ARMs (mean of 21.43 as opposed to 27.53mT). It appears that the Eacham cores may satisfy quite well the criteria required of uniformity of magnetic mineralogy and grain size. Figure 4.3 compares a typical AF demagnetizing curve for NRM with that of the ARM. They are quite similar despite the difference of about 7mT in MDF.

Table 4.1 Median Demagnetising Fields for Core E2 NRM and ARM AF Pilot Studies.

Depth	MDF of NRM (mT)	MDF of ARM (.01/100mT)
75.0	22.7	27.6
175.0	22.2	28.9
275.0	21.5	27.7
375.0	20.7	27.5
475.0	20.7	27.5
575.0	20.8	26.0

Table 4.2 Some Magnetic Properties of Specimens form Core B1.

Depth (cm)	SIRM mA/m	χ emu/ccx10^{-6}	SIRM/χ	$(B_o)_{cr}$ (mT)	S
105.0	245	35	7	27	0.92
202.5	137	27	5	21	0.87
267.5	175	39	4	22	0.95
270.0	6711	560	11	18	1.00
302.5	74.6	29	2.5	29	0.76
332.5	61.5	25	2.5	29	0.64
400.0	1031	115	9	27	0.93
502.5	3920	342	11	23	0.98
595.0	622	90	7	24	0.88
700.0	410	49	9	26	0.89
730.0	97	28	3.5	28	0.69
732.5	2909	215	13	24	0.82
767.5	21200	1950	11	22	0.97
802.5	4657	407	11	23	0.95
902.5	8586	710	12	23	0.94
1002.5	28600	1040	25	48	0.78
1012.5	62800	832	40	67	0.66
1022.5	1909	136	12	22	0.82
1102.5	1676	186	10	22	0.90
1190.0	2300	172	14	25	0.91

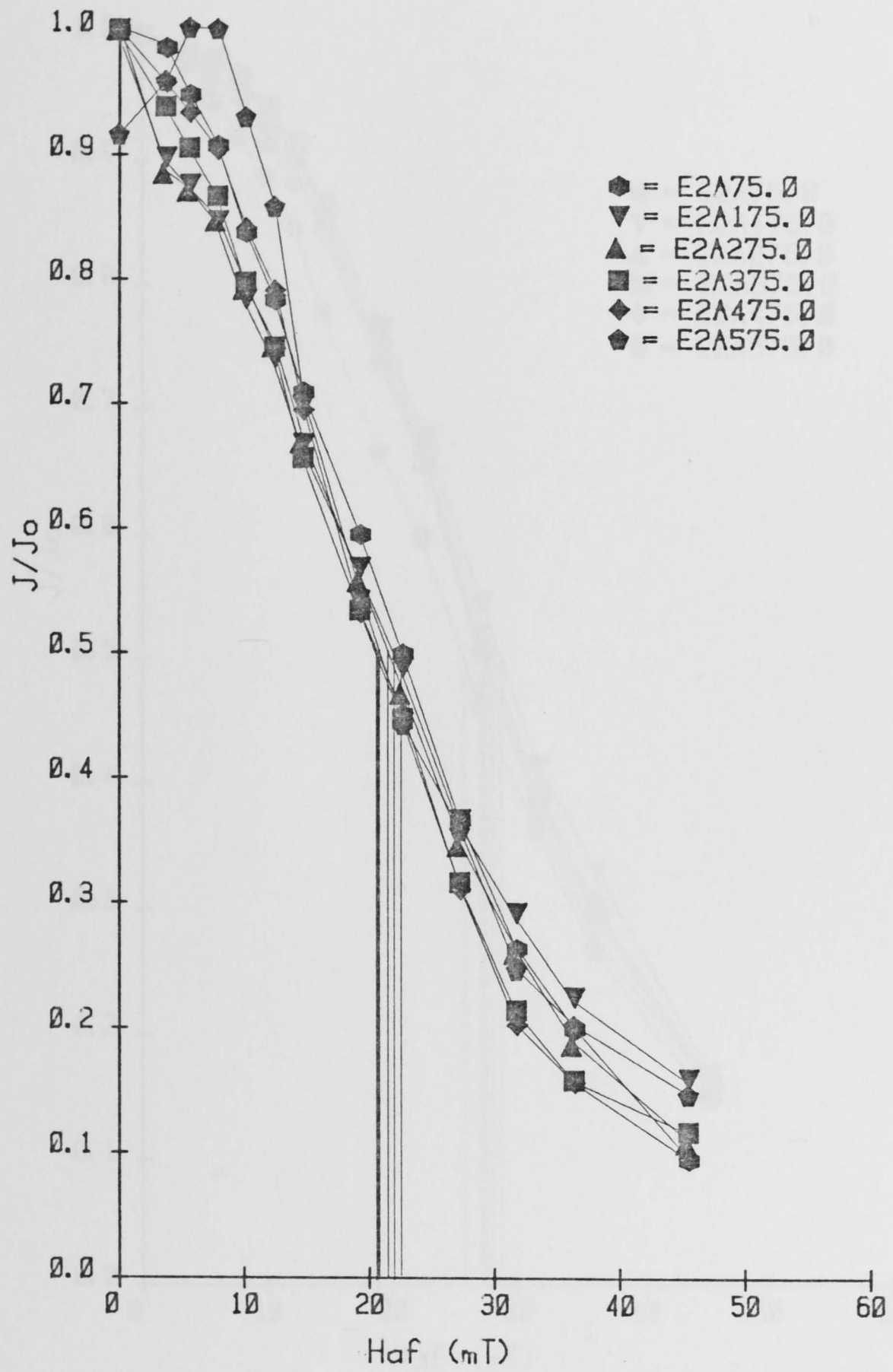

Figure 4.1 Normalised AF intensity demagnetization curves of the NRM for selected specimens from core E2.

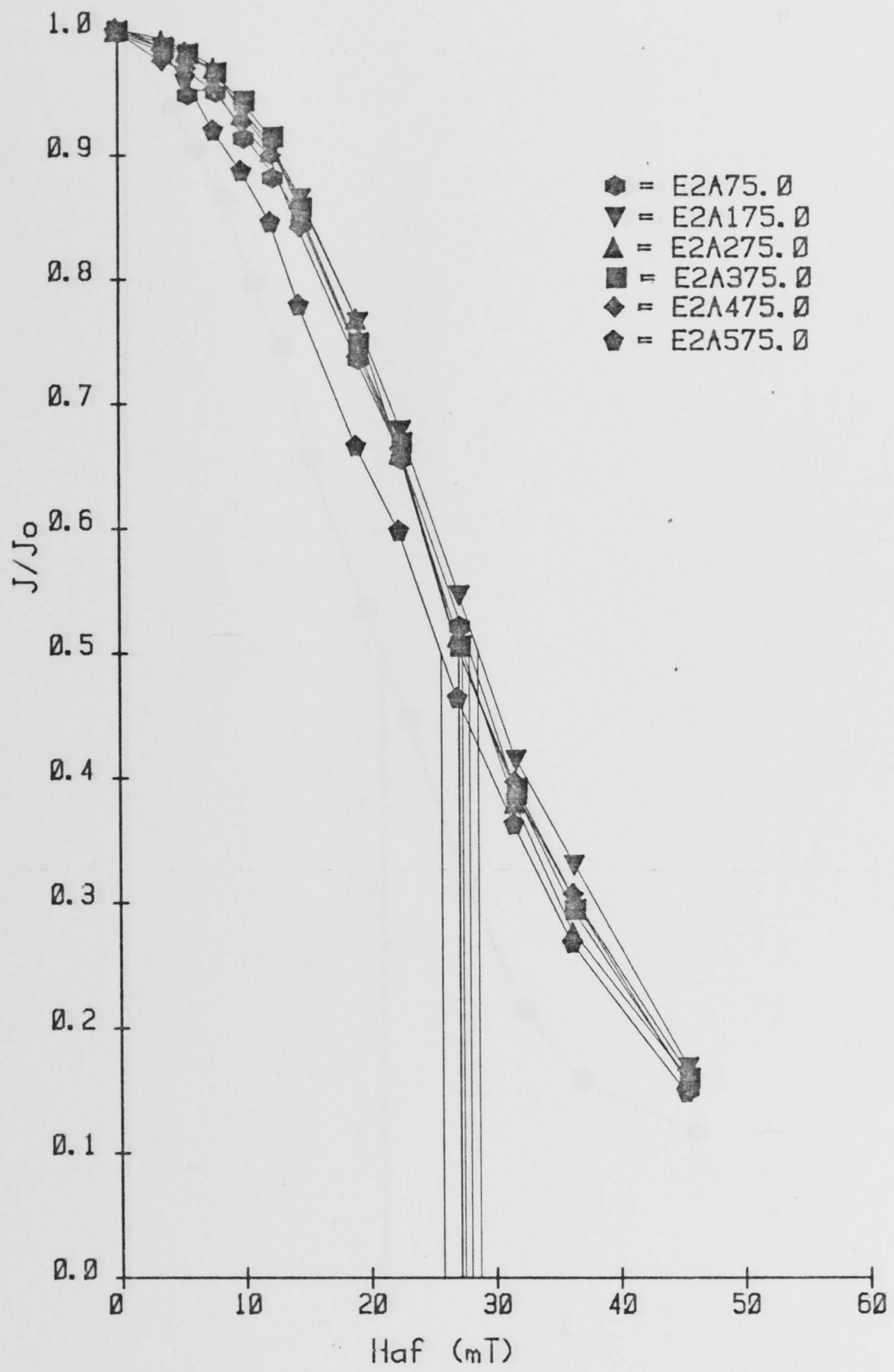

Figure 4.2 Normalised AF intensity demagnetization curves of the ARM for selected specimens from core E2.

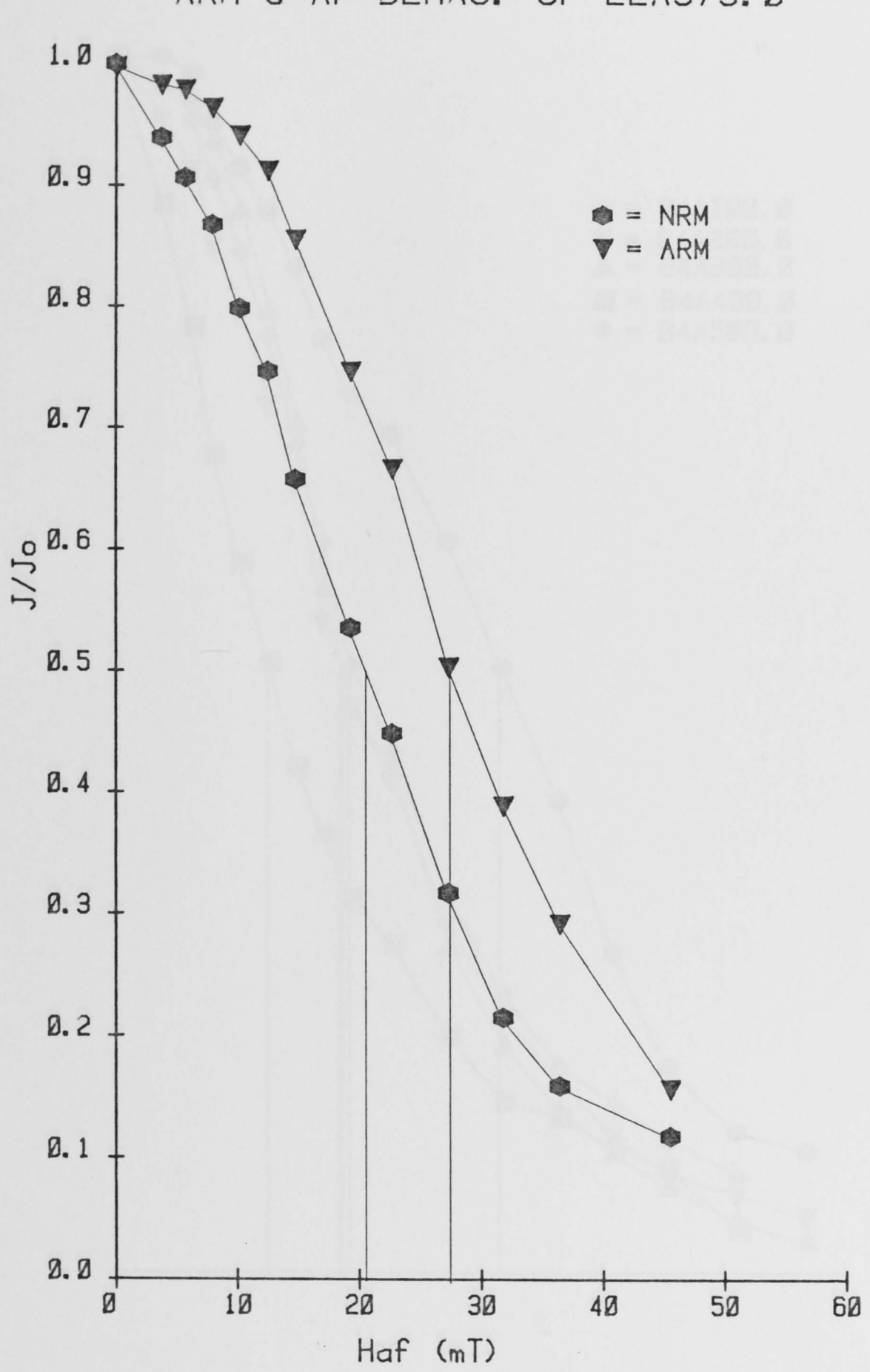

Figure 4.3 Comparison of typical AF demagnetizing curve for NRM and ARM from L. Eacham.

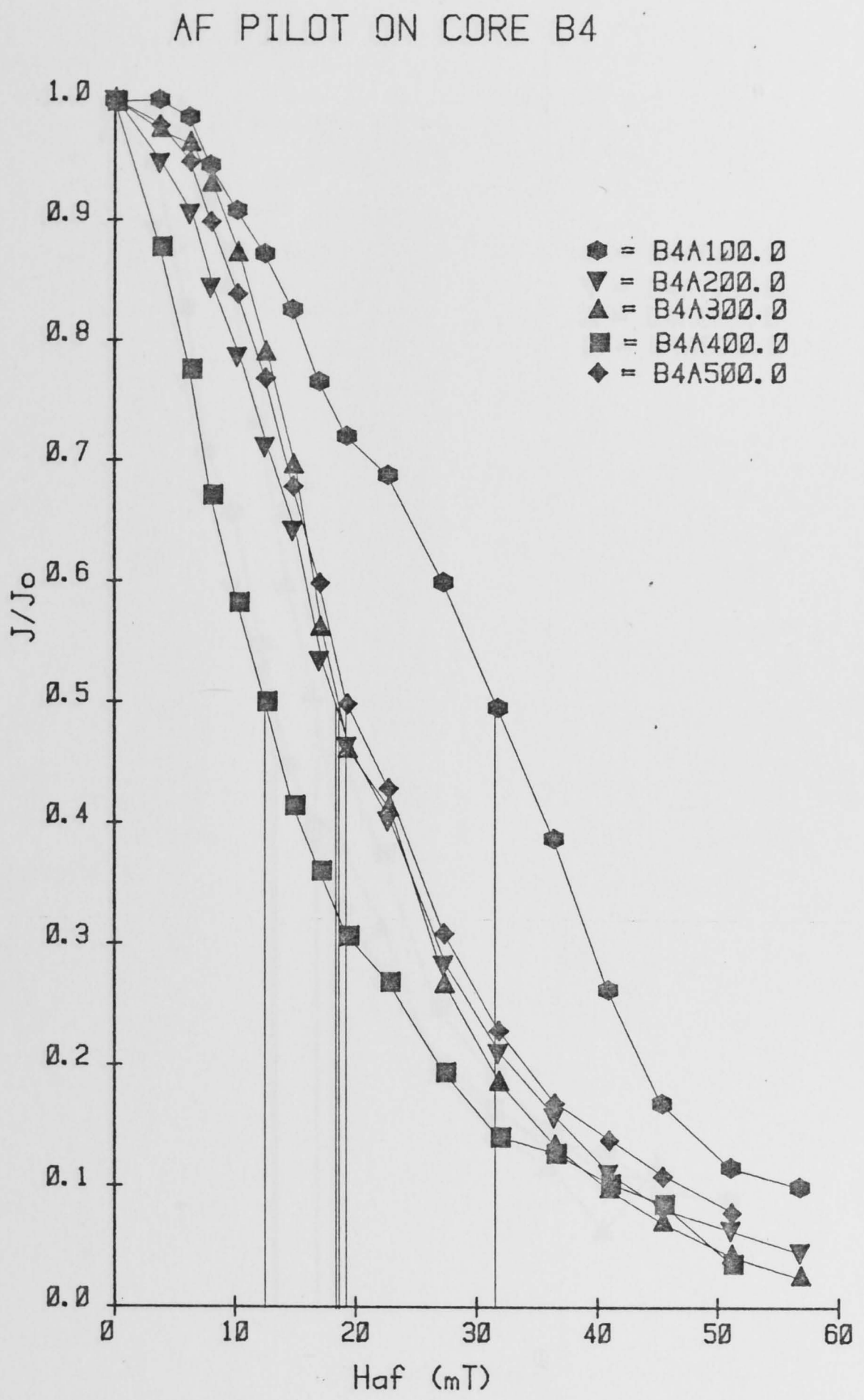

Figure 4.4 (a) Normalised AF intensity demagnetization curves of the NRM for pilot specimens from core B4.

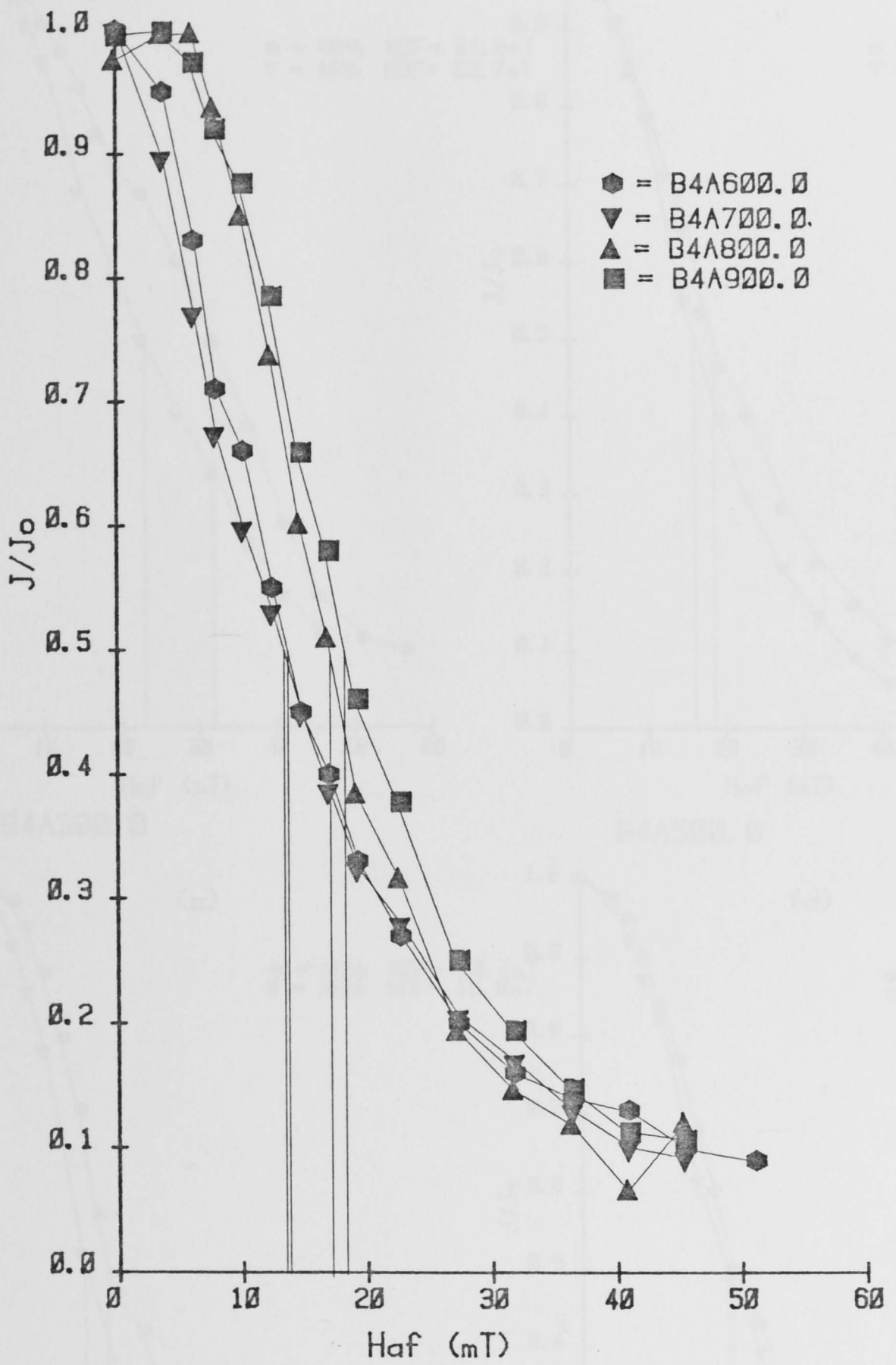

Figure 4.4 (b) Normalised AF intensity demagnetization curves of the NRM for pilot specimens from core B4.

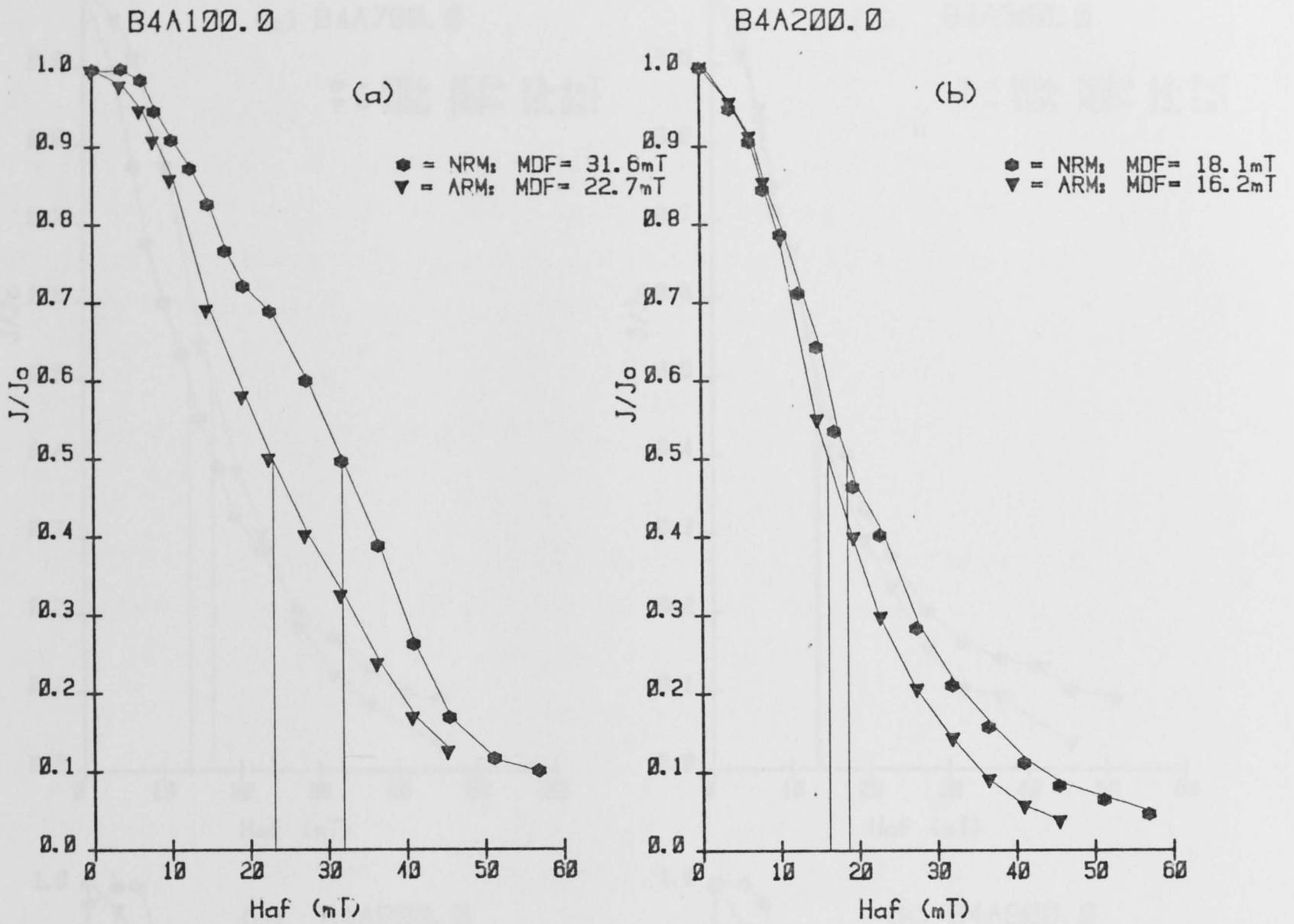

Figure 4.5 (a)-(d) Comparison of AF demagnetization of NRM and ARM for pilot specimens from core B4.

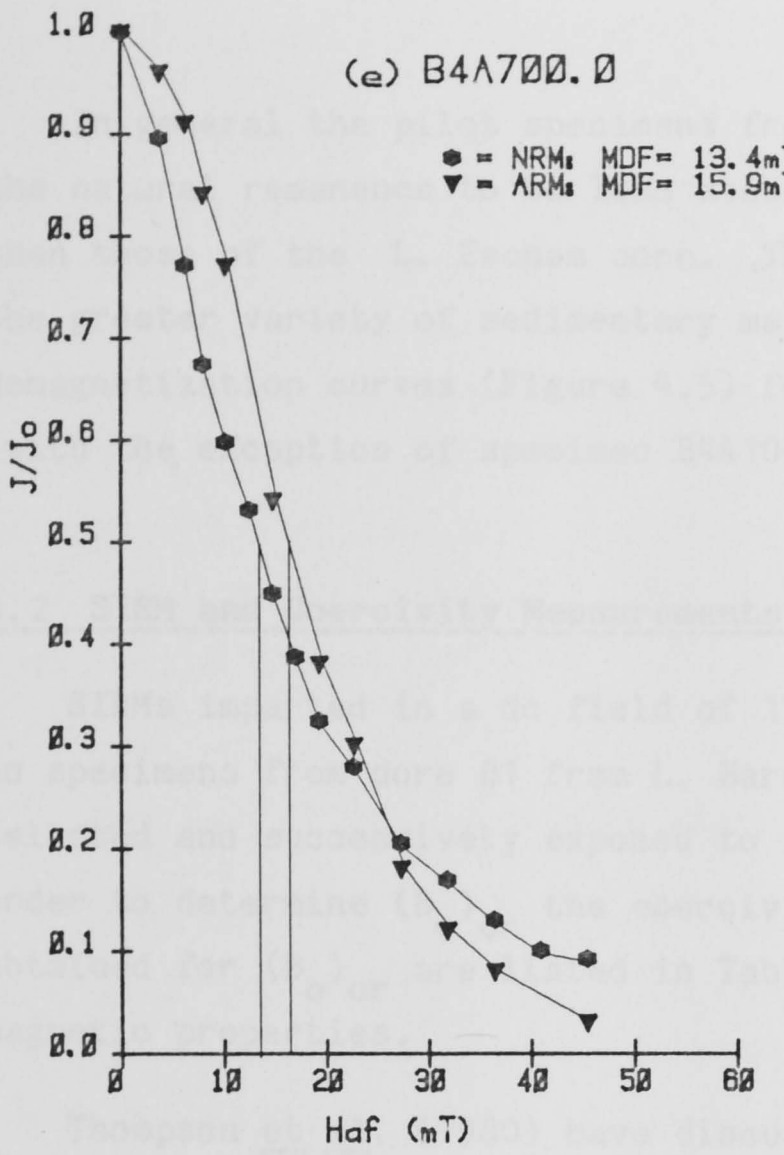

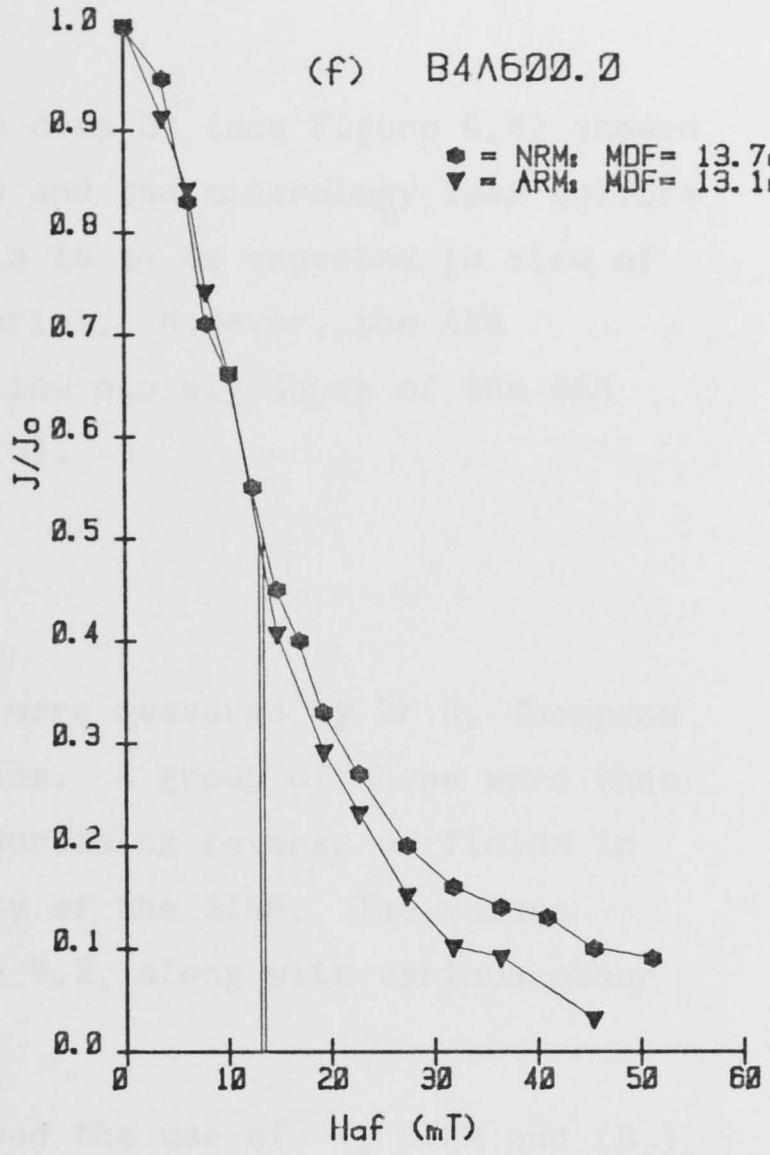

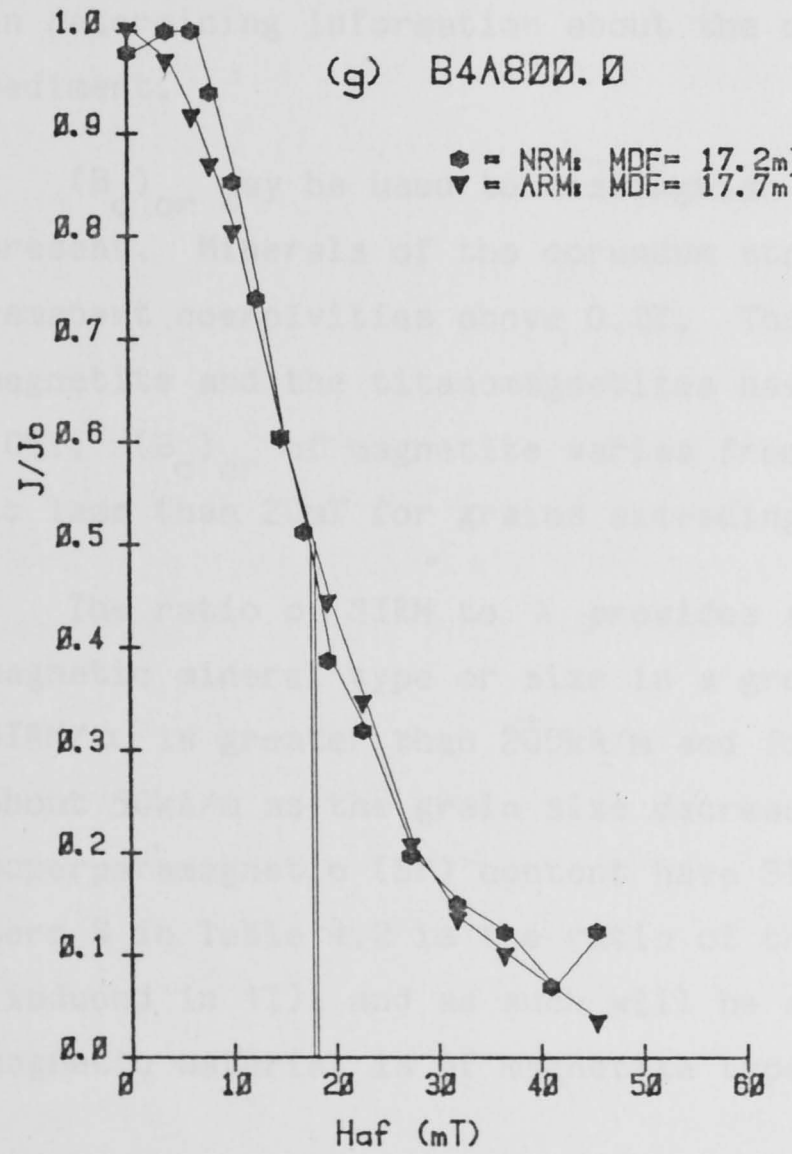

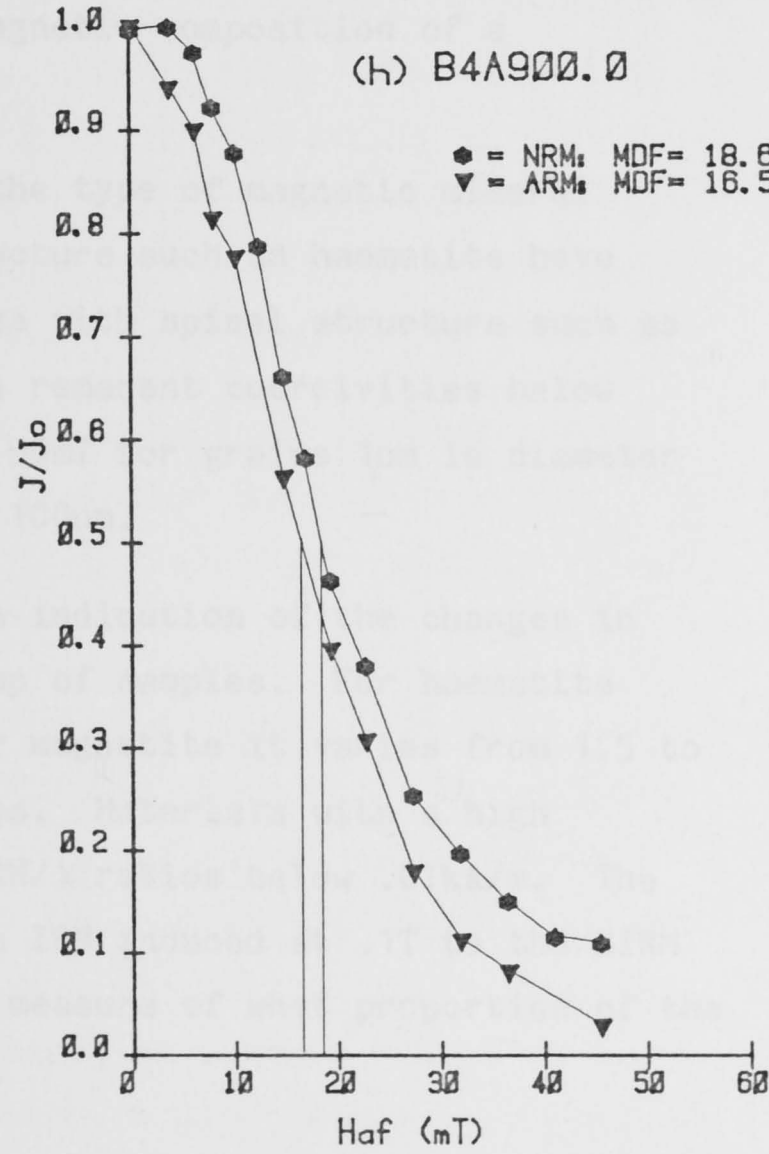

Figure 4.5 (e)-(g) Comparison of AF demagnetization of NRM and ARM for pilot specimens from core B4.

In general the pilot specimens from core B4 (see Figure 4.4) showed the natural remanence to be less stable and the mineralogy less uniform than those of the L. Eacham core. This is to be expected in view of the greater variety of sedimentary material. However, the ARM demagnetization curves (Figure 4.5) follow closely those of the NRM (with the exception of specimen B4A100.0).

4.2 SIRM and Coercivity Measurements.

SIRMs imparted in a dc field of 1T were measured by Dr R. Thompson on specimens from core B1 from L. Barrine. A group of these were then selected and successively exposed to increasing reverse dc fields in order to determine $(B_o)_{cr}$ the coercivity of the SIRM. The values obtained for $(B_o)_{cr}$ are listed in Table 4.2, along with various other magnetic properties.

Thompson et al. (1980) have discussed the use of χ, SIRM and $(B_o)_{cr}$ in determining information about the magnetic composition of a sediment.

$(B_o)_{cr}$ may be used to distinguish the type of magnetic mineral present. Minerals of the corundum structure such as haematite have remanent coercivities above 0.2T. Those with spinel structure such as magnetite and the titanomagnetites have remanent coercivities below .05T. $(B_o)_{cr}$ of magnetite varies from 50mT for grains 1μm in diameter to less than 20mT for grains exceeding 100μm.

The ratio of SIRM to χ provides an indication of the changes in magnetic mineral type or size in a group of samples. For haematite SIRM/χ is greater than 200kA/m and for magnetite it varies from 1.5 to about 50kA/m as the grain size decreases. Materials with a high superparamagnetic (SP) content have SIRM/χ ratios below .01kA/m. The term S in Table 4.2 is the ratio of the IRM induced at .1T to the SIRM (induced in 1T), and as such will be a measure of what proportion of the magnetic material is of magnetite type.

It is apparent from the $(B_o)_{cr}$ and S values of Table 4.2 that magnetite type minerals generally dominate the remanence characteristics of the L. Barrine sediment. However, occasional low values of S indicate that there are significant quantities of haematite present at some levels in the core. Only around the 10m level are these supported by correspondingly high values of $(B_o)_{cr}$. The AF demagnetization curves of Figure 4.4 suggest that haematite is not contributing significantly to the NRM of the sediment, since in general less than 10% of the NRM is left by the time a field of 50mT has been reached.

4.3 ARM versus Susceptibility Plots.

Banerjee et al. (1981) have proposed a method for determining the fine scale variation in the grain size of magnetite in long cores of sediment. This method consists of making a comparitive plot of the depth variation of low field (less than 0.1mT) susceptibility and anhysteretic remanent magnetization imparted by a smoothly decreasing AF field in the presence of a weak (0.01-0.1mT) dc field. The magnitude of the ARM will be sensitive to the finer grain size fraction of the magnetic material (single domain (SD) and smaller pseudo-single domain (PSD) grains), while the low field susceptibility will be relatively more sensitive to the coarser grain sizes (larger PSD and MD grains).

King et al. (1982) have tested this technique on sediments from three lakes which contain magnetite or a similar magnetic carrier. Their interpretations are supported by high field hysteresis measurements on the same sediments.

A simple idealized model based on magnetite samples of known size is proposed by King et al. (1982) to explain the use of the ARM versus χ plot for detecting relative grain size changes in the magnetite content of natural materials. Figure 4.6 shows the variations expected in the ARM/χ ratio for different grain sizes and the data on which these are based. Changes in amount of magnetic material present will result in progression along a line of constant slope, while changes in grain size will result in a change of slope.

than 1m.

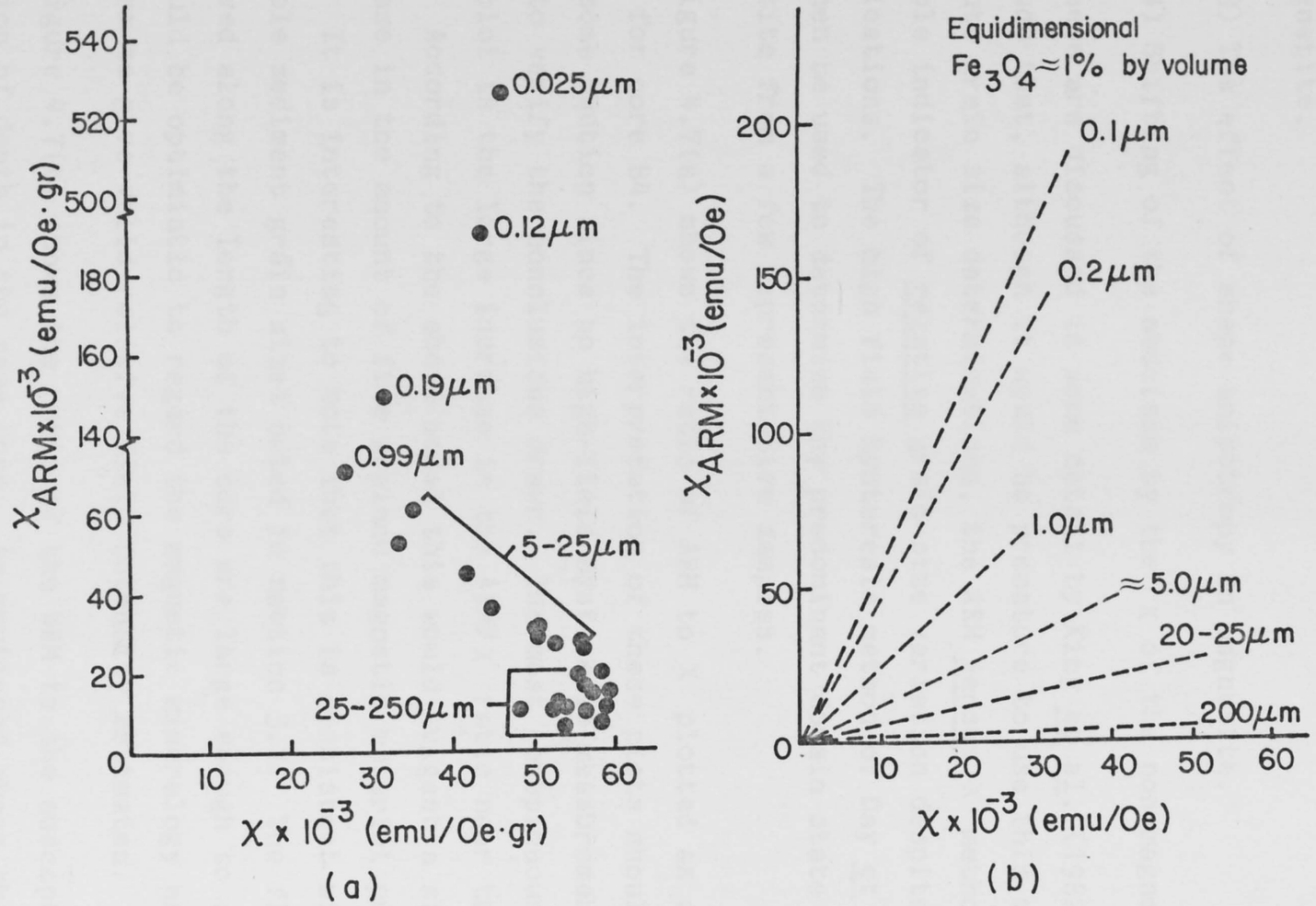

Figure 4.6 (a) Variations in ARM as a function of χ for equidimensional Fe_3O_4 (data from Özdemir and Bannerjee, 1981; Dankers, 1978). (b) King et al.'s (1982) idealized model of ARM versus χ variations.

There are a number of complications associated with this model.

(1) Possible presence of SP magnetite grains which will contribute only to χ and not to the ARM.

(2) The effect of magnetic interactions with varying concentrations of magnetite.

(3) The effect of shape anisotropy in magnetite.

(4) Shifting of the abscissa by the χ of the non-magnetic matrix.

These are discussed in some detail by King *et al*. (1982). They conclude that, although it would be premature to use this method for absolute grain size determinations, the ARM *versus* χ method is a reliable indicator of *relative* grain size variation despite the above complications. The high field hysteresis method of Day *et al*. (1977) can then be used to determine the predominant domain state of the magnetite from a few representative samples.

Figure 4.7(a) shows the ratio of ARM to χ plotted as a function of depth for core B4. The interpretation of these plots should be viewed with some caution since no high-field hysteresis measurements have been made to verify the conclusions drawn. The most conspicuous feature of this plot is the large increase in the ARM/χ ratio near the top of the core. According to the above model this would suggest a significant increase in the amount of fine grained magnetic material present in the core. It is interesting to note that this is consistent with the trend in whole sediment grain sizes noted in section 3.2. The fluctuations observed along the length of the core are large enough to suggest that it would be optimistic to regard the magnetic mineralogy as sufficiently uniform to give valid relative field intensity estimates.

Figure 4.7(b) shows the ratio of the NRM to the susceptibility as a function of depth in the same core. As mentioned above these Q-ratios are sometimes used as relative intensity estimates, but have generally fallen out of favour because they are thought to over-emphasise the role of SP particles, which will not contribute to the NRM. The Q-ratios and ARM to χ ratios are very similar. This suggests that if the ARM/χ is providing a valid estimate of the relative grain sizes present, then the variation in Q-ratio is almost exclusively controlled by changes in magnetic grain size down the length of the core. This would render it a

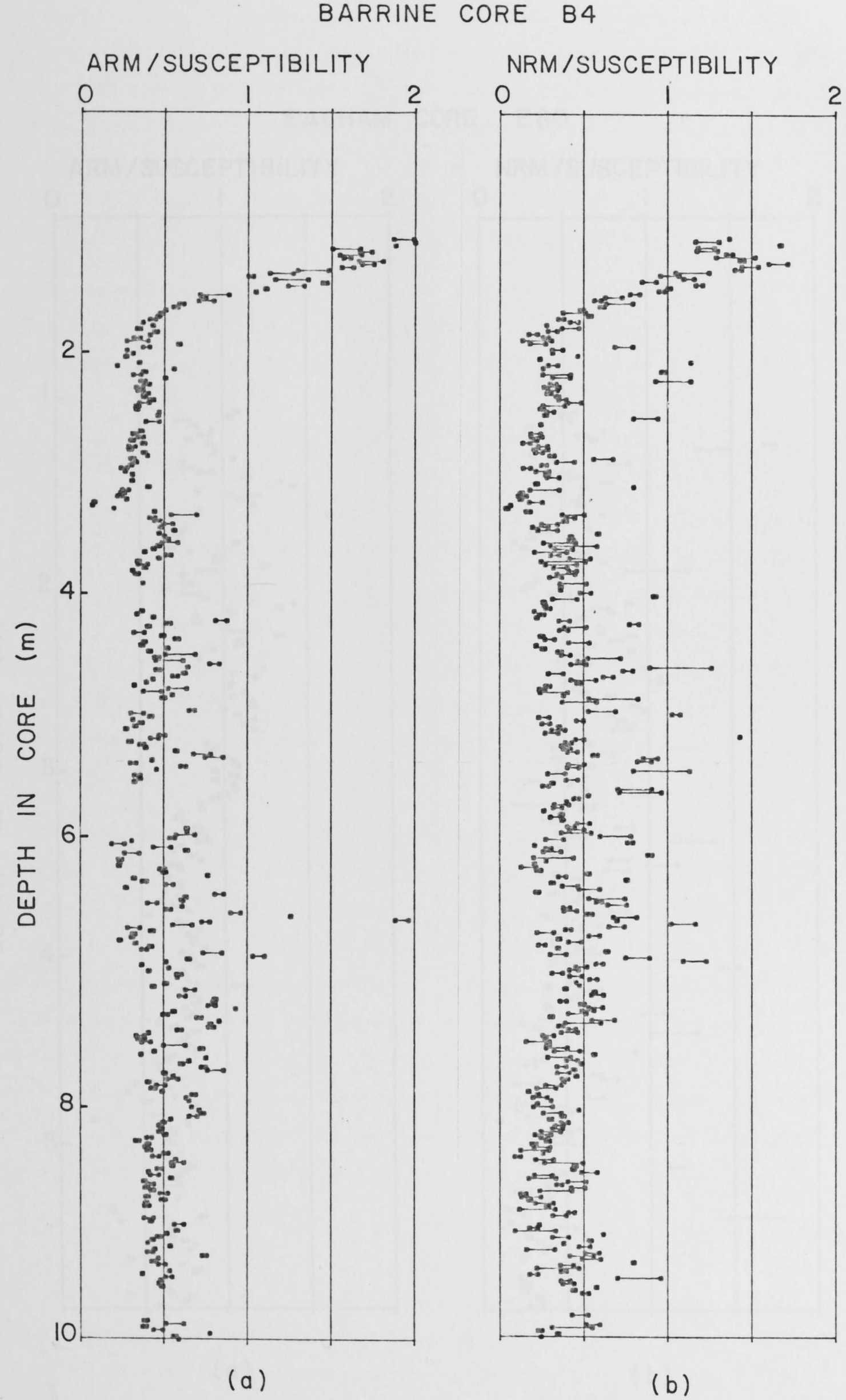

Figure 4.7 Ratio of (a) ARM to susceptibility and (b) NRM to susceptibility as a function of depth in core B4.

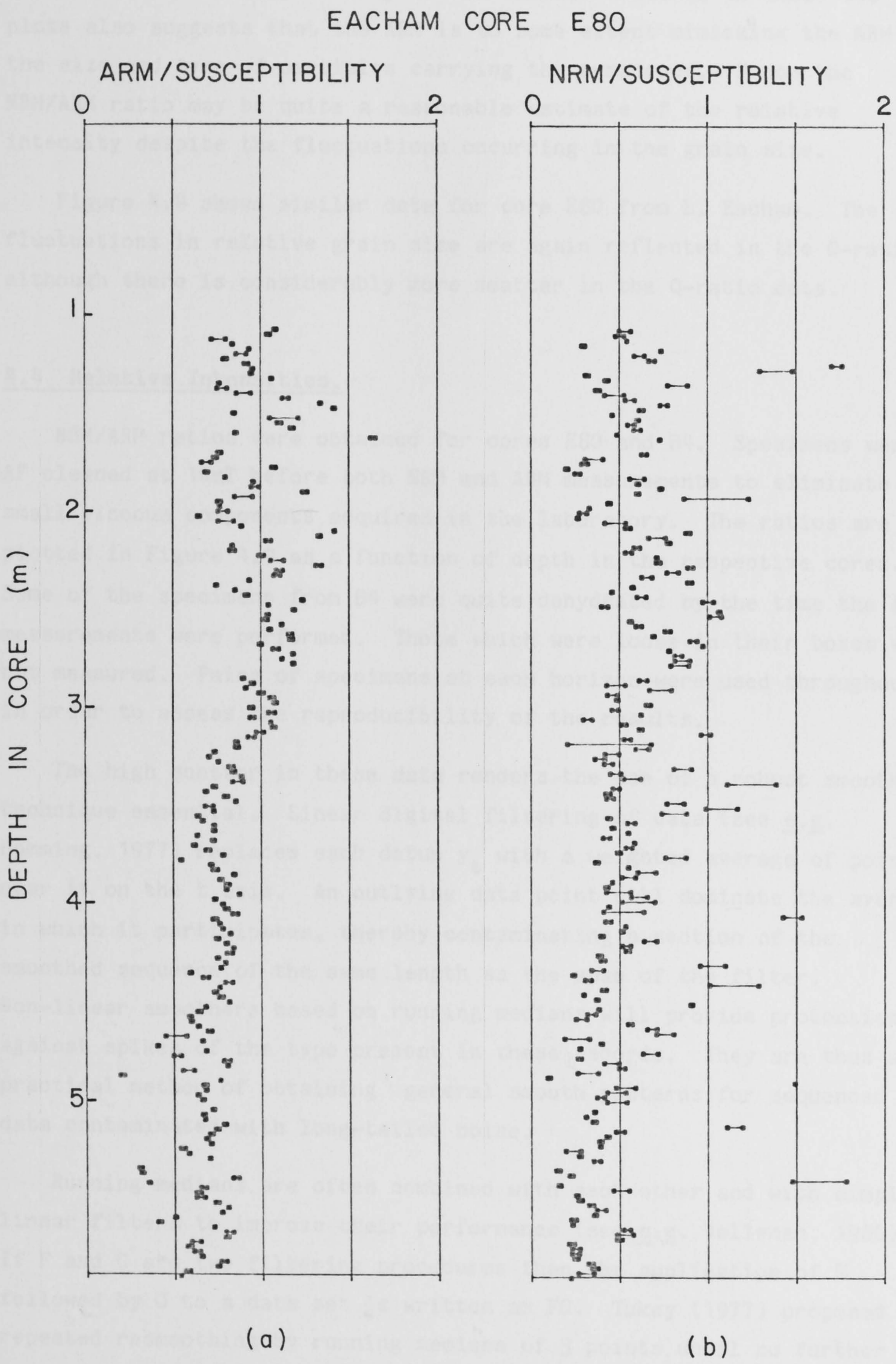

Figure 4.o Ratio of (a) ARM to susceptibility and (b) NRM to susceptibility as a function of depth in core E80.

very poor estimate of relative intensity fluctuations in the geomagnetic field. The similarity of many of the smaller features on these two plots also suggests that the ARM is to some extent mimicking the NRM in the size and type of particles carrying the remanence. Hence the NRM/ARM ratio may be quite a reasonable estimate of the relative intensity despite the fluctuations occurring in the grain size.

Figure 4.8 shows similar data for core E80 from L. Eacham. The fluctuations in relative grain size are again reflected in the Q-ratios, although there is considerably more scatter in the Q-ratio data.

4.4 Relative Intensities.

NRM/ARM ratios were obtained for cores E80 and B4. Specimens were AF cleaned at 10mT before both NRM and ARM measurements to eliminate small viscous components acquired in the laboratory. The ratios are plotted in Figure 4.9 as a function of depth in the respective cores. Some of the specimens from B4 were quite dehydrated by the time the ARM measurements were performed. Those which were loose in their boxes were not measured. Pairs of specimens at each horizon were used throughout in order to assess the reproducibility of the results.

The high scatter in these data renders the use of a robust smoothing technique essential. Linear digital filtering of data (see e.g. Hamming, 1977) replaces each datum y_t with a weighted average of points near it on the t axis. An outlying data point will dominate the average in which it participates, thereby contaminating a section of the smoothed sequence of the same length as the span of the filter. Non-linear smoothers based on running medians will provide protection against spikes of the type present in these records. They are thus a practical method of obtaining general smooth patterns for sequenced data contaminated with long-tailed noise.

Running medians are often combined with each other and with simple linear filters to improve their performance (see e.g. Velleman, 1980). If F and G are two filtering procedures then the application of F followed by G to a data set is written as FG. Tukey (1977) proposed repeated resmoothing by running medians of 3 points until no further changes take place. A running median of 3 is denoted by "3" and the repetition until no further change by R, so that this combined filter is

represented as 3R. Tukey also recommended a splitting algorithm called S to modify resulting flat stretches of two consecutive points.

The splitting algorithm is such that:
for data sequence

$$[\ldots y_{t-2},\ y_{t-1},\ y_t,\ y_u,\ y_{u+1},\ \ldots],\quad \text{where } u=t+1,$$

and its smoothed sequence after 3R,

$$[\ldots z_{t-2},\ z_{t-1},\ z_t,\ z_u,\ z_{u+1},\ \ldots],$$

then whenever

$$z_t = z_u \text{ and } \operatorname{sign}(z_t - z_{t-1}) = \operatorname{sign}(z_u - z_{u+1}) \neq 0$$

replace z_t by

$$\operatorname{median}[\ 3z_{t-1}-2z_{t-2},\ z_t,\ z_{t-1}\ ]$$

and z_u by

$$\operatorname{median}[\ 3z_{u+1}-2z_{u+2},\ z_u,\ z_{u+1}\ ].$$

S is usually repeated once, (SS), or until no further changes take place, (SR).

The end points of the data series may be treated using Tukey's (1977) end point rule

$$z_1 = \operatorname{median}[\ 3z_2-2z_3,\ y_1,\ z_2\ ].$$

This makes use of the slope of the line joining the second and third points to smooth the first point.

Tukey (1977) has also suggested using a slightly different feature from a running median as the basic component of the smoother, namely

$$\underline{3} = \operatorname{median}[u, v, w]$$

where

$$u = \operatorname{median}[y_{t-1},\ y_t,\ y_{t+1}\ ]$$
$$v = \operatorname{median}[y_{t-1},\ (3y_{t-1}-y_{t-2})/2,\ y_t\ ]$$
$$w = \operatorname{median}[y_{t+1},\ (3y_{t+1}-y_{t+2})/2,\ y_t\ ]$$

The effect of using $\underline{3}$RSR rather than 3RSR is to preserve local peaks in the data to a greater extent (McNeil, 1977).

After spikes have been removed from the record by non-linear smoothing linear filters can be applied with safety. Hanning (H), applying a three point moving average with weights 0.25, 0.5, 0.25 is often used to complete the smoothing process and remove small steps in the median smoothed record.

Fortran subroutines to implement the median smoothing were taken from McNeil (1977). Dr R.M. Clark of the Department of Statistics, Monash University wrote the rest of the package used here.

The smoother used on the relative intensity data was 3RSRH. Prior to its application the data from each core was split up into an A and a B series corresponding to the A and B samples at each depth in the core. The smoother was then applied separately to each of these series in order to assess the reproducibilty of the data.

The smoothed data are shown in Figure 4.10 after having been adjusted to the calibrated time scales derived in section 3.4. The A and B series for each lake have been recombined and lines join data pairs at the same level. The agreement between the As and Bs for each lake is in general quite good. An inter-lake comparison shows that the two records are very similar, although their coeval time span is rather short, due to the fact that the top section of core B4 was too disturbed to sample. The record for B4 appears to lag that for Eacham very slightly, by about 200 years. This is within the error associated with the radiocarbon time scale.

The only absolute intensity estimates covering this time span which are available for comparitive purposes come from S.E. Australian archaeomagnetic work carried out on Aboriginal fireplaces by Dr M. Barbetti (pers. comm.). These span the last 7 000 calendar years and are illustrated in Figure 4.11 with the L. Eacham relative intensity estimates. It can be seen that the agreement is good. Considerably more detail is apparent in the lake sediment record than the archaeointensity one as is to be expected from the continuous sampling throughout time. Some of this detail will undoubtedly be spurious, caused by departures from uniformity in the remanence acquisition in ways which cannot be compensated by the normalization procedure. Other features such as the rapid fall in intensity at about 4 000 B.P. may well represent real geomagnetic intensity fluctuations which have not

previously been discovered (note the lack of archaeomagnetic data between 3 500 and 4 500 B.P.).

It is concluded that these relative intensity estimates do represent a valid measure of geomagnetic field fluctuation. The good agreement between the two lakes also suggests that, at least over this section of the record, the time scale derived for the L. Barrine record in section 3.4 cannot be in error by more than two or three hundred years.

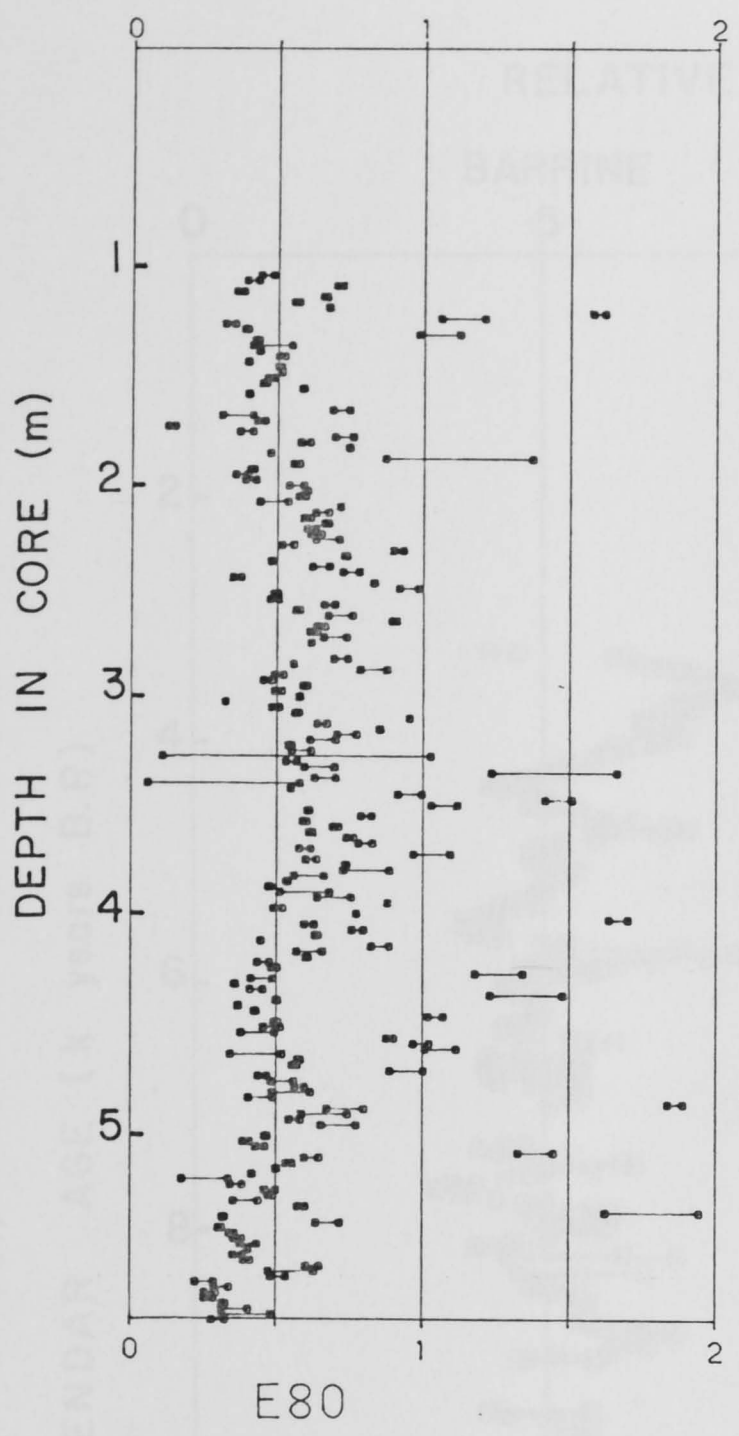

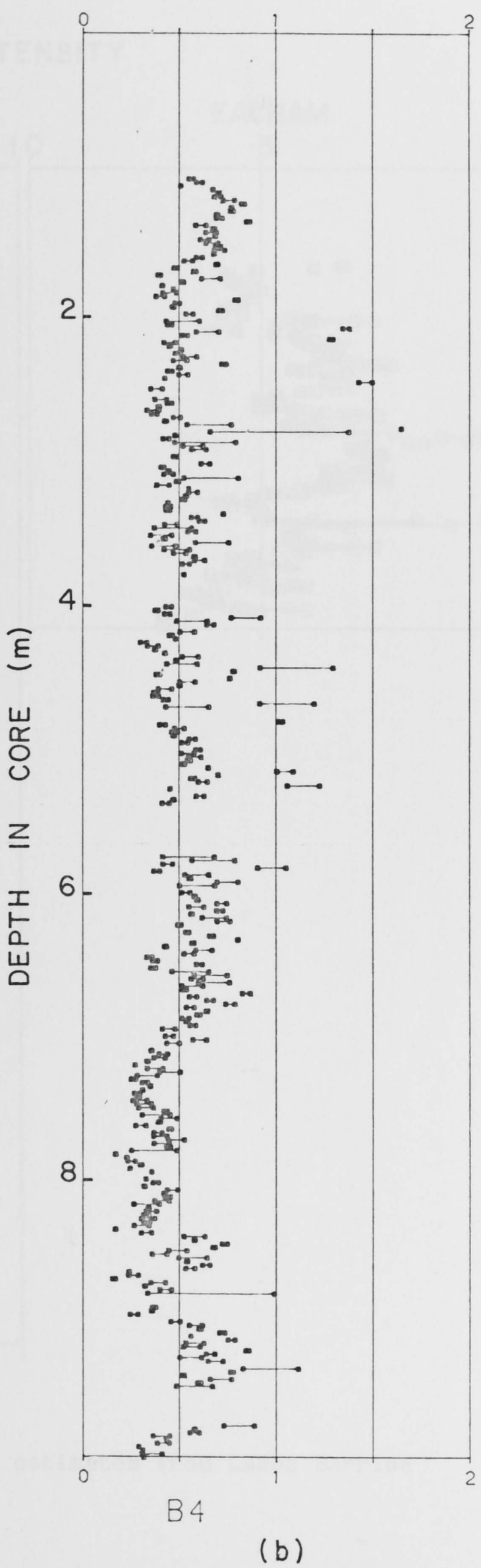

Figure 4.9 Ratios of NRM to ARM for cores E80 and B4 as a function of depth in core.

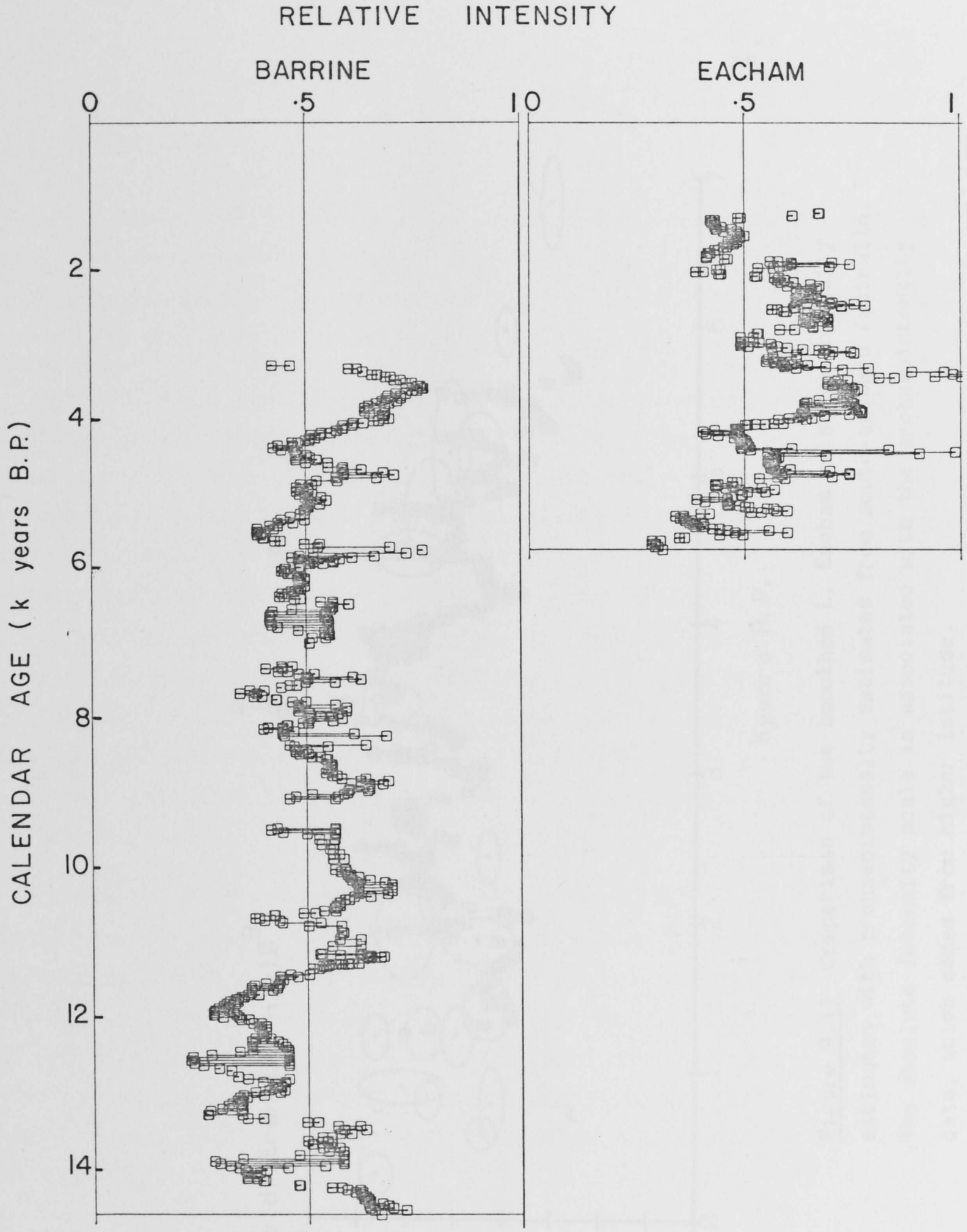

Figure 4.10 Smoothed relative intensity estimates from Lakes Barrine and Eacham.

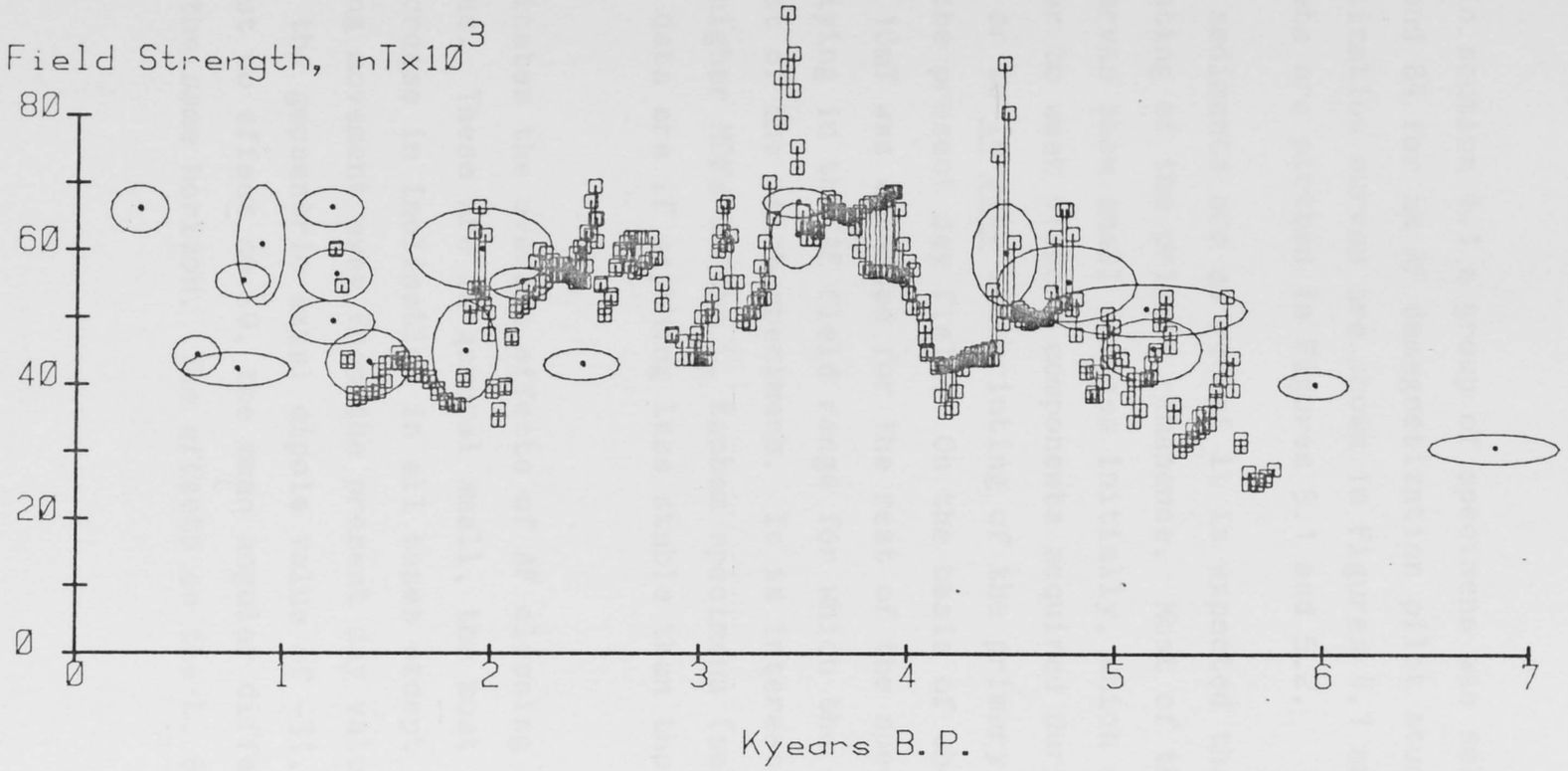

Figure 4.11 Comparison of the smoothed L. Eacham relative intensity estimates with archaeointensity estimates from south-eastern Australia. The absolute intensity scale is associated with the archaeointensity data, which comes from higher latitude.

5 DIRECTIONAL DATA.

5.1 AF Cleaning.

As described in section 4.1 a group of specimens was selected from each of cores E2 and B4 for an AF demagnetization pilot study. The intensity demagnetization curves are shown in Figures 4.1 and 4.4, while the directional data are plotted in Figures 5.1 and 5.2.

Because these sediments are so recent it is expected that there will be little overprinting of the primary remanence. Most of the demagnetization curves show small changes initially, which are probably attributable either to weak viscous components acquired during storage in the laboratory or to *in situ* overprinting of the primary magnetization by the present day field. On the basis of these data a cleaning field of 10mT was selected for the rest of the specimens from both lakes, this lying in the AF field range for which the directions are stable for most of the pilot specimens. It is interesting to note that despite the higher MDFs of the L. Eacham specimens (see Table 4.1) their directional data are if anything less stable than those from L. Barrine.

Table 5.1 indicates the average effects of AF cleaning at 10mT on the L. Eacham cores. These are in general small, the most obvious trend being a slight decrease in inclination in all cases except E77. This is probably reflecting movement away from the present day value at the site of -45.5^{o} towards the geocentric axial dipole value of -31.9^{o}. AF cleaning had almost no effect on $\Delta\theta$, the mean angular difference between pairs of data at the same horizon. The effects on the L. Barrine cores were similar.

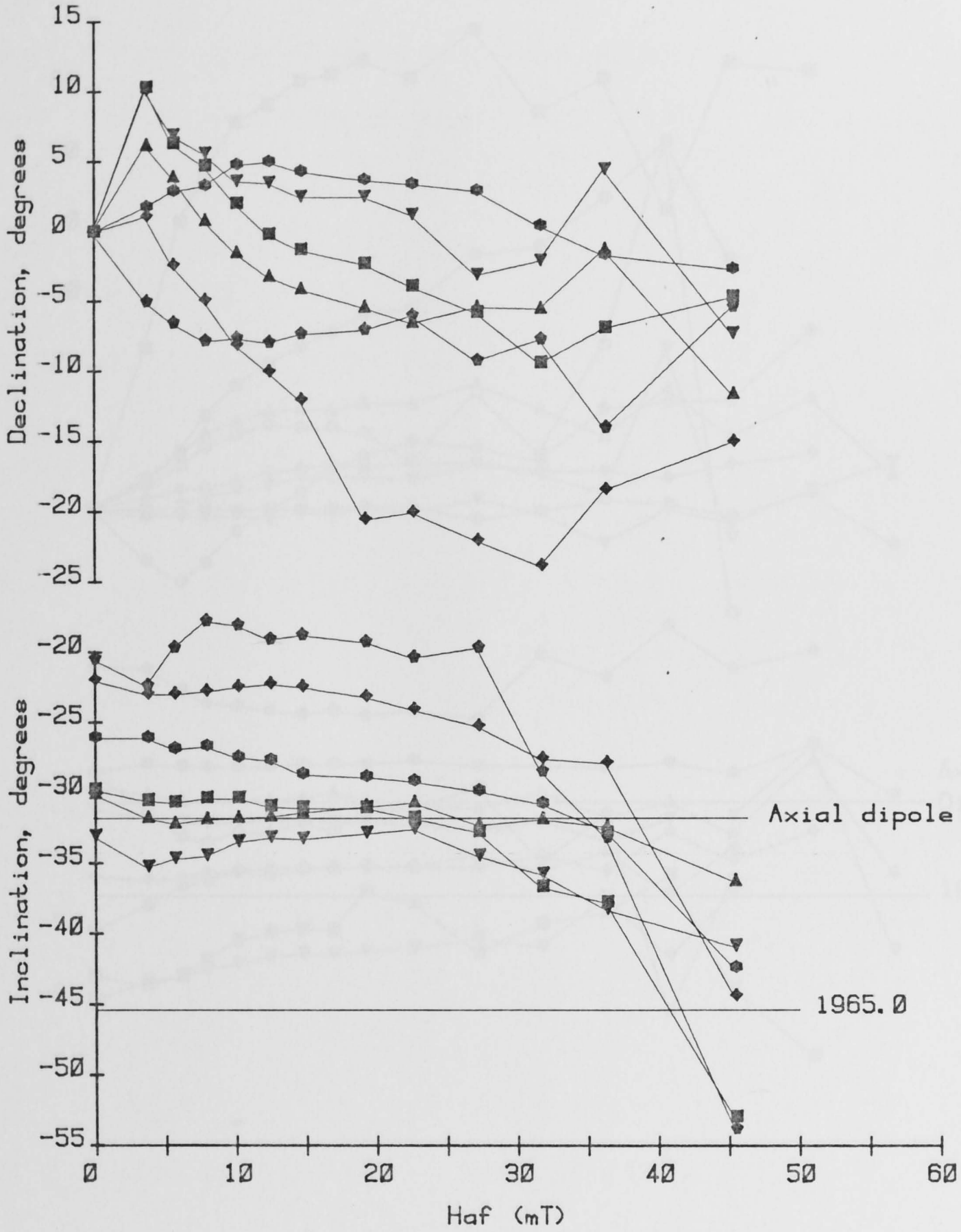

Figure 5.1 Effect of AF cleaning on core E2 pilot specimens.

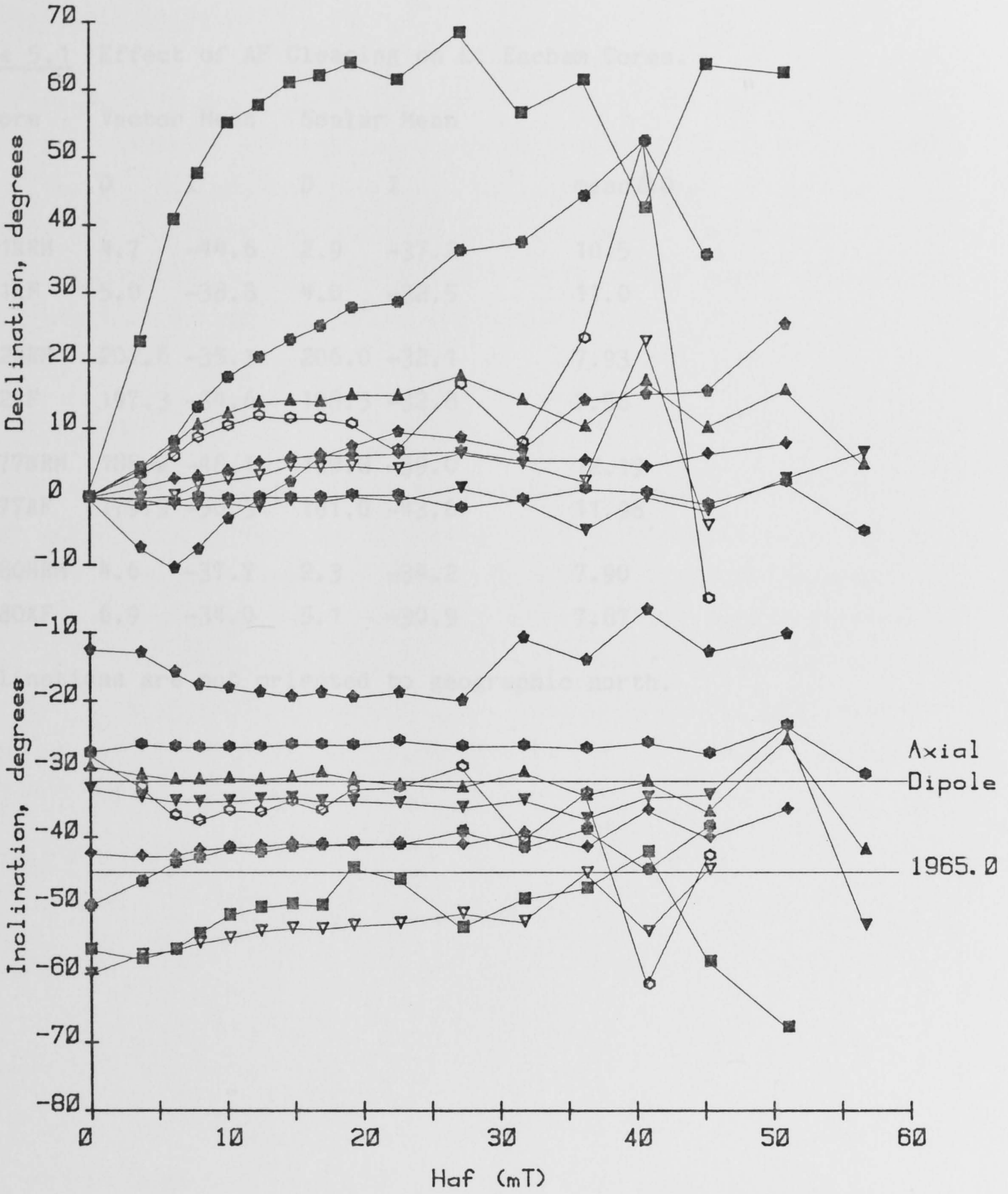

Figure 5.2 Effect of AF cleaning on core B4 pilot specimens.

Table 5.1 Effect of AF Cleaning on L. Eacham Cores.

Core	Vector Mean		Scalar Mean		
	D	I	D	I	mean $\Delta\theta$
E1NRM	4.7	-44.6	2.9	-37.2	10.5
E1AF	5.0	-38.8	4.0	-32.5	11.0
E2NRM	202.6	-35.1	206.0	-32.1	7.93
E2AF	197.3	-34.6	198.5	-32.8	7.56
E77NRM	188.2	-48.1	189.8	-39.0	12.19
E77AF	179.9	-50.3	181.0	-43.6	11.98
E80NRM	4.6	-37.7	2.3	-34.2	7.90
E80AF	6.9	-34.0	5.1	-30.9	7.87

*Declinations are not oriented to geographic north.

5.2 Data Processing.

Before data from the different cores within a lake can be stacked there are a number of corrections which must be applied to them. These include the gap corrections and depth scaling described in section 3.3 and 'sieving' to remove inconsistent pairs of data. It is also necessary to compensate for non-vertical entry of the corer and twisting of the core tube during the coring process.

5.2.1 Sieving.

Pairs of specimens were taken from each horizon in a core. The angular difference between the directions for each of the pairs may be used to detect highly abberrant data. Barton (1978, p1.17) suggests using a sieving procedure and rejecting data with an angular difference greater than some set value, which is determined by the quality of the data. The mean angular differences, $\Delta\theta$, between pairs of specimens at the same level in each core are listed below for L. Barrine. Similar data for L. Eacham are in Table 5.1.

Table 5.2

Core	mean $\Delta\theta(^{o})$
B1AF	23.79
B3AF	10.61
B4AF	11.36
B5AF	8.22
B7AF	12.80

It may be seen that the data quality is poor compared with, for example, the L. Keilambete sequence from S. E. Australia. In the L. Keilambete cores the mean $\Delta\theta$ after AF cleaning varied only between 3.6^{o} and 6.6^{o} (Barton 1978, p3.39).

A compromise must be achieved between inclusion of unreliable data and a loss of information through eliminating too much data. A value of 20^{o} was chosen as the critical divergence angle, which for most of the cores resulted in a culling of slightly less than 10% of the data. In core B1 however the percentage was much higher (about 30%). This may have been due to the different AF cleaning procedure used. However, in view of the low Q-ratios in this core it seems more likely that it is a

reflection on the stability of the magnetic remanence.

Figure 5.3 shows the effect of sieving on core B4. Even after sieving there remain a number of outlying points, particularly in the declination record. Physical disturbance of the sediment during coring, transportation or measurement on the spinner magnetometer may be contributing to these.

5.2.2 Detrending of Declinations.

As noted earlier (sect. 2.2.2) most cores showed a trend in declination along their lengths as a result of twisting of the core tube during coring. These trends were estimated by performing a least squares linear regression, and are given in Table 5.3.

A right hand screw (RHS) of the core tube is here taken to mean that the trend of the declination is to decrease along the length of the core.

One of the problems with detrending the data is that it might well obscure real trends in the geomagnetic field. However, in the above procedure all the trends averaged to zero. This suggests

(1) that there is no linear trend in real declination and no bias in the direction of twisting of the corer or

(2) that the combination of a real trend in declination and the synthetic trend introduced by the corer is self-cancelling.

The second alternative seems unlikely.

5.2.3 Correction for the Tilt of Corer.

In a number of the L. Barrine cores which were opened it was evident from the orientation of the laminae that the corer had entered the sediment at an angle. An attempt was made to correct for this.

The apparent dips Θ and $\emptyset$ from the X and Y directions respectively were measured at a number of points along the length of the core (Figure 5.4). The angle $\emptyset$ could only be measured at gaps in the sediment. Some difficulty was experienced in doing this with any accuracy as the sediment had not always separated cleanly along a

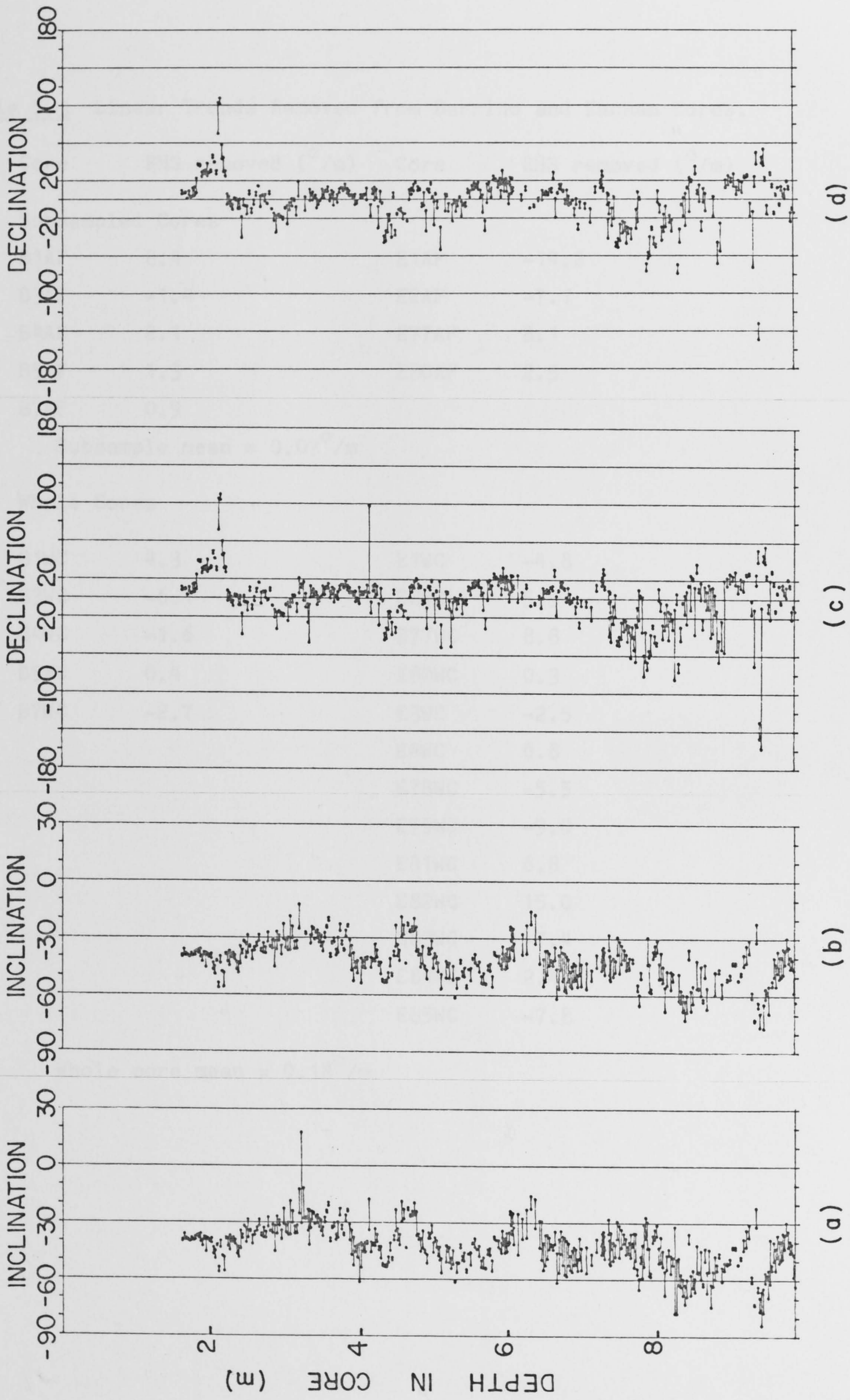

Figure 5.3 Effect of sieving on core B4. (a) and (c) are before, and (b) and (d) after sieving.

Table 5.3 Linear Trends Removed from Barrine and Eacham Cores.

Core	RHS removed (^{o}/m)	Core	RHS removed (^{o}/m)
Subsampled Cores			
B1AF	8.4	E1AF	-14.2
B3AF	-1.4	E2AF	-7.1
B4AF	2.1	E77AF	8.1
B5AF	1.3	E80AF	2.5
B7AF	0.9		
Subsample mean = 0.07^{o}/m			
Whole Cores			
B1WC	4.3	E1WC	-4.8
B3WC	-6.1	E2WC	5.9
B4WC	-1.6	E77WC	8.8
B5WC	0.4	E80WC	0.3
B7WC	-2.7	E3WC	-2.5
		E4WC	6.8
		E78WC	-5.5
		E79WC	-9.0
		E81WC	6.8
		E82WC	15.0
		E83WC	-7.4
		E84WC	2.4
		E85WC	-7.8

Whole core mean = 0.18^{o}/m

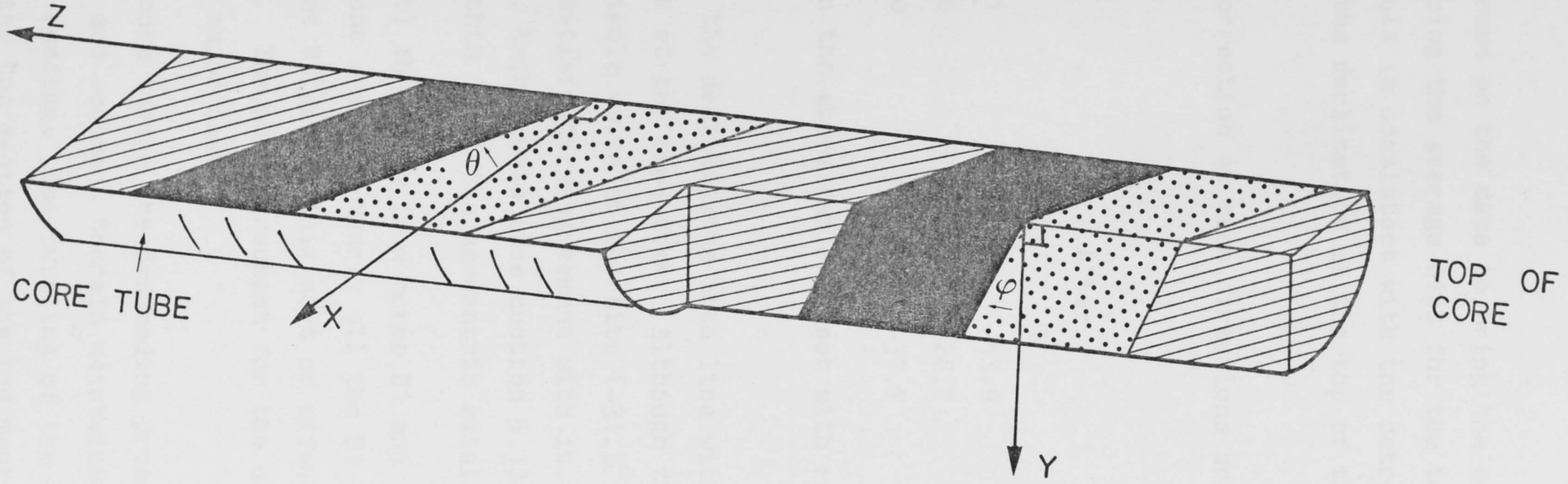

Figure 5.4 Section of core showing apparent dips from the X and Y directions. Cores are normally sectioned for sampling in the XZ plane.

lamination, thereby providing the true Y direction. Θ and Ø varied somewhat with depth probably due to the twisting of the core as it penetrated the sediment.

A rotation was performed on the data to bring the coordinate system back to the horizontal using the average dips for the top metre of sediment in the core. This is consistent with the detrending procedure which left the value of the declination at the top of the core unchanged.

The effects of the correction on mean directions are shown in Table 5.4.

Table 5.4

Core	Before		After	
	D	I	D	I
B1	114.5	-66.1	2.3	-43.9
B3	313.6	-40.6	325.2	-28.7
B4	39.8	-44.0	348.4	-37.7

The before declination in the above table is not with respect to geographic north.

Corrections to bring the declinations into line with geographic north were also performed at the same time. Although the data means move towards the axial dipole value at the site (-31.8^{o} for inclination) there is still far from satisfactory agreement with it. This is in direct contrast to the L. Eacham data (see section 5.1) for which the mean inclinations lie within 1^{o} of the geocentric axial dipole value.

Figures 5.5(a) and (b) show data from cores B1 and B3 plotted on the same diagram with different symbols. Nearly all the B1 data lie well to one side of the equivalent B3 data. This sort of offset is typical for all the L. Barrine cores. The poor agreement for the declination data can be attributed to two major causes

(1) Twisting of the core tube - the detrending procedure assumes that the top of the core and sediment therein maintained the same direction as the compass reading. The twisting of the core tube is likely to have affected the top section of the sediment most as it was subject to twisting throughout the coring process as the corer penetrated to the deeper sediment.

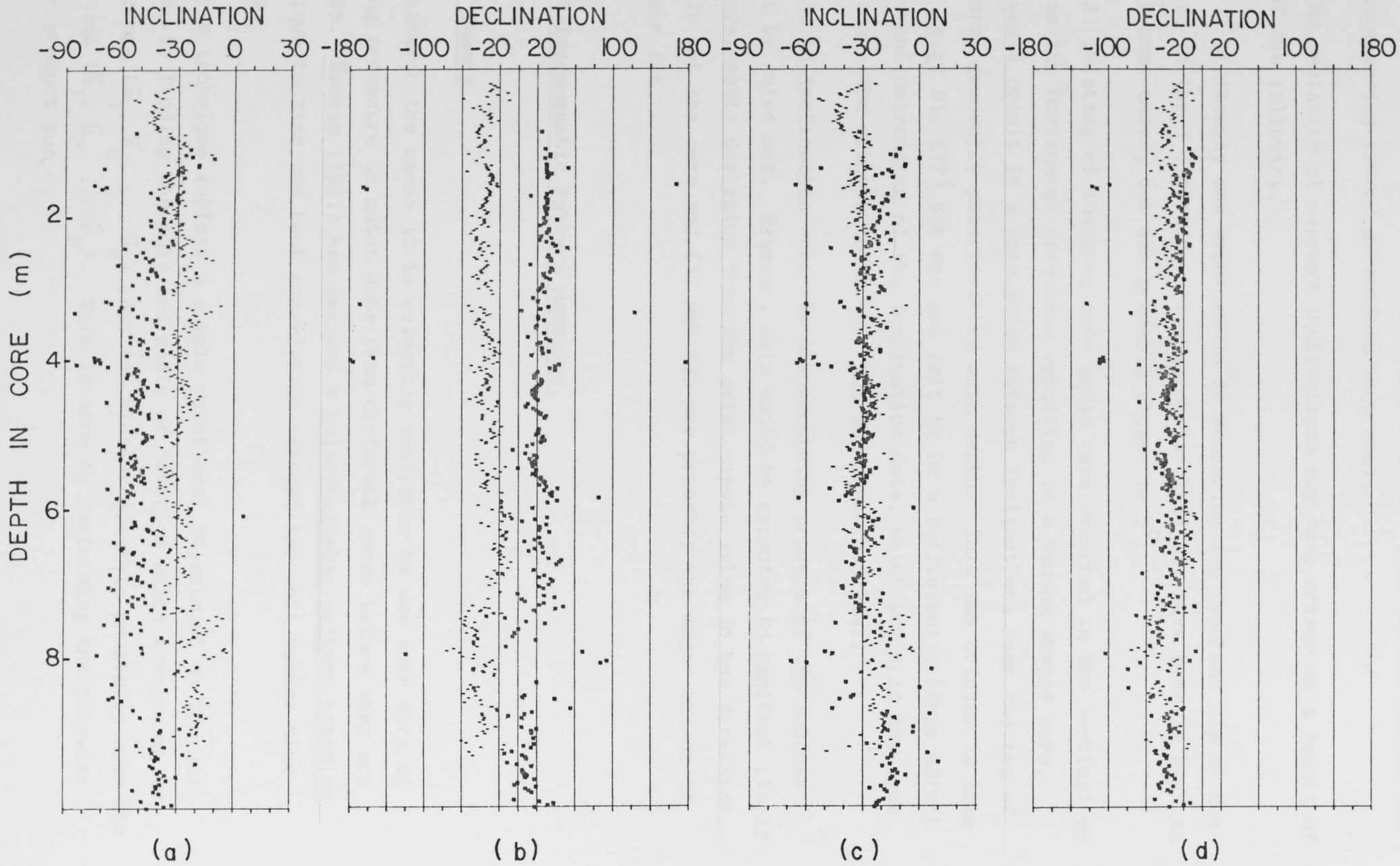

Figure 5.5 Directional data from cores B1(▪) and B3 (′). (a) and (b) before, and (c) and (d) after palaeomagnetic pattern matching.

(2) Tilting of the compass - the compass was only intended to operate when level and if tilted at more than 10 or 15° from the horizontal did not necessarily record directions accurately.

The deviation of average inclinations may have arisen as a result of one of the following.

(1) Difficulty was experienced in measuring the apparent dip of the laminae in the Y direction - the error involved may have been as high as 10° in some cases, but was probably closer to 5°.

(2) Twisting of the core tube could have occurred in the vertical as well as the horizontal direction resulting in a banana shaped core. This would result in a good match between inclinations near the top of the core, gradually deteriorating with depth. This was evident in some cores (e.g. B1, E77) but was not felt to be a sufficiently large effect to warrant detrending of the inclination data, which would in any case complicate the attempt to recover the geomagnetic signal.

(3) An inclination error in the recording process of the sediment cannot be ruled out. However, this would be expected to manifest itself in a systematic deviation from the axial dipole value in one direction. This is not the case and (1) and (2) are probably the major causes of the poor fit.

5.3 Palaeomagnetic Pattern Matching.

5.3.1 Theory

Whatever the cause it is evidently desirable to use some sort of fitting procedure to match data from different cores before they are stacked. Denham (1981) has devised a palaeomagnetic pattern matching technique to find the best correlation between two unit vector time series.

This technique employs a simple rotational adjustment on the unit sphere, by finding the pole and angle of rotation which brings one set of vectors ($\bar{a}_1$, $\bar{a}_2$, ... $\bar{a}_N$) into the closest possible proximity with the other set ($\bar{b}_1$, $\bar{b}_2$, ... $\bar{b}_N$). This is done by maximising the pairwise scalar product sum

$$R = \sum_{i=1}^{N} r\bar{a}_i.\bar{b}_i \qquad (1)$$

where r is the unknown pure rotation operator required on the $\bar{a}_i$.

The conventional least squares formulation of this problem has no unique solution (since the data are unit vectors), so Denham suggests the following iterative procedure to solve (1). Given an arbitrary trial pole of rotation $\bar{P}$ (a unit vector) the optimum rotation angle Θ about $\bar{P}$ is given by

$$\Theta = \arctan \frac{\bar{P}. \sum_{i=1}^{N} \bar{a}_i x \bar{b}i}{\sum_{i=1}^{N} (\bar{a}_i x \bar{P}).(\bar{b}_i x \bar{P}).} \qquad (2)$$

On finding Θ series $\bar{a}_i$ is rotated towards series $\bar{b}_i$ about $\bar{P}$. A new $\bar{P}$ is chosen, Θ recalculated and the iteration proceeds until R no longer increases.

Denham suggests using the successive values of the pairwise vector cross product sum scaled to unit length for the successive directions of $\bar{P}$, i.e.

$$\bar{P} = \frac{\sum \bar{a}_i x \bar{b}_i}{\left| \sum \bar{a}_i x \bar{b}_i \right|} \qquad (3).$$

This seems reasonable since for any two vectors $\bar{a}_i$ and $\bar{b}_i$ in the matching time series, with angular difference Θ_i

$$\sin(\Theta_i) = \bar{a}_i x \bar{b}_i$$

$$\cos(\Theta_i) = \bar{a}_i.\bar{b}_i$$

$$= (\bar{a}_i x \frac{\bar{a}_i x \bar{b}_i}{\left|\bar{a}_i x \bar{b}_i\right|}). \quad (\bar{b}_i x \frac{\bar{a}_i x \bar{b}_i}{\left|\bar{a}_i x \bar{b}_i\right|}).$$

Hence

$$\Theta_i = \arctan\left(\frac{\bar{a}_i x \bar{b}_i}{\bar{a}_i.\bar{b}_i} \right).$$

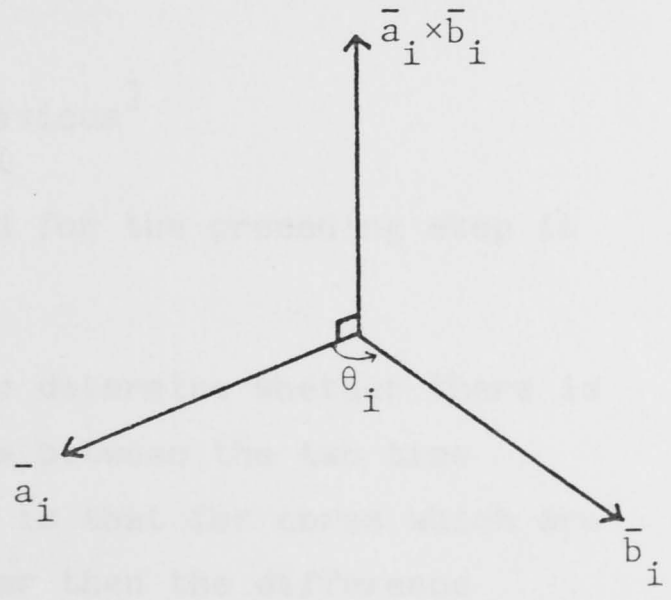

The Θ obtained in (2) is thus effectively a core average of the individual Θ_i.

McFadden (1982) has pointed out that as the iteration proceeds towards completion there is the potential for (3) to provide an inaccurate estimate of the pole. This results from the estimate of the pole $\bar{P}_{est}$ being made up of two parts

$$\bar{P}_{est} = \bar{P}_1 + \bar{P}_2$$

where $\bar{P}_1 = (r\bar{a}_i x \bar{b}_i)$ for those terms with

$$\text{signum}[(r\bar{a}_i x \bar{b}_i).\bar{P}_c] = +1$$

and $\bar{P}_2 = (r\bar{a}_i x \bar{b}_i)$ for those terms with

$$\text{signum}[(r\bar{a}_i x \bar{b}_i).\bar{P}_c] = -1$$

$\bar{P}_c$ being the correct pole of rotation. The signum function is defined by

$$\begin{aligned} \text{signum}(x) &= +1, \quad x > 0 \\ &= -1, \quad x < 0 \\ &= 0, \quad x = 0. \end{aligned}$$

$\bar{P}_1$ and $\bar{P}_2$ will be oppositely directed estimates of the correct axis of rotation and will tend to cancel each other in (3) the estimate of $\bar{P}_c$. The resulting direction calculated for $\bar{P}_{est}$ will then depend on the errors in the axis estimates $\bar{P}_1$ and $\bar{P}_2$ rather than on $\bar{P}_1$ and $\bar{P}_2$ themselves. McFadden suggests improving the efficiency of the iteration by choosing each new pole of rotation $\bar{P}_{est}$ as the direction of

$$\bar{P}_{est} = \sum_{i=1}^{N} (r\bar{a}_i x \bar{b}_i) \text{ signum}[(r\bar{a}_i x \bar{b}_i).\bar{P}_{previous}]$$

where $\bar{P}_{previous}$ is the pole of rotation used for the preceding step in the iteration.

McFadden (1982) also suggested a test to determine whether there is actually any significant rotation detectable between the two time series. The basic assumption for this test is that for cores which are correctly aligned with respect to one another then the difference vectors will be randomly distributed without any systematic component.

The effective pole of rotation as a result of the successive iterations $\bar{P}_{eff}$ is calculated from

$$\bar{P}_{eff} = (r\bar{X} - \bar{X})x(r\bar{Y} - \bar{Y})$$

(Denham, 1981), where $\bar{X}$ and $\bar{Y}$ are unit vectors in those directions.

The difference vectors are then transformed into a set of measurements s_i on the nominal scale

$$s_i = \text{signum}[(\bar{a}_i x \bar{b}_i).\bar{P}_{eff}].$$

The sign of s_i just determines in which direction about $\bar{P}_{eff}$ a given datum $\bar{a}_i$ would have to be rotated in order to lie closest to its counterpart $\bar{b}_i$. If the cores are correctly aligned then the number n of a given sign in the sequence will be a random observation from a binomial distribution of size N with probability 0.5. θ_{eff} determines the direction of rotation so a one tailed test is performed and provided

$$(1/2)^N \sum_{i=1}^{n} \frac{N!}{(N-i)!i!} \quad < .05 \text{ or } > .95$$

it may be assumed that, at the 95% level of confidence the 2 cores are rotated relative to each other.

In practice the values of N are generally too large for use of the binomial distribution to be convenient and a chi-square test with one degree of freedom and 0.1 level of significance is used instead (0.1 significance level is used because the upper tail of the chi-square distribution includes both the tails of the binomial distribution). Then if

$$d^2/N > 2.71 \qquad (4)$$

where d = (no. of +'s) - (no. of -'s) , then the null hypothesis of no relative rotation of the two cores can be rejected at the .05 level of significance. If no a priori assumption is made about the direction of rotation then a two tailed test is required. The critical value in (4) then becomes 3.84.

The order of the signs in the sequence s_i for the completely rotated cores provide information regarding trends in the data. For example a sequence (++++++-----) would suggest that there are different trends superimposed in the variations in the two cores. A one sample runs test (Siegel 1956, p52-55) can be used to determine how many runs of +'s and -'s one might expect in a sample of size N.

Let r be the number of runs in the sequence s_i and n_1 and n_2 be the number of +'s and -'s respectively. For large samples (n_1 or n_2 > 20) a good approximation to the sampling distribution of r is the normal distributuion with

$$\mu = \frac{2n_1n_2}{n_1+n_2} + 1$$

and $$\sigma^2 = \frac{2n_1n_2(2n_1n_2-n_1n_2)}{(n_1+n_2)^2(n_1+n_2-1)}$$

The normal distribution table for $z = (r-\mu)/\sigma$ can be used to determine whether r is significantly less than would be expected and hence whether there is a difference trend.

5.3.2 Practical Application.

Denham's (1981) algorithm described above along with the modifications and tests described by McFadden (1982) were used to provide a matching routine for all the cores collected. Although it was only really essential for the L. Barrine data it was found that a considerable improvement in the resolution occured when it was applied to the Eacham data before stacking.

One core from each lake was chosen as a master core using the criteria that the mean inclination should be close to the expected axial dipole value and that the record should be as smooth as possible (this avoided the problem of trying to match spikes in the record). B3 was used for Barrine and E2 for Eacham.

Linear interpolation was then applied to the declination and inclination records separately, in order to provide data for matching pairs on an equally spaced grid. The interpolated records were truncated to the length of the shorter one. Then an optimum fit was found using the pattern matching algorithm. The effective pole and angle of rotation were calculated and these applied to the original data.

In practice only 1 or 2 iterations were usually required to reach the stage where a rotation between the 2 cores could no longer be detected at the 95% significance level used. However, none of the cores passed the one sample runs test. This seemed to suggest that as far as these data are concerned the original postulate that the θ_i are independent may not have been very reasonable. This is attributable to two causes.

(1) The detrending may be inadequate. Possibly a more sophisticated detrending procedure should have been used for the declinations, although this might have masked real field trends.

(2) Physical disturbance of blocks of sediment containing several specimens could have occured during coring, transportation, measurement on long core spinner, or even as a result of slumping of the sediment <u>in situ</u> after acquisition of its PDRM.

The final s_i sequences were examined and it appeared that generally the failure to pass the 1-sample runs test resulted from clumping of the signs into larger groups than expected, rather than from a trend down the cores. This seemed to suggest that the second of the above causes is more influential.

Figure 5.5 shows data from cores B1 and B3 on the same plot before and after the application of the pattern matching. The table below shows the improvement on Denham's (1981) fitting criterion $\Delta = \cos^{-1}(R/N)$ between the fitted core and the master core as a result of the pattern matching. The within core value is calculated from successive pairs of data down the core and provides some indication of the <u>best</u> possible match that might be expected (N.B. these are from cores which have been sieved at 20^{o}).

Table 5.5

Core	Δ_{before}	Δ_{after}	$\Delta_{within\ core}$
B1	37.4	24.9	9.1
B3	not rotated		9.0
B4	30.0	22.2	14.8
B5	36.1	25.7	10.1
B7	27.5	19.3	10.2
E1	34.2	25.7	14.9
E2	not rotated		9.5
E77	38.4	26.1	17.7
E80	30.0	22.2	14.5

5.4 Stacked Results.

After the above corrections had been applied all the data within each lake were combined to yield a stack of the results. These are shown in Figures 5.6 (Barrine) and 5.7 (Eacham), plotted as a function of depth in the master core from each lake.

These were then transformed to a time scale using the fits derived in section 3.4 from the radiocarbon dates. Figure 5.8 shows the Eacham data on an uncalibrated time scale while Figure 5.9 is the calibrated version. Figure 5.10 shows Barrine data adjusted to the calibrated time scale.

These records are still extremely scattered, despite the sieving procedure used to discard inconsistent data. Figure 5.11 shows the standard deviations from the mean intensity (+ signs), inclination (triangles) and declination (circles), when their scalar values are averaged over 100 year blocks for Barrine and 60 year blocks for Eacham. Intensity means and standard deviations were calculated on a log normal basis. Standard deviations of declinations and inclinations are in degrees. Low standard deviations of intensity should arise as a direct consequence of the stacking technique used. However, the rapid fluctuations in intensity occurring in many sections of the cores mean that high standard deviations can result from very small mismatches in the depth scales.

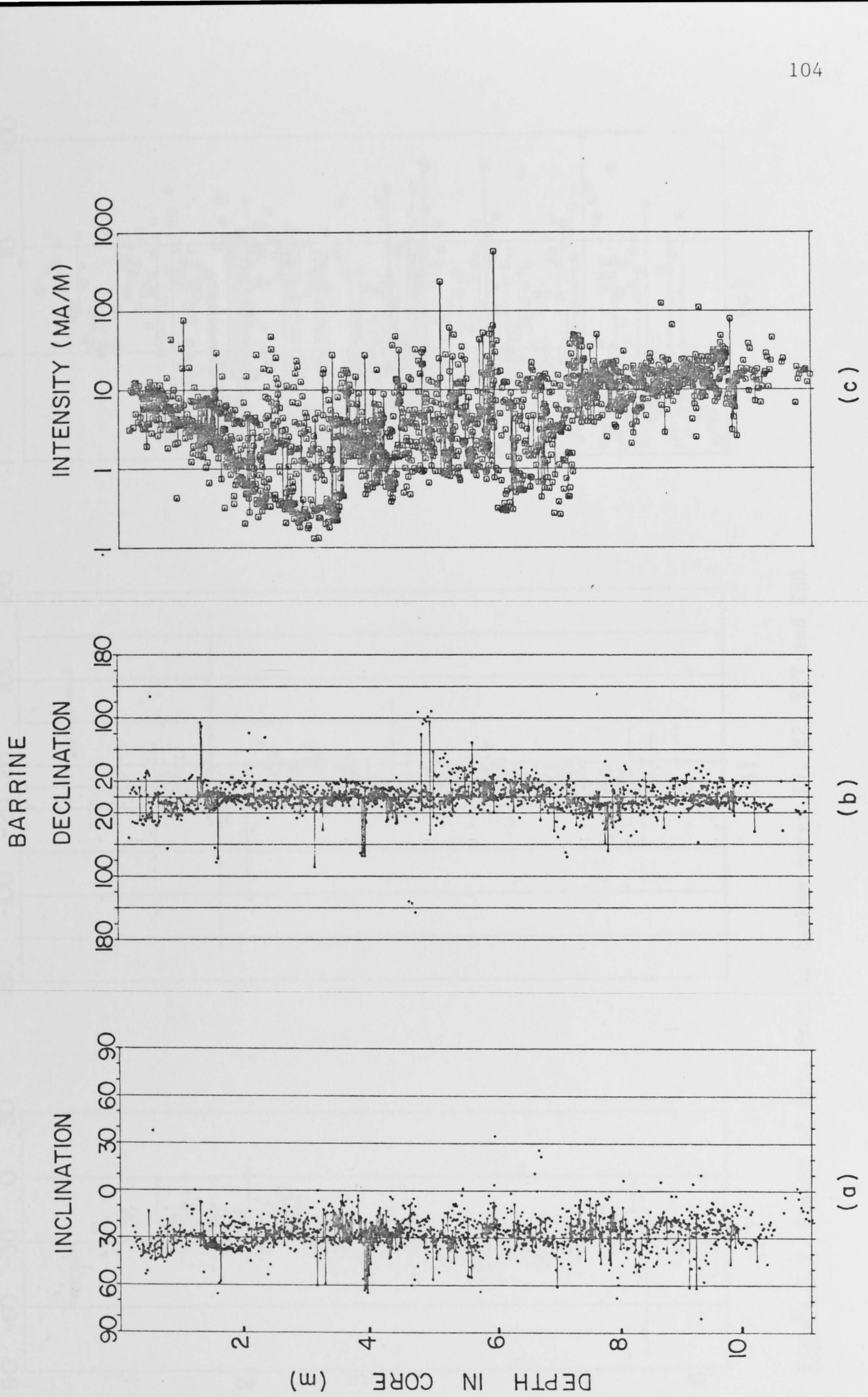

Figure 5.6 Stacks of data from L. Barrine cores B1, B3, B4, B5 and B7.

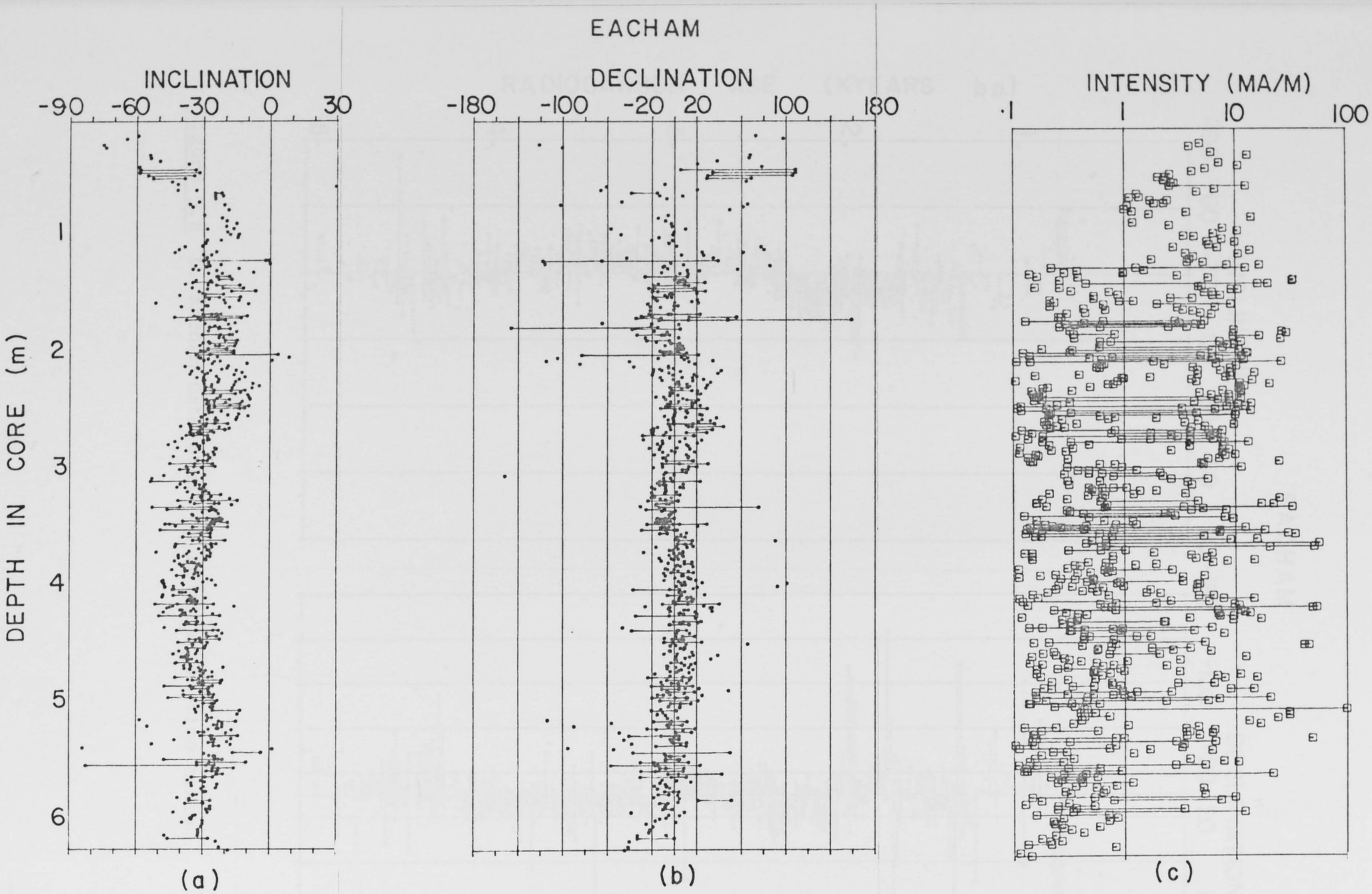

Figure 5.7 Stacks of data from L. Eacham cores E1, E2, E77 and E80.

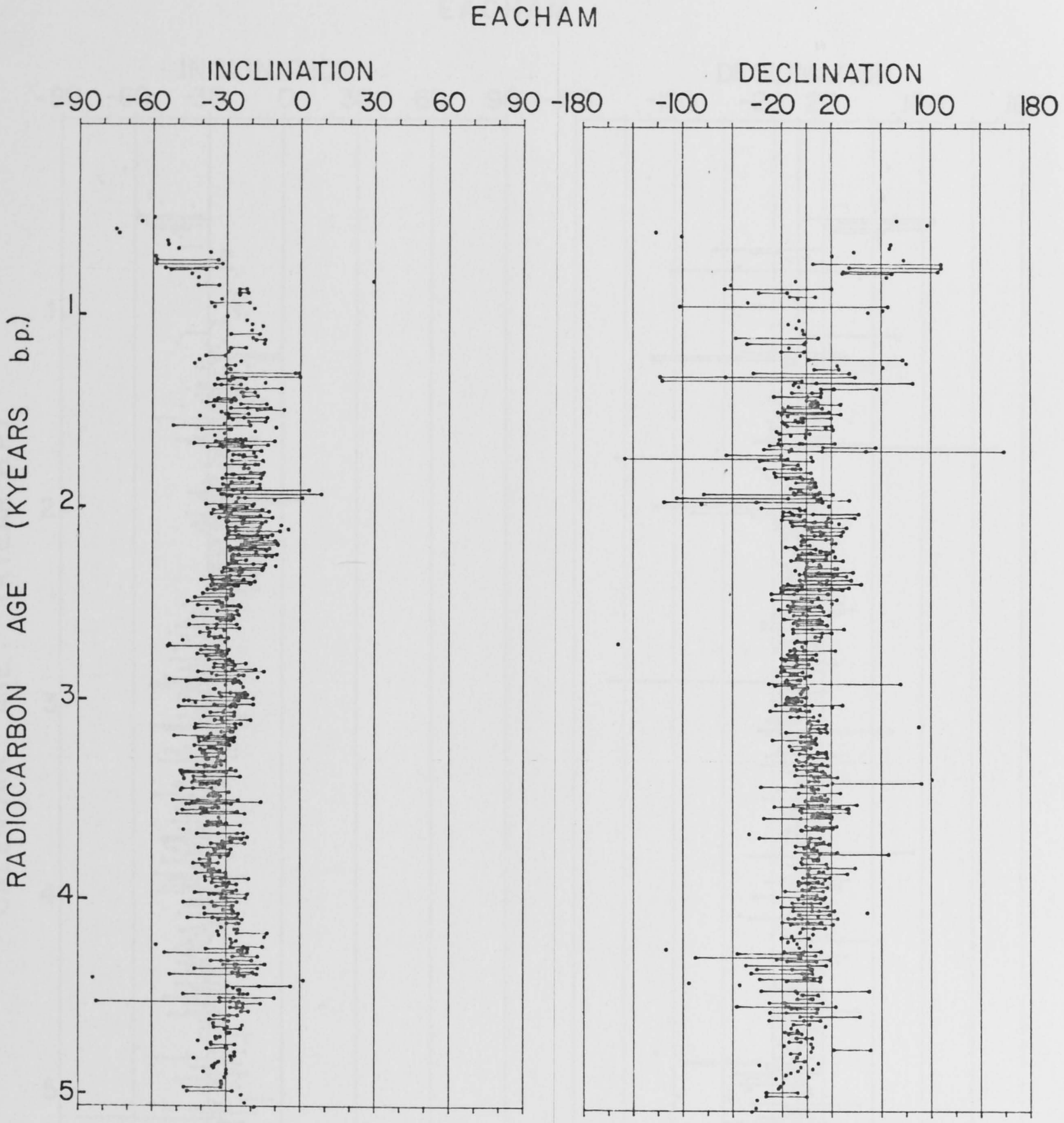

Figure 5.8 L. Eacham data stack on radiocarbon time scale.

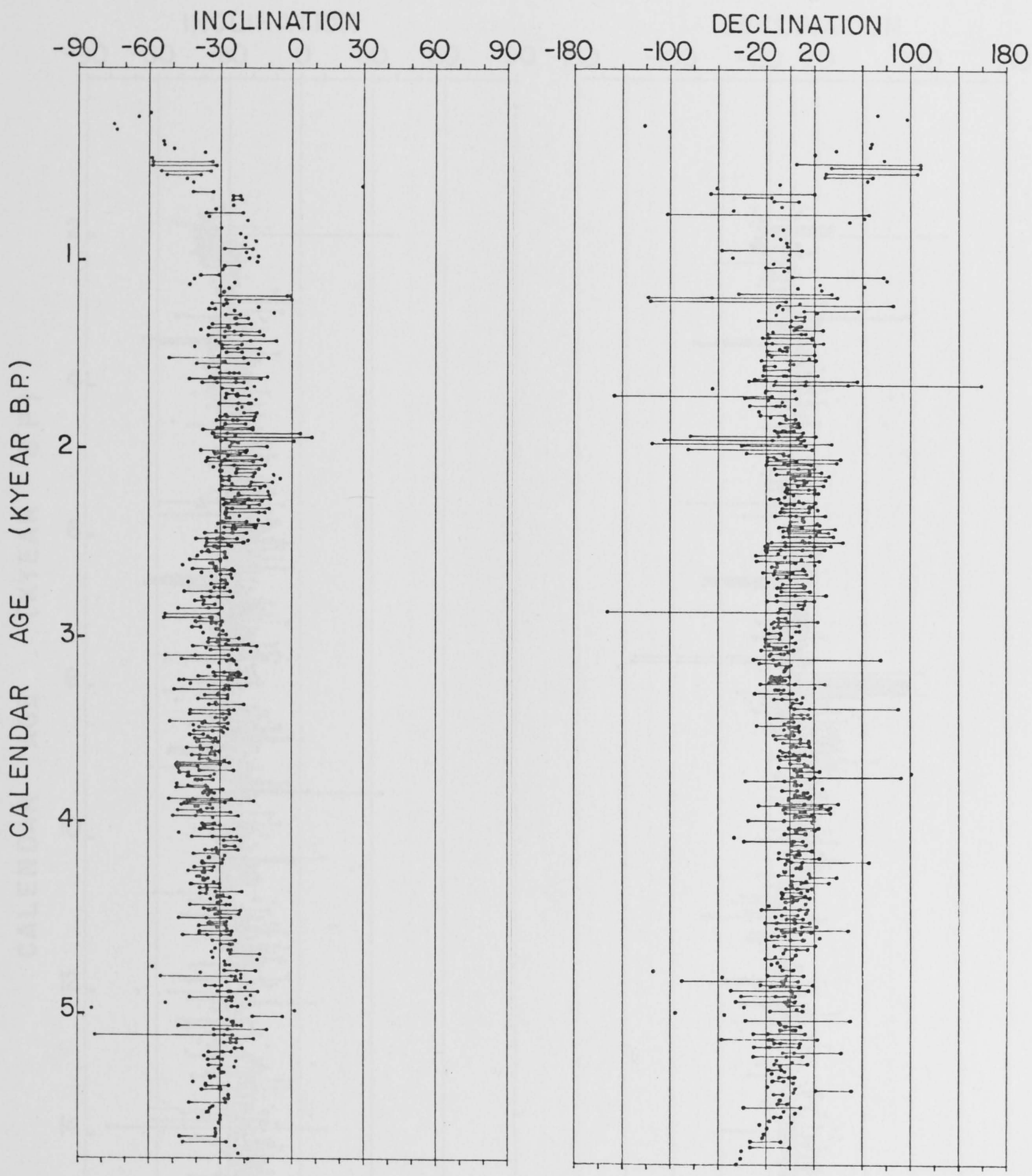

Figure 5.9 L. Eacham data stack on calibrated time scale.

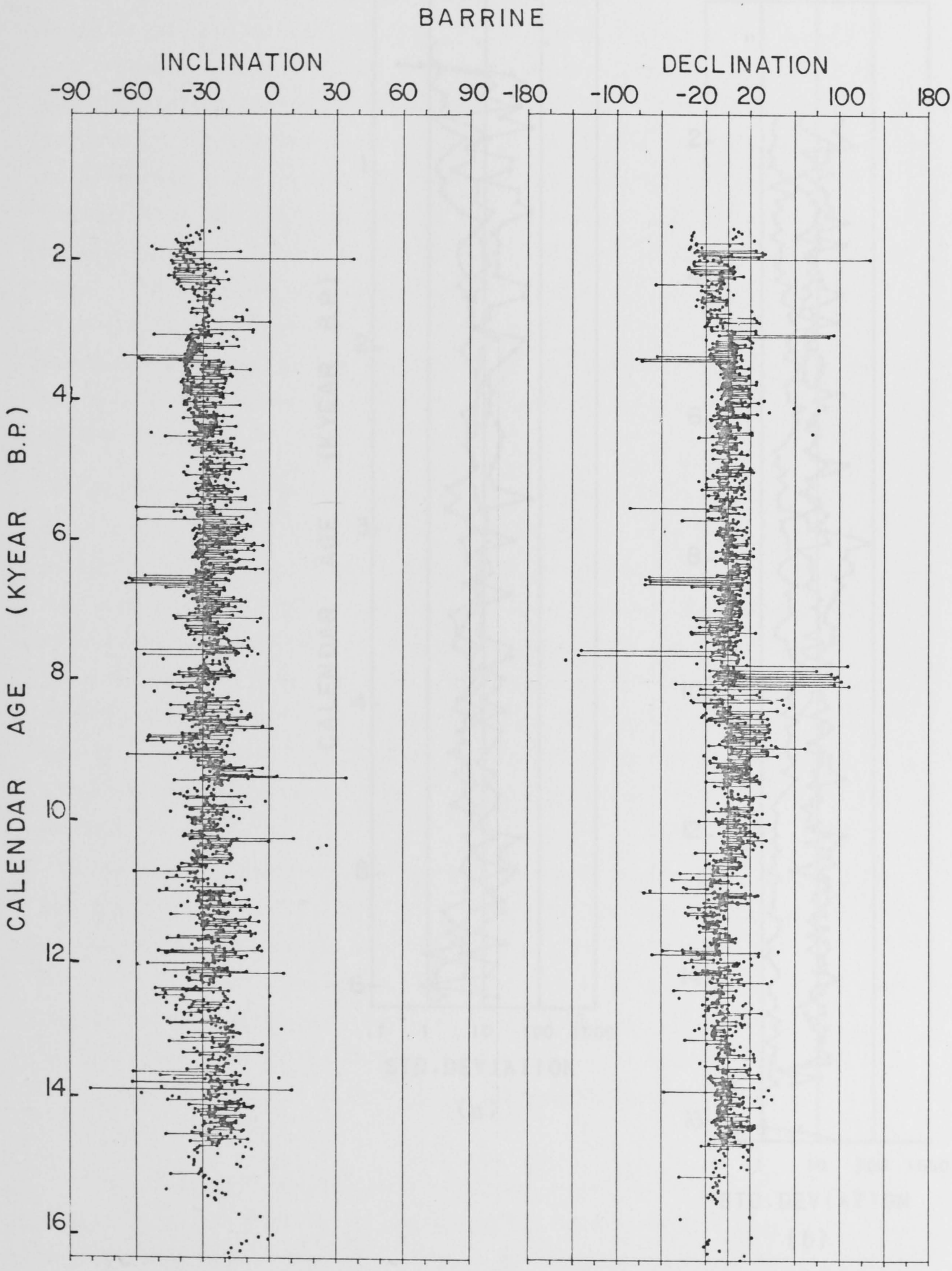

Figure 5.10 L. Barrine data stack on calibrated time scale.

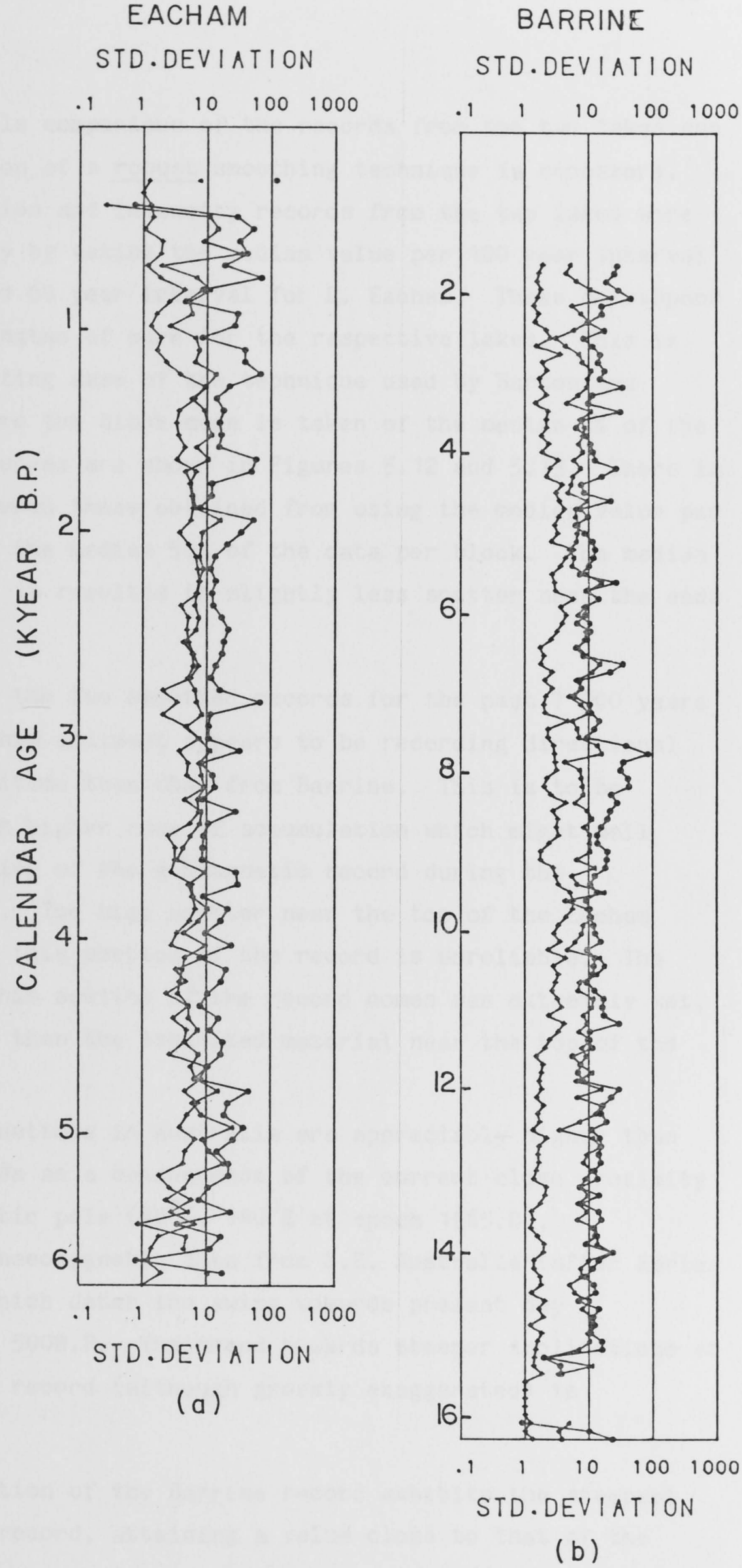

Figure 5.11 Standard deviations from the mean for intensities (+ signs), inclinations (triangles) and declinations (circles). Barrine data are averaged over 100 year blocks and Eacham over 60 year blocks.

Before a reasonable comparison of the records from the two lakes can be made the application of a robust smoothing technique is necessary. Declination, inclination and intensity records from the two lakes were smoothed independently by taking the median value per 100 year interval for the L. Barrine and 60 year interval for L. Eacham. These correspond to 7.5cm and 6.5cm lengths of core for the respective lakes. This is analogous to the limiting case of the technique used by Barton and McElhinny (1981), where the block mean is taken of the median x% of the data. The smoothed curves are shown in Figures 5.12 and 5.13. There is little difference between those obtained from using the median value per block and the mean of the median 50% of the data per block. The median was used here because it resulted in slightly less scatter near the ends of the records.

Figure 5.14 shows the two smoothed records for the past 7 000 years side by side. L. Eacham sediment appears to be recording directional swings of higher amplitude than that from Barrine. This is to be expected from its much higher rate of accumulation which might well result in less smoothing of the geomagnetic record during the acquisition of a PDRM. The high scatter near the top of the Eacham record indicates that this section of the record is unreliable. The material from which this section of the record comes was extremely wet, and less consolidated than the laminated material near the top of the L. Barrine cores.

Present day inclinations in Australia are appreciably higher than the axial dipole values as a consequence of the current close proximity of the southern magnetic pole (66^{o}S, 140^{o}E at epoch 1965.0). Figure 5.15 shows archaeomagnetic data from S.E. Australia (after Barton and Barbetti, 1982) which dates the swing towards present day inclinations at about 500B.P. The trend towards steeper inclinations at the top of the Eacham record (although grossly exaggerated) is consistent with this.

The uppermost section of the Barrine record exhibits the steepest inclinations in that record, attaining a value close to that of the present day field. However, in view of the poor reproducibility between the two lakes of the rest of the records it would be unreasonable to draw any inferences from this. The shortness of the Eacham record,

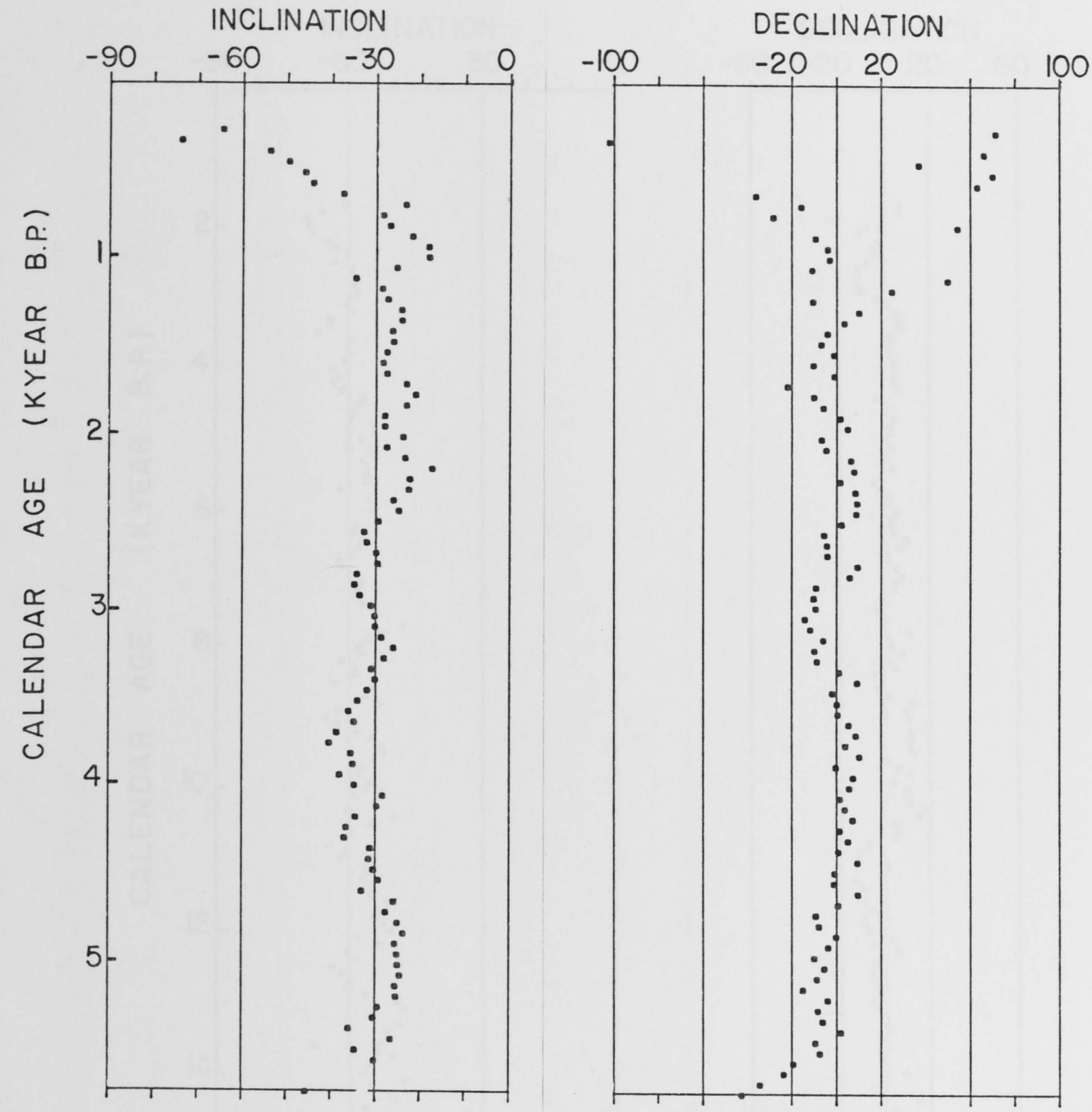

Figure 5.12 Smoothed declination and inclination records for L. Eacham.

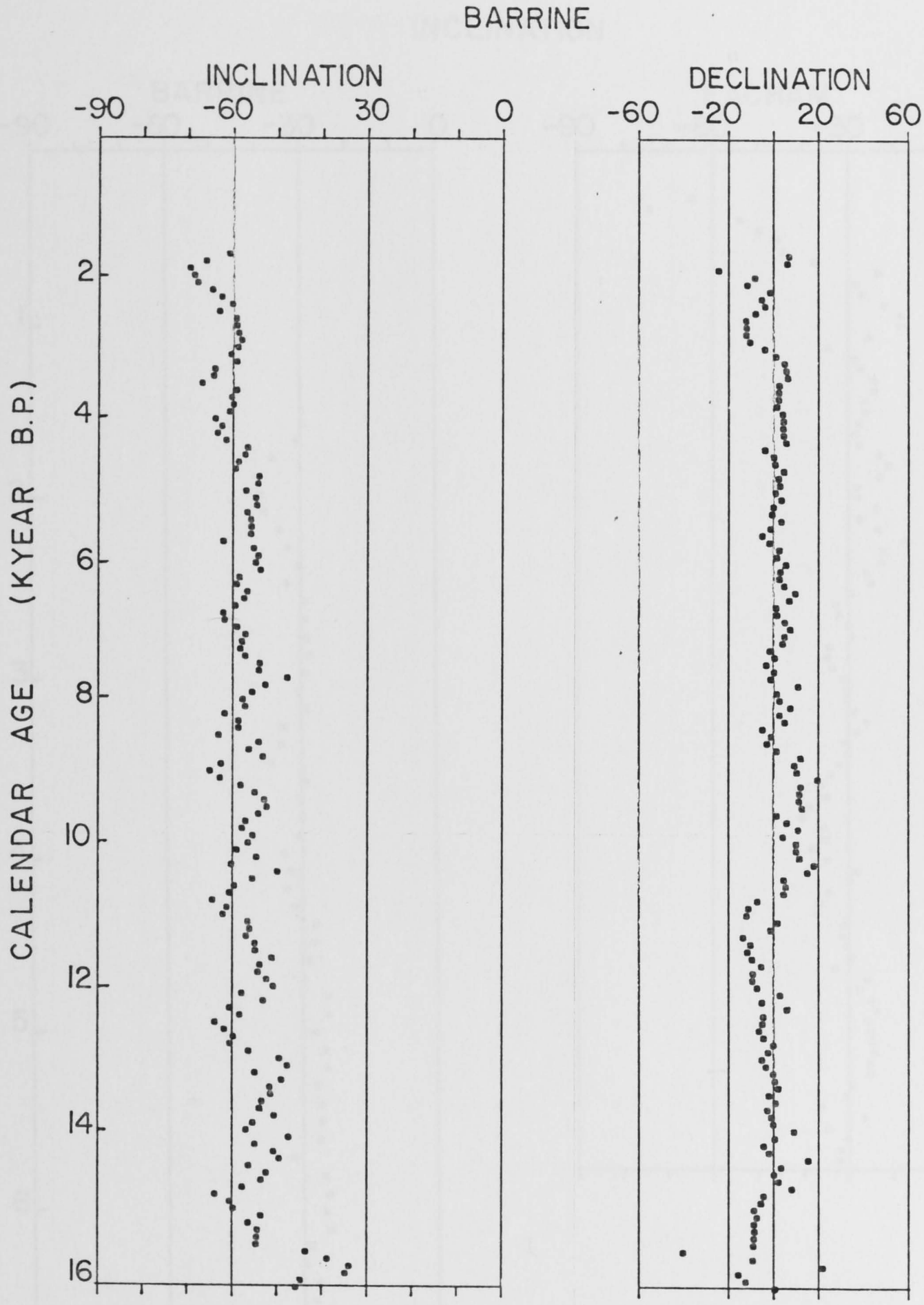

Figure 5.13 Smoothed declination and inclination records for L. Barrine.

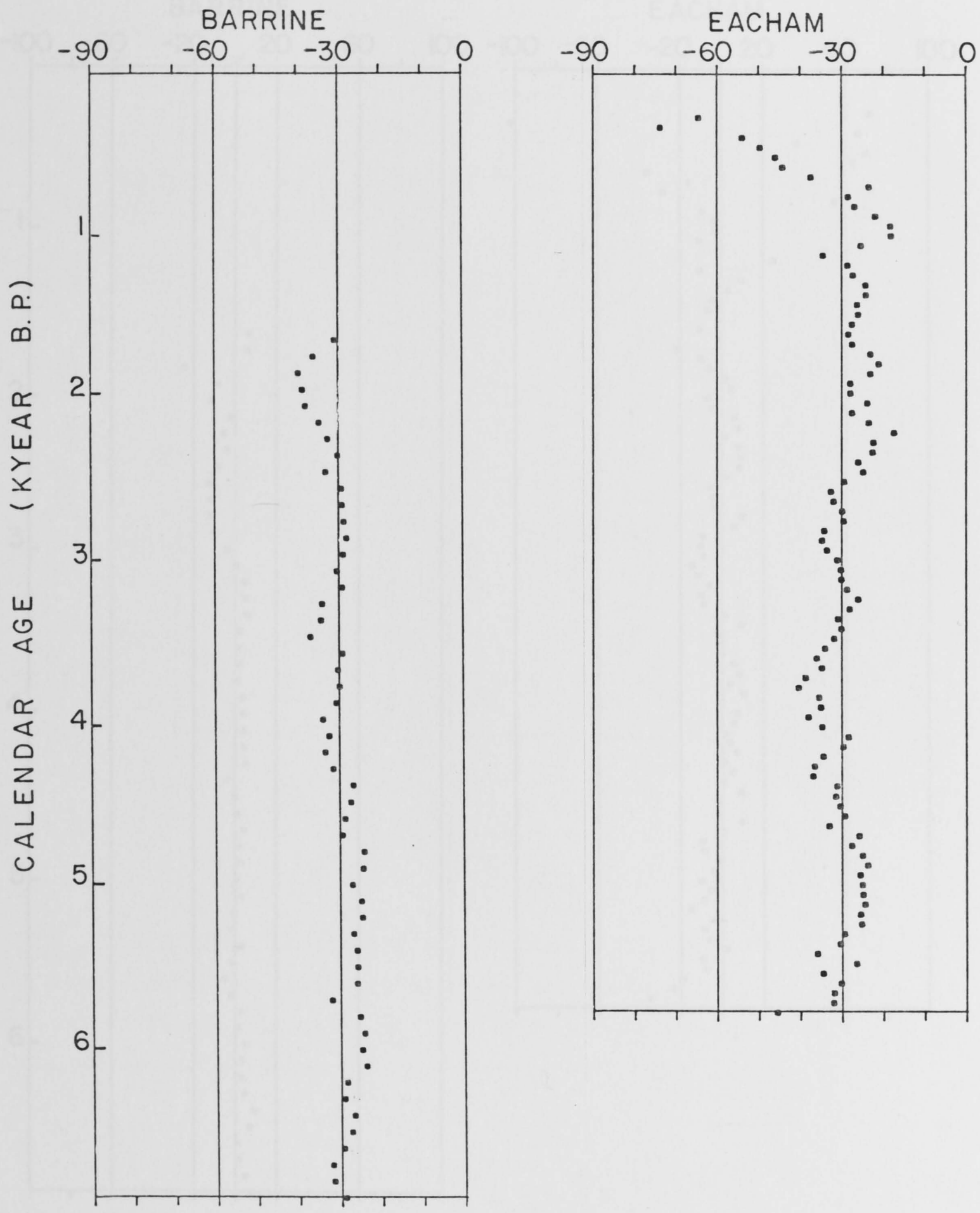

Figure 5.14 (a) Smoothed inclination records from Barrine and Eacham over the past 7 000 years.

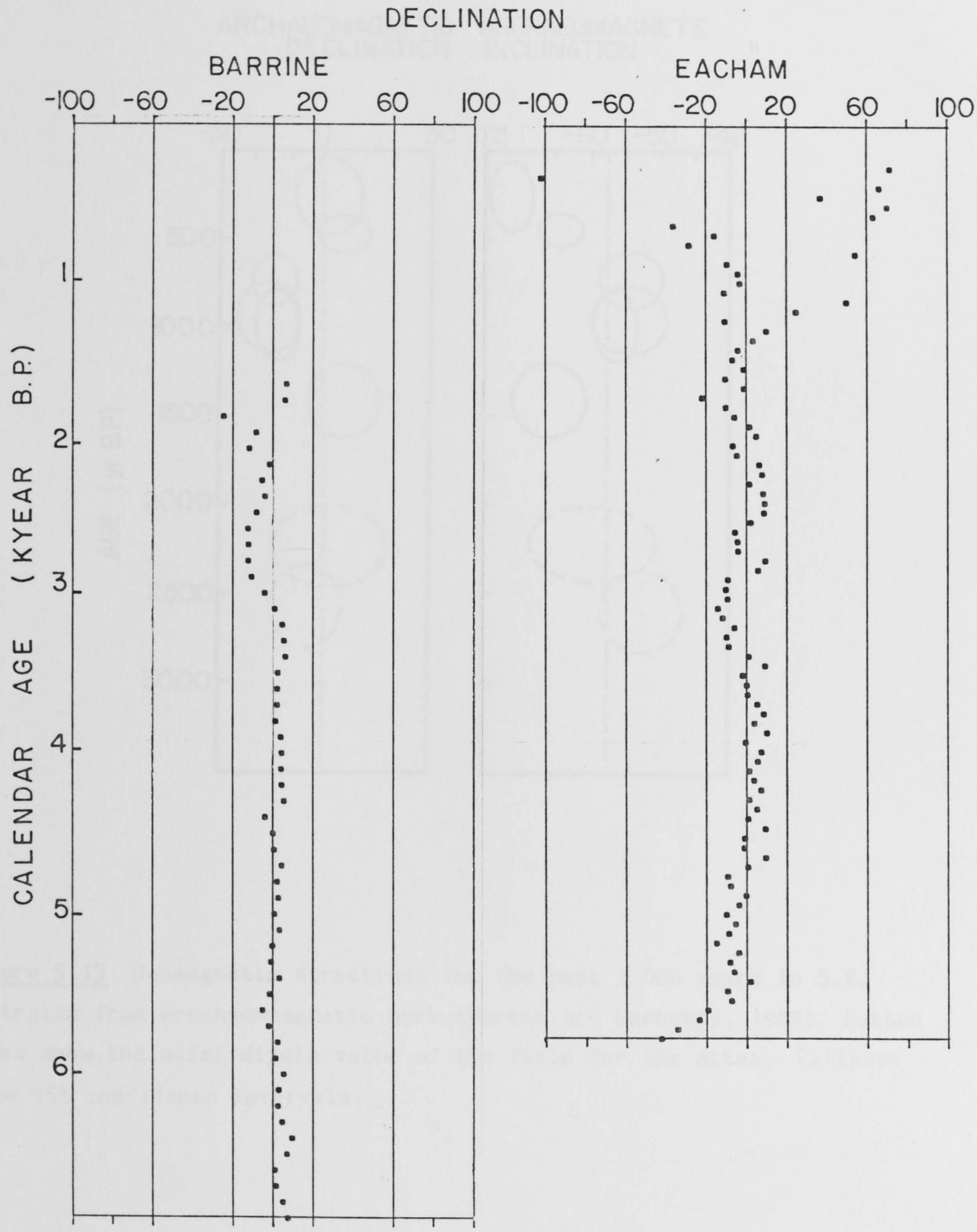

Figure 5.14 (b) Smoothed declination records from Barrine and Eacham over the past 7 000 years.

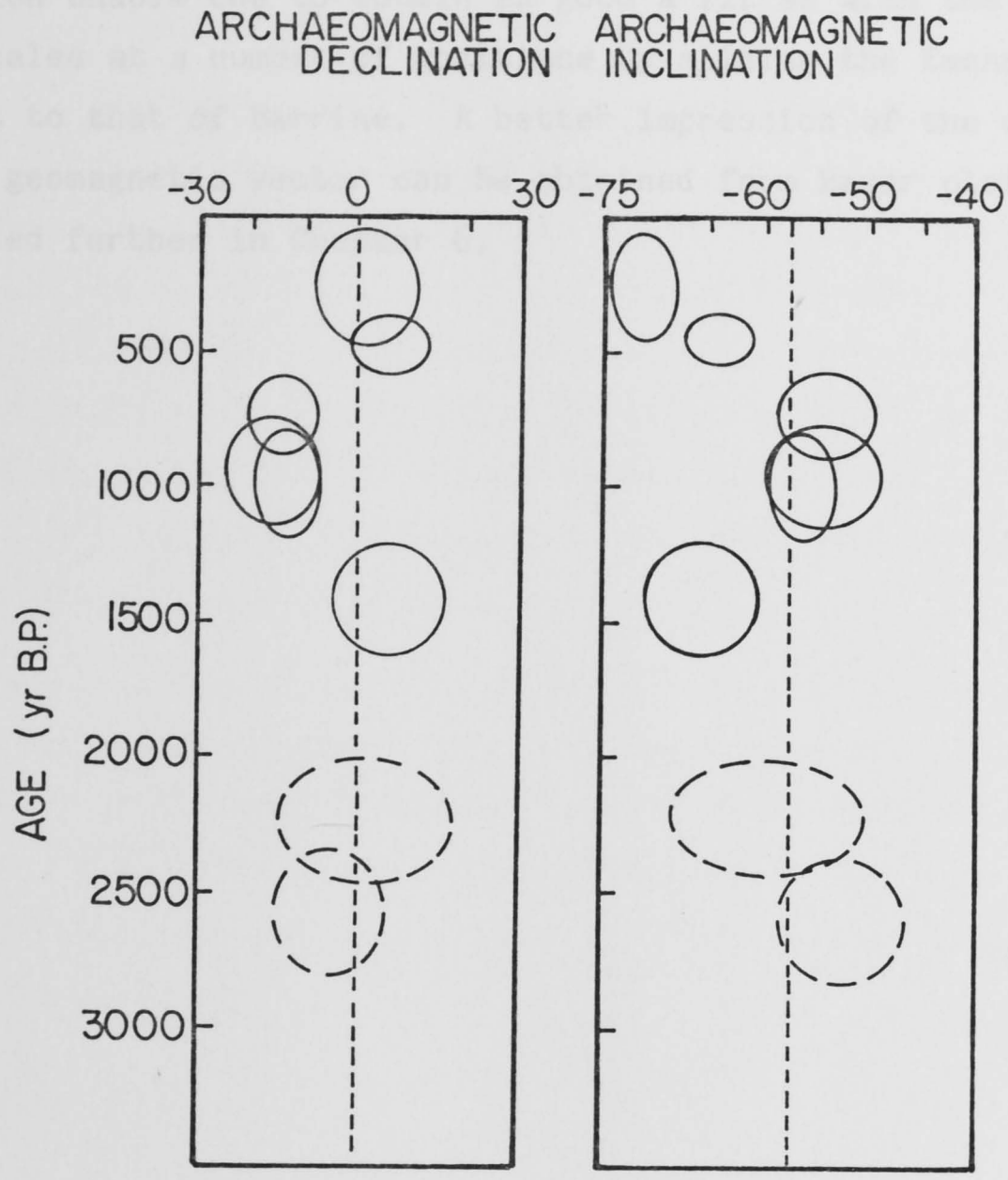

Figure 5.15 Geomagnetic directions for the past 3 000 years in S.E. Australia from arcahaeomagnetic work (Barton and Barbetti, 1982). Dotted lines show the axial dipole value of the field for the sites. Ellipses show 95% confidence intervals.

together with the quasi-periodic nature of the swings in the field direction enable one to obtain as good a fit as with the radiocarbon time scales at a number of positions by sliding the Eacham record with respect to that of Barrine. A better impression of the complete motion of the geomagnetic vector can be obtained from Bauer plots. This is discussed further in Chapter 6.

6 TIME SERIES ANALYSIS.

Time series analysis, that is the representation of the data in the frequency rather than the time domain, may be a useful method of obtaining information about the time constants associated with the sources of the secular variation. Denham (1975) first proposed the use of spectral analysis on lake sediment secular variation records. A useful discussion of this application is to be found in Barton (1978) and a condensed version in Barton and McElhinny (1982). The computer programs used here for periodogram and maximum entropy spectral analysis are those used by these authors.

In spectral analysis, a function of time x(t) is decomposed into a sum of sine and cosine functions with amplitudes a(f). In this way it is possible to estimate the power (at any given frequency f) in the underlying stochastic process generating x(t). The power S(f) will actually be spread over a continuum of frequencies. The variance of the process is given by

$$\sigma^2 = \int_{-\infty}^{\infty} S(f)df$$

The time series actually observed is one sample from an infinite set of realizations of the process. In spectral analysis the problem is to estimate the power spectrum of the process from the limited amount of information available in the length of data which has been sampled. There are a number of ways in which this may be done.

6.1 The Periodogram Method.

The periodogram was the earliest method of spectral analysis employed. The Fourier transform (FT) of the record is computed and the squared amplitude of the transform used as the spectral estimate. This is physically equivalent to performing a least squares fit of a series of sinusoids of periods $1/f_j$ to the data x(t). The periods used are integer divisors of the record length. See for example Bloomfield (1976) Chapter 3.

$$x(t) = A_o + 2\sum_{j=1}^{n}(A_j \cos w_j t + B_j \sin w_j t)$$

where

$w_j = 2\pi f_j$

$2n + 1$ = the number of points in the series $x(-n),...x(0),...x(n)$.

A_o is the mean value of $x(t)$ and

$$A_j = 1/(2n+1) \sum_{t=-n}^{n} x(t)\cos w_j t$$

$$B_j = 1/(2n+1) \sum_{t=-n}^{n} x(t)\sin w_j t.$$

The spectrum actually obtained from this procedure is that of the infinite time series generated by periodic extension of the data.

The periodogram method was computationally expensive for long time series until the advent of the discrete fast Fourier transform (DFFT) (Cooley and Tukey, 1965). This algorithm reduces the number of operations from about n^2 to about nlogn, where n is the number of terms in the time series.

The periodogram is a poor estimate of the power spectrum, because the variance of the estimate exceeds its mean value. Bingham *et al.* (1967) note that leakage of power to adjacent frequencies can be a large effect in a raw periodogram. The spectral estimate can be improved by the use of suitable smoothing techniques (*e.g.* Hanning the Fourier coefficients, or equivalently, multiplying the input data by a cosine bell). It will then provide a reasonable spectral estimate except at low frequencies. When the periods of interest are comparable to the record length the assumption of a periodic extension of the record may result in poor resolution and shifts in spectral peaks.

In geomagnetic secular variation records it is frequently the case that the periods of interest are almost of the same length as the records themselves. Under these circumstances the use of a data adaptive method is desirable.

6.2 Parametric Modelling.

In the data adaptive methods for estimating the power spectrum of a time series it is assumed that the underlying process generating the data is linear and satisfies one of 3 parametric models, namely the autoregressive, moving average or autoregressive moving average model.

1. The Autoregressive (AR) Model.

The value of the variable y_t at time t is derived linearly from the previous n values of the variable, i.e.

$$y_t = x_t - b_1 y_{t-1} - b_2 y_{t-2} - \ldots - b_n y_{t-n} \qquad (1)$$

where t is a discrete time variable, $b_1 \ldots b_n$ have to be determined and the system input x_t is usually taken to be ε_t, a Gaussian white noise series with mean $E(\varepsilon_t) = 0$ and variance $E(\varepsilon_t^2) = \sigma^2$. x_t is thus effectively the error in predicting y_t from the previous n values of y. The constants $1, -b_1, \ldots\ldots, -b_n$ are known as the prediction error filter. The order of the autoregressive process is n.

2. Moving Average (MA) Model.

$$y_t = x_t + a_1 x_{t-1} + a_2 x_{t-2} + \ldots + a_m x_{t-m} \qquad (2)$$

where $a_1 \ldots a_m$ are to be determined and x_t is again a random Gaussian series.

3. Autoregressive Moving Average (ARMA) Model.

This is an extension of the above two models.

$$\begin{aligned} y_t = x_t &- b_1 y_{t-1} - b_2 y_{t-2} - \ldots - b_n y_{t-n} \\ &+ a_1 x_{t-1} + a_2 x_{t-2} + \ldots + a_m x_{t-m}. \end{aligned} \qquad (3)$$

Both the AR coefficients b_i and the MA coefficients a_j remain to be determined.

Let z be the unit delay operator. Then (1), (2) and (3) become

$$Y(z) = \frac{1}{B_n(z)} X(z) \qquad \text{.....AR} \qquad (4)$$

$$Y(z) = A_m(z)X(z) \qquad \text{.....MA} \qquad (5)$$

$$Y(z) = \frac{A_m(z)}{B_n(z)} X(z) \qquad \text{.....ARMA} \qquad (6)$$

where X(z) and Y(z) are the z-transforms of the input x_t and output y_t respectively, and the m^{th} order polynomial $A_m(z)$ and n^{th} order $B_n(z)$ are defined in the form

$$A_m(z) = 1 + a_1 z + a_2 z^2 + ... + a_m z^m$$

$$B_n(z) = 1 + b_1 z + b_2 z^2 + ... + b_n z^n .$$

Spectra of the three processes (taking $x_t = \varepsilon_t$) may be computed by evaluating the autocorrelation funtion Ø(z) on the unit circle ($z = e^{-i2\pi f}$ where f is the circular frequency in Hz).

$$Ø(f) = \frac{\sigma^2}{B_n(f)^2} \qquad \text{AR process} \qquad (7)$$

$$Ø(f) = \sigma^2 A_m(f)^2 \qquad \text{MA process} \qquad (8)$$

$$Ø(f) = \frac{A_m(f)^2}{B_n(f)^2} \sigma^2 \qquad \text{ARMA process} \qquad (9)$$

To obtain the power spectrum of a finite data window one should use the estimator corresponding to the model which is correct for the data. Unfortunately the correct model for the data is usually unknown. In geomagnetism the underlying process is generally assumed to be autoregressive and the maximum entropy method used to provide a spectral estimate.

6.3 The Maximum Entropy Method.

Traditional methods of spectral analysis such as the periodogram and autocorrelation methods often make unrealistic assumptions about the behaviour of the time series outside the sampled windows, such as periodic or null extension. The maximum entropy method (MEM), first proposed by Burg (1967, 1968), involves fitting an AR model to the data using the principle that the spectral estimate should represent all the information in the record and assume as little information as possible from outside the record. Ables (1972) has discussed the connection between the maximum entropy method and information theory.

There are two general techniques for estimating the prediction error filter of the AR process b_1, b_2, ... b_n. These are described by Ulrych and Bishop (1975). The Yule-Walker (Yule, 1927; Walker, 1931) estimates of these coefficients require explicit knowledge of the autocorrelation function of the input data. Burg (1968) on the other hand estimates the AR parameters without prior knowledge of the autocorrelation function. This is a considerable advantage since techniques for estimating the autocorrelation function directly generally violate the concept of MEM, by assumptions regarding data outside the record.

Burg's method for estimating the coefficients essentially fits successively higher order prediction and retrospection error series x_t to the series by convolving the filter both backwards and forwards over the data (but not off the ends). The squares of the two resulting error series are then summed for each order. Filter coefficients for a particular order are determined by minimising this sum with respect to the last coefficient b_n and then using recursion relations to find b_1 .... b_{n-1} (Anderson, 1974). The autocorrelation function can then be obtained from the prediction error coefficients (Ulrych and Bishop, 1975).

The b_n derived by the Burg method represents the partial correlation coefficient which, for a particular order N, measures the correlation between the prediction and retrospection error series for N-1, (Gutowski et al., 1977). If the order of the prediction error series filter is less than or equal to the actual order of the AR system, there will be significant correlation between the two error series and $b_n \sim 1$. However, if the prediction error filter order exceeds that of the AR

system all the predictable information in the data has been removed and the two error series should be uncorrelated (i.e. $b_n \sim 0$). This has been proposed by Akaike (1969a,b, 1970) as a means of determining the correct order for the AR process.

A fundamental problem in the use of MEM is this choice of the order of the underlying AR process. Too low a value for m will result in an over-smoothed spectrum, while too high a value results in high frequency shifting and splitting of peaks. Ulrych and Bishop (1975) conclude that Akaike's criterion of choosing the minimum final prediction error is an objective one for selecting the filter length. Berryman (1978) has reviewed briefly other criteria for choosing the filter length and proposed the use of $m = 2N/\ln(2N)$ to avoid the ambiguity of data adaptive methods. Barton and McElhinny (1982) point out that since most of the criteria are justified on empirical grounds using both real and synthetic data the lack of concensus indicates that the best choice of criterion depends on the length and characteristics of the data set.

6.4 Spectral Analysis of Complex Equivalent Directions.

Denham (1975) has pointed out that spectral analysis of palaeomagnetic directions mapped onto the complex plane may be used to detect clockwise or anticlockwise looping of the geomagnetic vector with time. Figure 6.1 shows the sort of power spectra expected from linear, circular and elliptical motions in the complex plane. From these it may be inferred that any periodic precession of the geomagnetic vector will show as an imbalance in the power at negative and positive frequencies.

The modification described by Barton and McElhinny (1982) of Denham's (1975) method for converting directional data into complex time series has been used here. Either the axial dipole value at the site or the vector mean of the data is subtracted from the data vectorially. The directions are projected onto a plane surface centred about this value, using a stereographic projection. The Cartesian coordinates of the projected directions were converted to complex numbers via

$$z(t) = x(t) + iy(t).$$

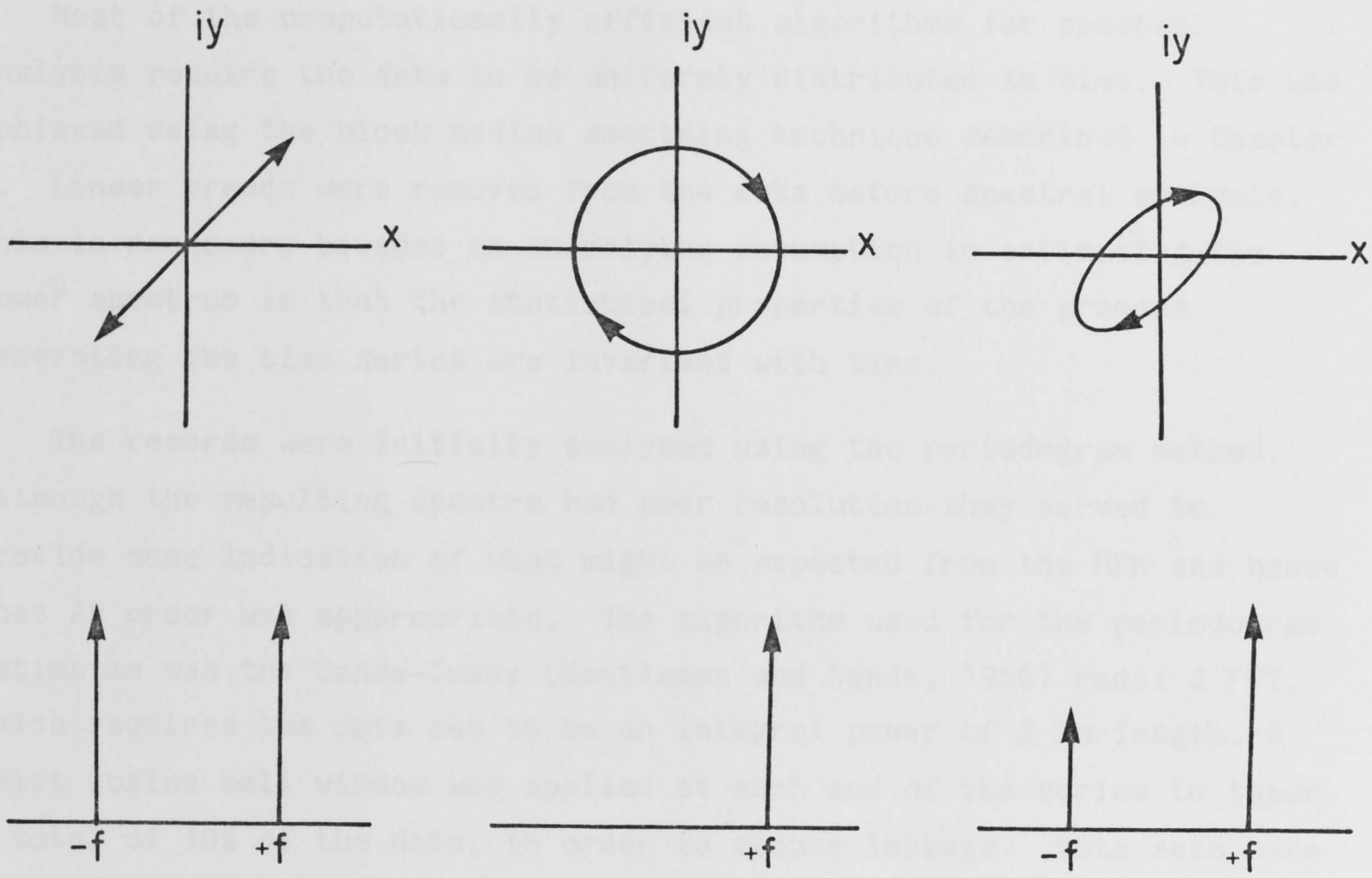

Figure 5.1 Balance of power at positive and negative frequencies in the power spectra generated by (a) planar, (b) circular and (c) elliptical motion in the complex plane.

The sign convention used is such that power at negative frequencies corresponds to clockwise looping of the tip of the geomagnetic vector when viewed towards its north seeking end.

6.5 Application to Barrine and Eacham Records.

Most of the computationally efficient algorithms for spectral analysis require the data to be uniformly distributed in time. This was achieved using the block median smoothing technique described in Chapter 5. Linear trends were removed from the data before spectral analysis. This is necessary because an underlying assumption in estimating the power spectrum is that the statistical properties of the process generating the time series are invariant with time.

The records were initially analysed using the periodogram method. Although the resulting spectra had poor resolution they served to provide some indication of what might be expected from the MEM and hence what AR order was apppropriate. The algorithm used for the periodogram estimates was the Sande-Tukey (Gentleman and Sande, 1966) radix 2 FFT, which requires the data set to be an integral power of 2 in length. A split cosine bell window was applied at each end of the series to taper a total of 10% of the data, in order to reduce leakage. Data sets were expanded to the nearest power of 2 by adding a null extension.

Declination and inclination records were analysed independently using both the periodogram and maximum entropy methods. Complex equivalents of the directional data were analysed using the MEM.

Scattered data near the ends of the records were deleted as they tended to introduce spurious spikes in the spectra.

6.5.1 Declination results.

Figure 6.2 shows the results from the L. Eacham calibrated record. The record covered the time interval 1 235 to 5 700 years B.P. and was equally spaced on a 60 year grid. Burg's method was used to calculate the prediction filter coefficients for the MEM, and a plot of the final prediction error for orders up to m = 40 is given in Figure 6.2(b). Berryman's criterion for selecting the order of the AR model yields a

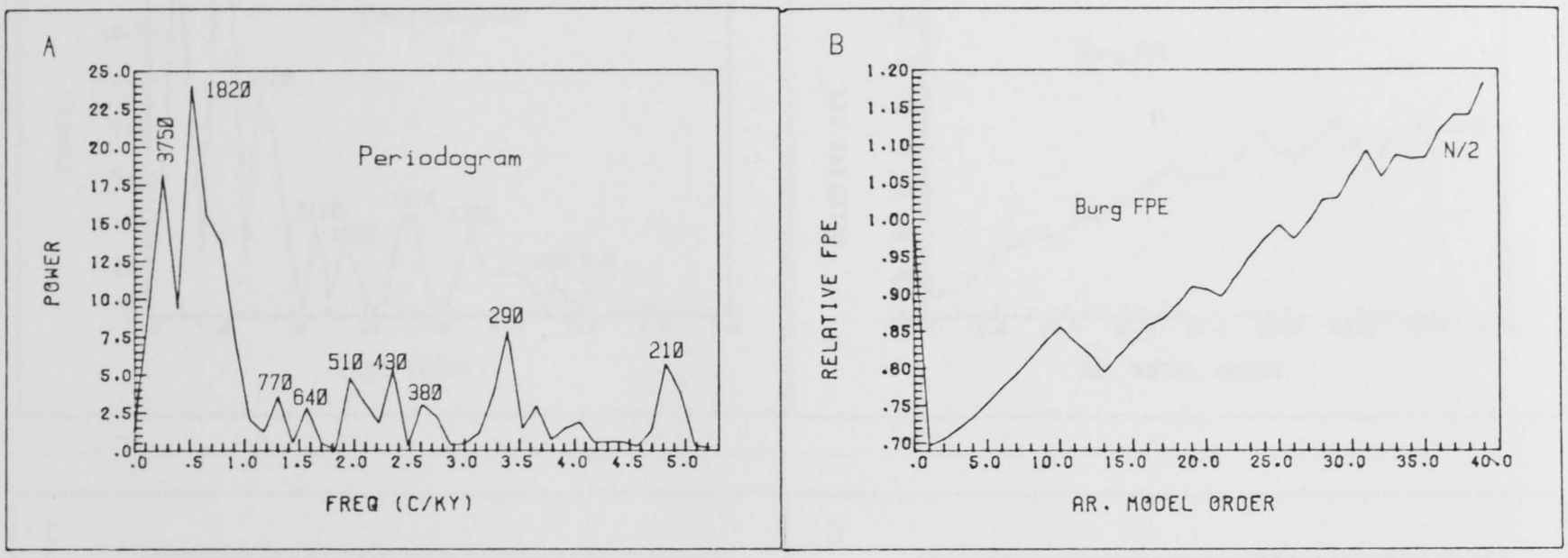

Figure 6.2 Power spectra of the L. Eacham calibrated declination record.

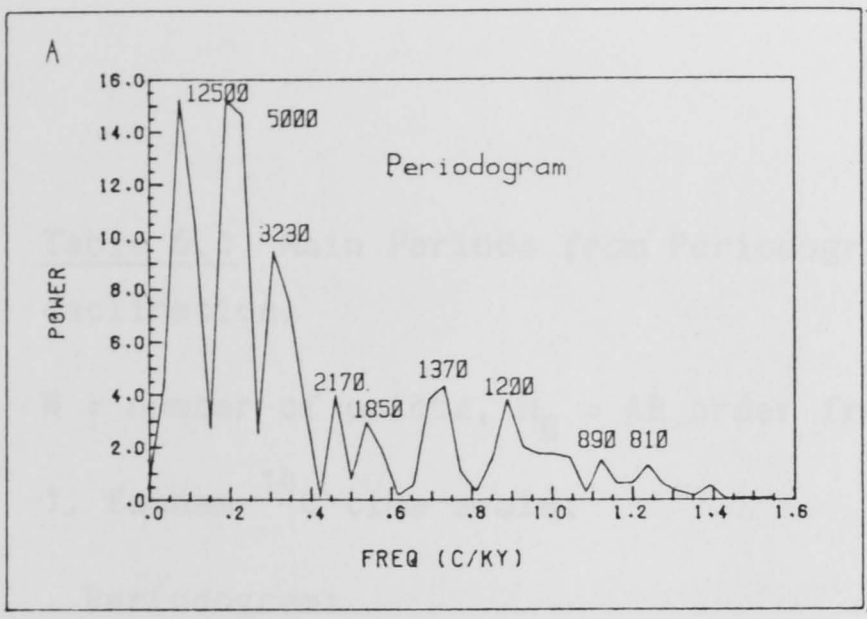

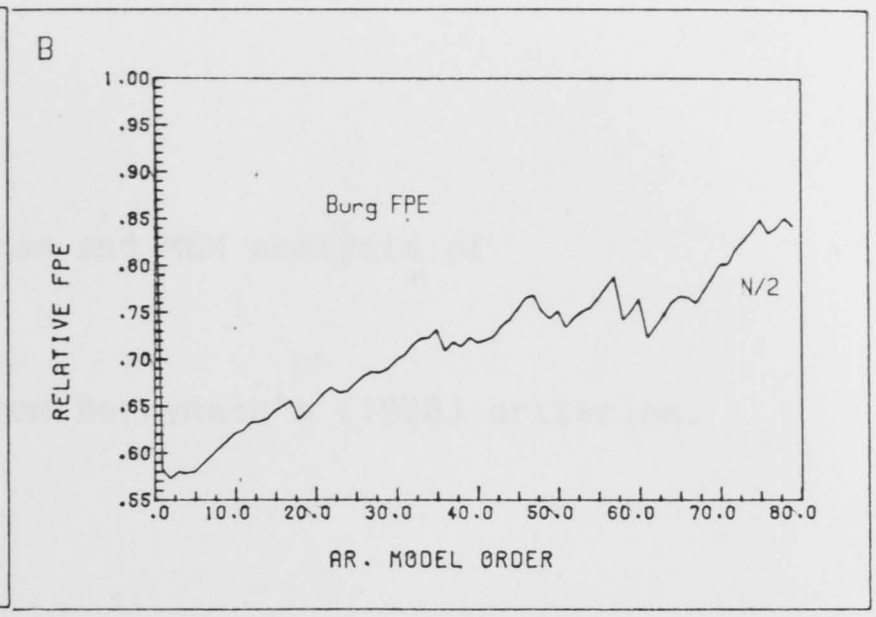

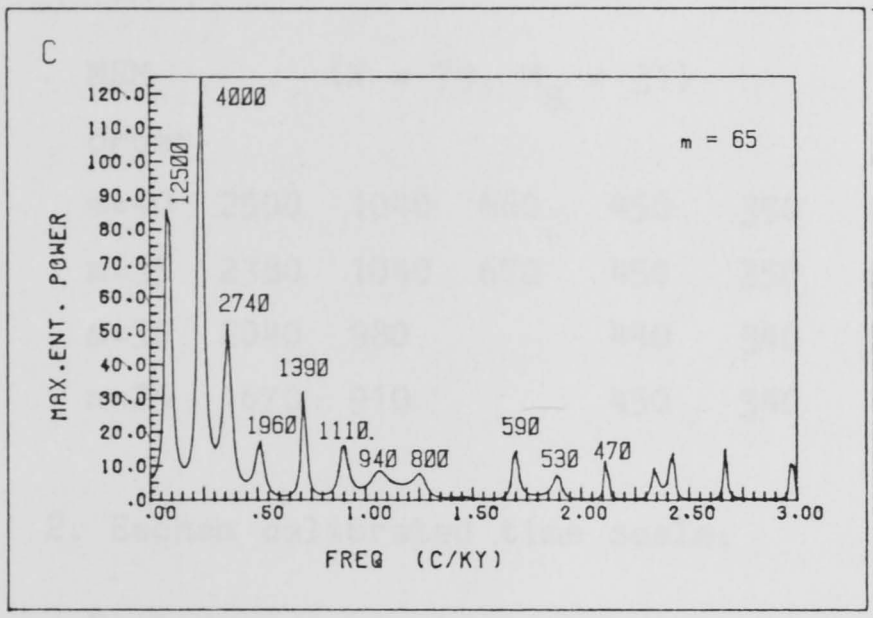

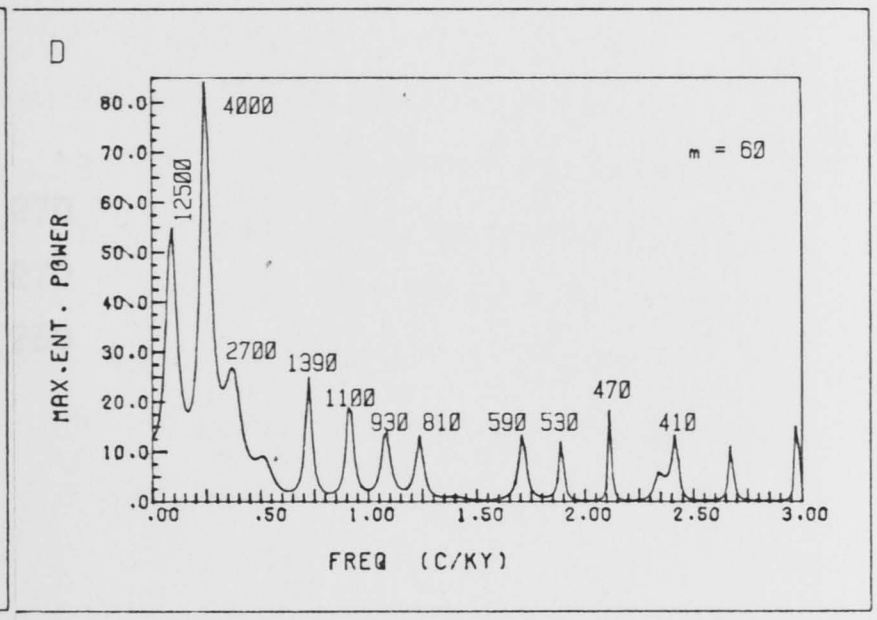

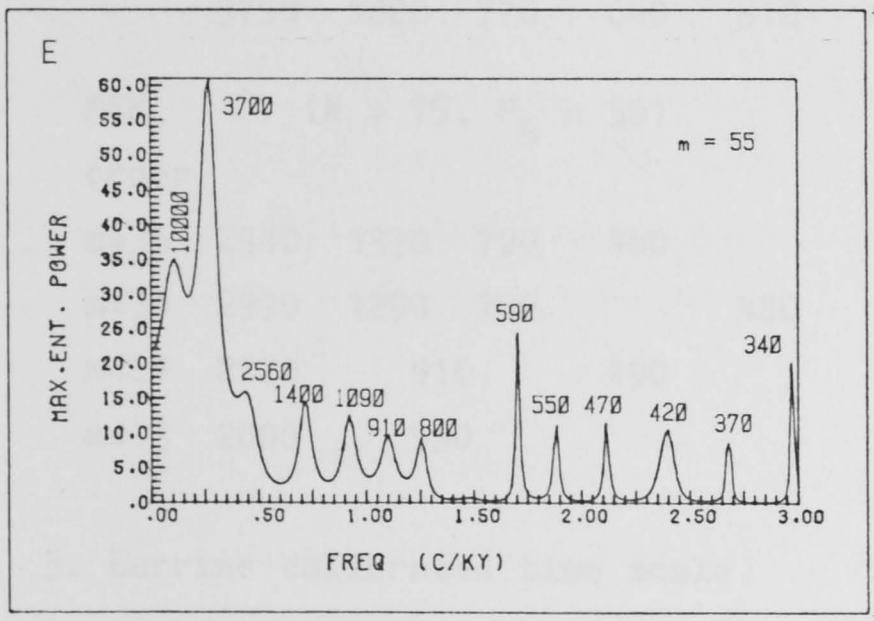

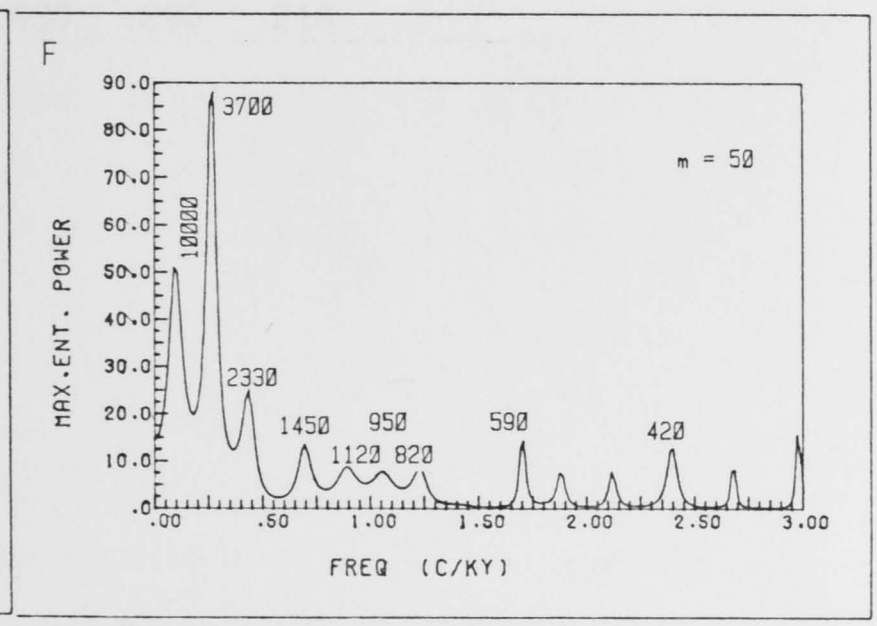

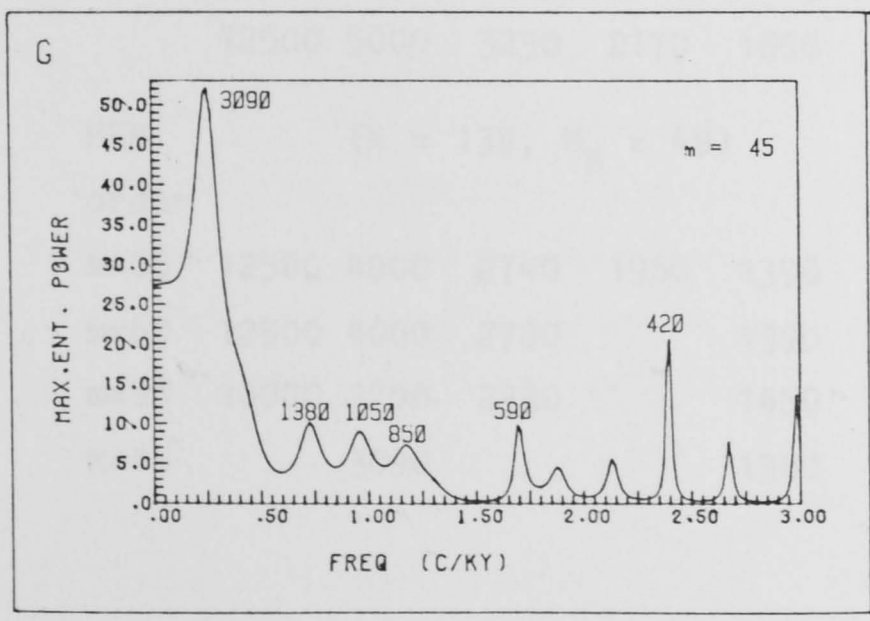

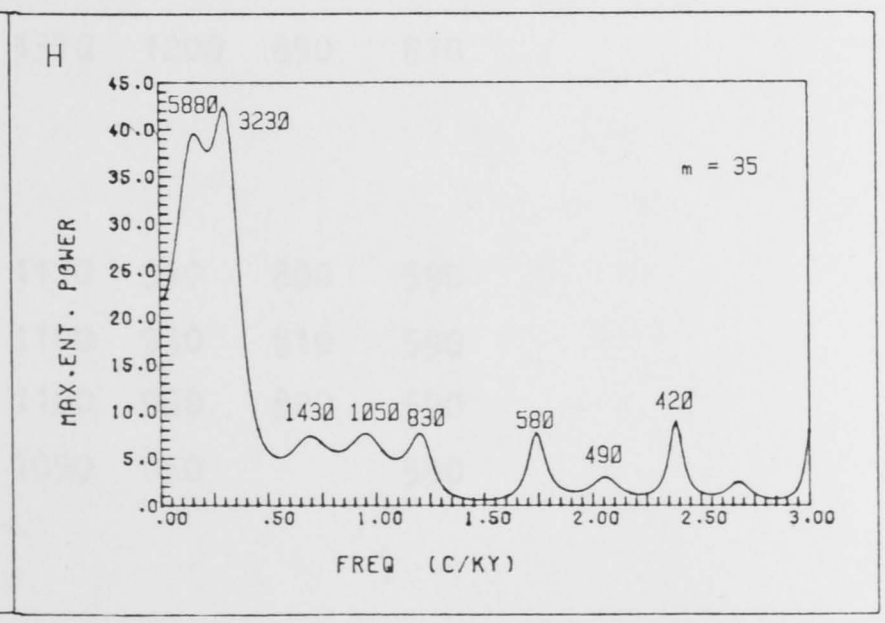

Figure 6.3 Power spectra of the L. Barrine calibrated declination record.

Table 6.1 Main Periods from Periodogram and MEM analysis of declination.

N = number of points, M_B = AR order from Berrymans's (1978) criterion.

1. Eacham ^{14}C time scale.

Periodogram:

	3130	1280	640	450	350	270	210

MEM (N = 79, M_B = 31)

order						
m=40	2500	1040	660	450	350	270
m=35	2380	1040	670	450	350	270
m=30	2040	980		440	340	260
m=25	1670	910		450	340	

2. Eacham calibrated time scale.

Periodogram:

	3750	1820	770	640	510	430	290	210

MEM (N = 75, M_B = 30)

order						
m=35	2940	1330	790	460		
m=30	2990	1290	750		480	
m=25	2270	910		490		
m=13	2000	550				

3. Barrine calibrated time scale.

Periodogram:

	12500	5000	3230	2170	1850	1370	1200	890	810

MEM (N = 139, M_B = 49)

order									
m=65	12500	4000	2740	1960	1390	1110	940	800	590
m=60	12500	4000	2700		1390	1100	930	810	590
m=50	10000	3700	2330		1450	1120	950	820	590
m=45		3090			1380	1050	850		590

value for m of 30. Figures 6.2(c) to 6.2(f) show the MEM spectra for m varying from 13 to 35. Those for m = 30 and 35 give the best resolution with peaks around 2 950, 1 300, 470 and 770 years in order of decreasing importance. The results are listed for various orders in Table 6.1 along with those from the uncalibrated series with block medians taken on a 50 year grid.

At first sight the periodogram result of Figure 6.2(a) appears to give better resolution than the MEM spectra. The peak at period 2 940 years in the MEM is split into two in the periodogram, where there are also more well defined peaks at low frequency. It should be borne in mind, however, that the record is only just over 4 000 years in length. Periodic extension of the data will probably result in a spurious peak in the power at periods of about the same length as the data set. Hence the periodogram peak at 3 750. The large number of peaks at higher frequencies is probably caused by leakage. The small width of the peaks in the MEM spectra suggests that they are giving better resolution than the periodogram despite appearances to the contrary.

Figure 6.3 shows the spectra of the L. Barrine declination record which spanned 1 650 to 15 640B.P. on a 100 year grid. There is a strong, well resolved peak at 3 700-4 000 years in the MEM spectra and others, weaker but still well defined, at 2 560-2 740, 1 390-1 450, 590, 420. The main periods are tabulated in Table 6.1 where the preferred orders for the MEM are indicated.

6.5.2 Inclination Results.

L. Eacham calibrated inclination records appear to be dominated by a component at 2 900-3 300 year period. 900, 1 500 and 450 year periods are also present in both the periodogram and higher order MEM spectra (see Figure 6.4 and Table 6.2). In the uncalibrated Eacham sequence the 2 900-3 300 year period appears as a 1 920-2 630 year period. This difference of about 25% in periods is typical for the calibrated and uncalibrated Eacham sequences and serves to indicate the approximate uncertainties in determining periods from the L. Barrine record which has relatively poor age control.

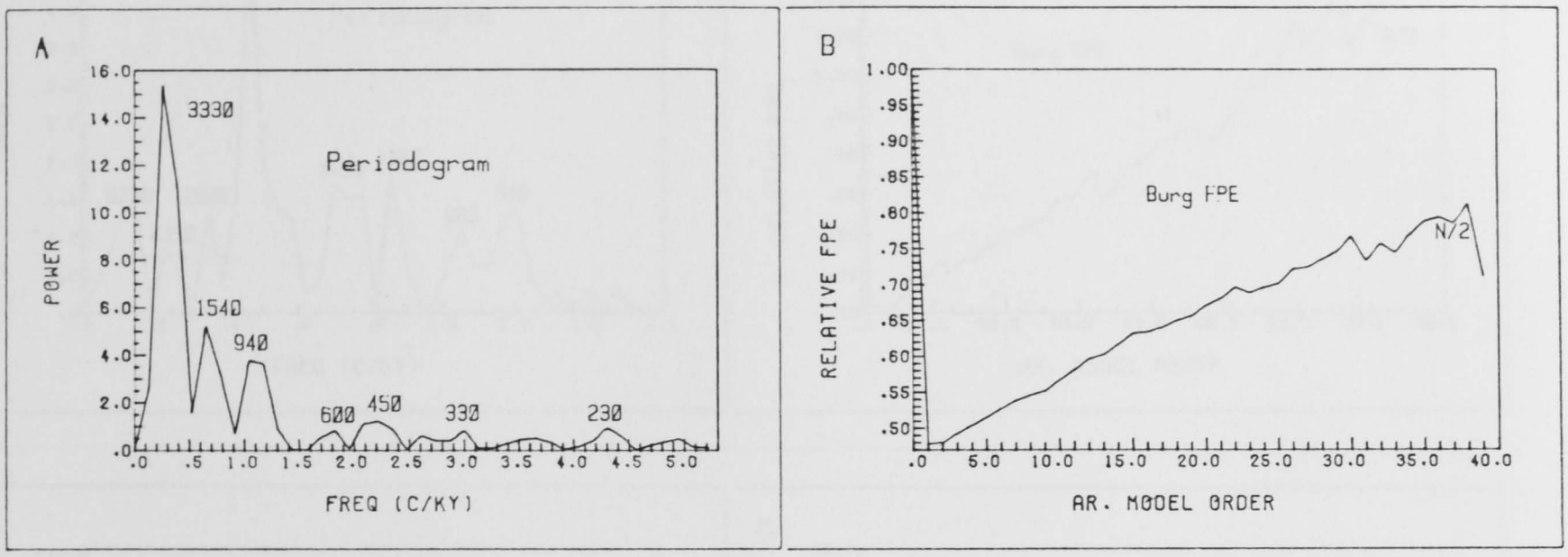

Figure 6.4 Power spectra of the L. Eacham calibrated inclination record.

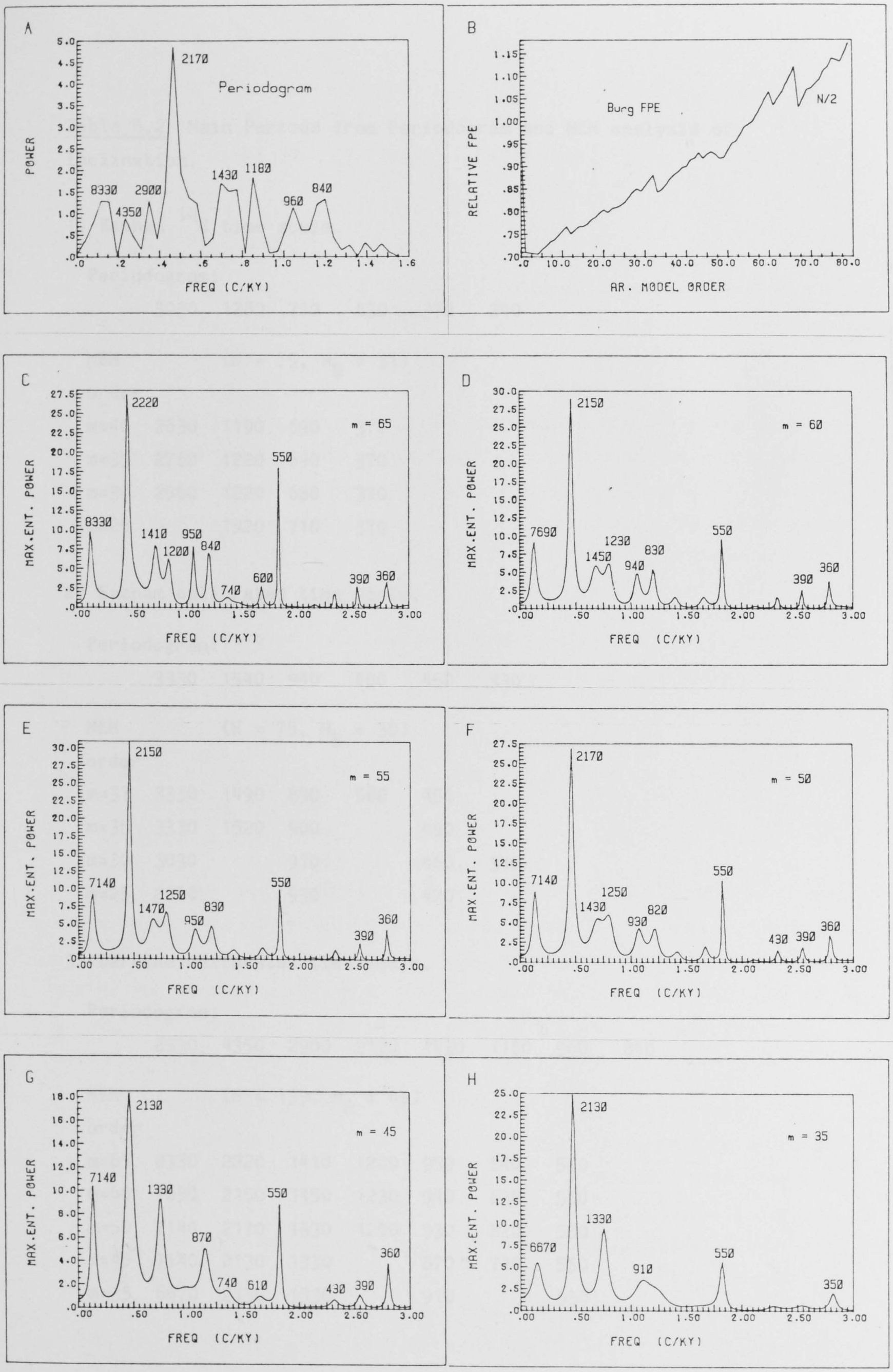

Figure 6.5 Power spectra of the L. Barrine calibrated inclination record.

Table 6.2 Main Periods from Periodogram and MEM analysis of inclination.

1. Eacham ^{14}C time scale.

Periodogram:	3030	1280	710	430	370	240
MEM order	(N = 79, M_B = 31)					
m=40	2630	1190	690	370		
m=35	2780	1220	690	370		
m=30	2560	1220	680	370		
m=25		1920	710	370		

2. Eacham calibrated time scale.

Periodogram:	3330	1540	940	600	450	330
MEM order	(N = 75, M_B = 30)					
m=37	3330	1490	890	560	450	
m=35	3330	1520	900		450	
m=30	3030		910		460	340
m=25	2860		930		470	

3. Barrine calibrated time scale.

Periodogram:	8330	4350	2900	2170	1430	1180	960	840
MEM order	(N = 139, M_B = 49)							
m=65	8330	2220	1410	1200	950	840	550	
m=60	7690	2150	1450	1230	940	830	550	
m=50	7140	2170	1430	1250	930	820	550	
m=45	7140	2130	1330		870	740	550	
m=35	6670	2130	1330		910		550	

In the Barrine series 2 130-2 220, 7 000-8 000, 1 330-1 450, 820-870, 550 and 350 are well resolved periods. The 2 130-2 220 year period is the strongest (see Figure 6.5 and Table 6.2).

6.5.3 Complex Spectra.

The complex equivalent directions were centred on the vector means for each record. Figure 6.6 shows MEM spectra for the Eacham calibrated and uncalibrated complex equivalent directions for a variety of AR orders. The uncalibrated data (a - d) provide consistent results for orders from m = 25 to 40. The 2 000 year period dominates the power spectrum and is associated with clockwise rotation of the geomagnetic vector. Anticlockwise rotation is indicated at a period of 1 000-1 100 years. At higher frequencies the power in the spectrum (which is given by the area under the curve) is fairly evenly distributed between positive and negative frequencies.

For the calibrated data the spectra were less stable. For m > 25 spectra had to be plotted on a log scale because of the dominant effects of peaks at 2 500 and 5 000 year periods. The much smaller peaks are of the same periods as found in the individual inclination and declination spectra. The peak at 2 500 in the complex spectrum is considered to be the same as that at 2 900-3 000 in the declination and 2 900-3 300 in the inclination.

The complex spectra from the Barrine record (see Figure 6.7) showed rather different power characteristics from the Eacham ones. There is a strong peak at a period of about 4 000 years associated with clockwise motion and two associated with anticlockwise motion at 5 500-7 500 and 2 100 years. There is also a weaker but still well defined peak at about 1 400 years in the anticlockwise half of the spectrum.

Table 6.3 lists the main periods found in the complex spectra for periodogram and various orders of MEM analysis. A comparison of data for the two lakes shows that in each sequence there is a bias towards anticlockwise rotation, at periods of about 2 100 years in Barrine and 1 000 in Eacham uncalibrated, (or about 1 300 calibrated). There is a bias towards clockwise rotation at approximately twice this period in each lake (2 000 in uncalibrated Eacham, 2 500 calibrated Eacham and 4 000 years in Barrine). Lower periods appear to be reasonably well

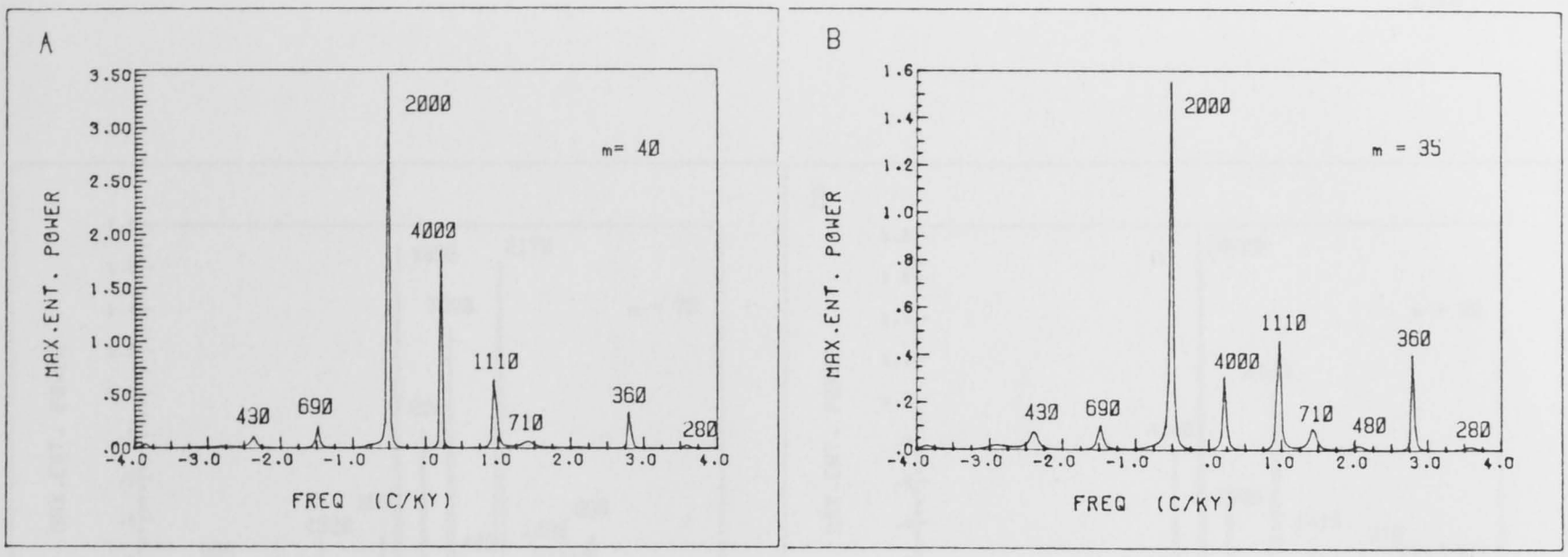

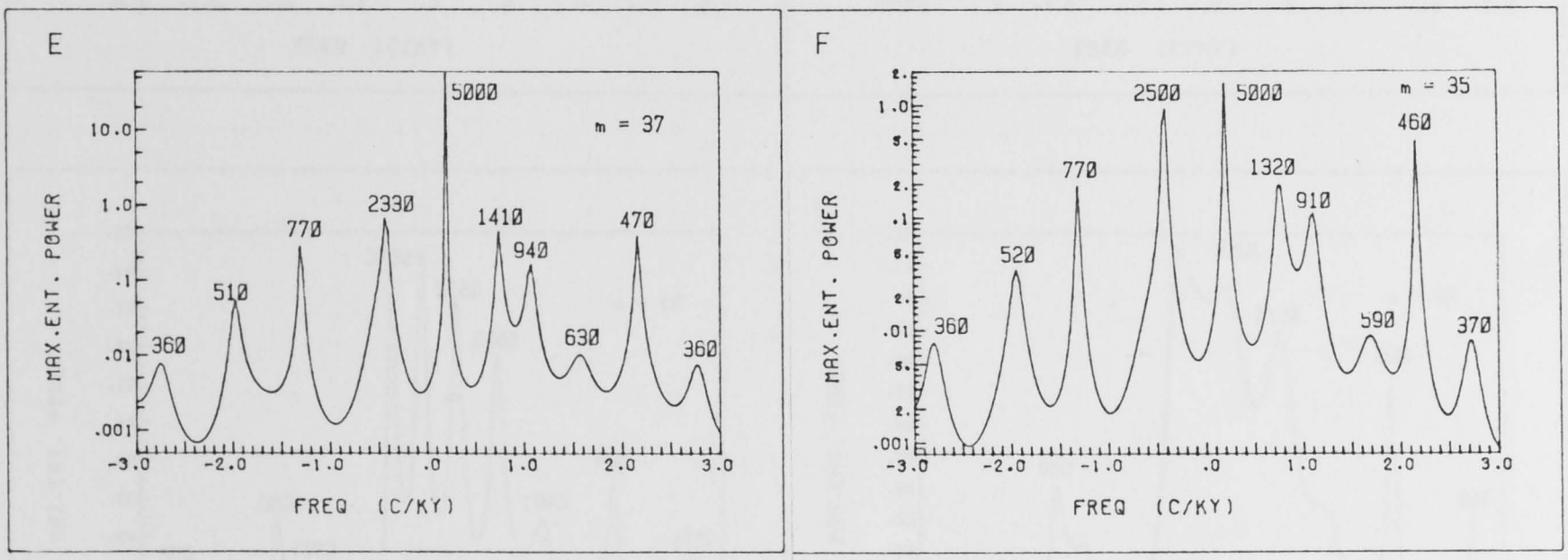

Figure 6.6 Complex MEM spectra for the L. Eacham series, uncalibrated time scale A-D and calibrated E-H.

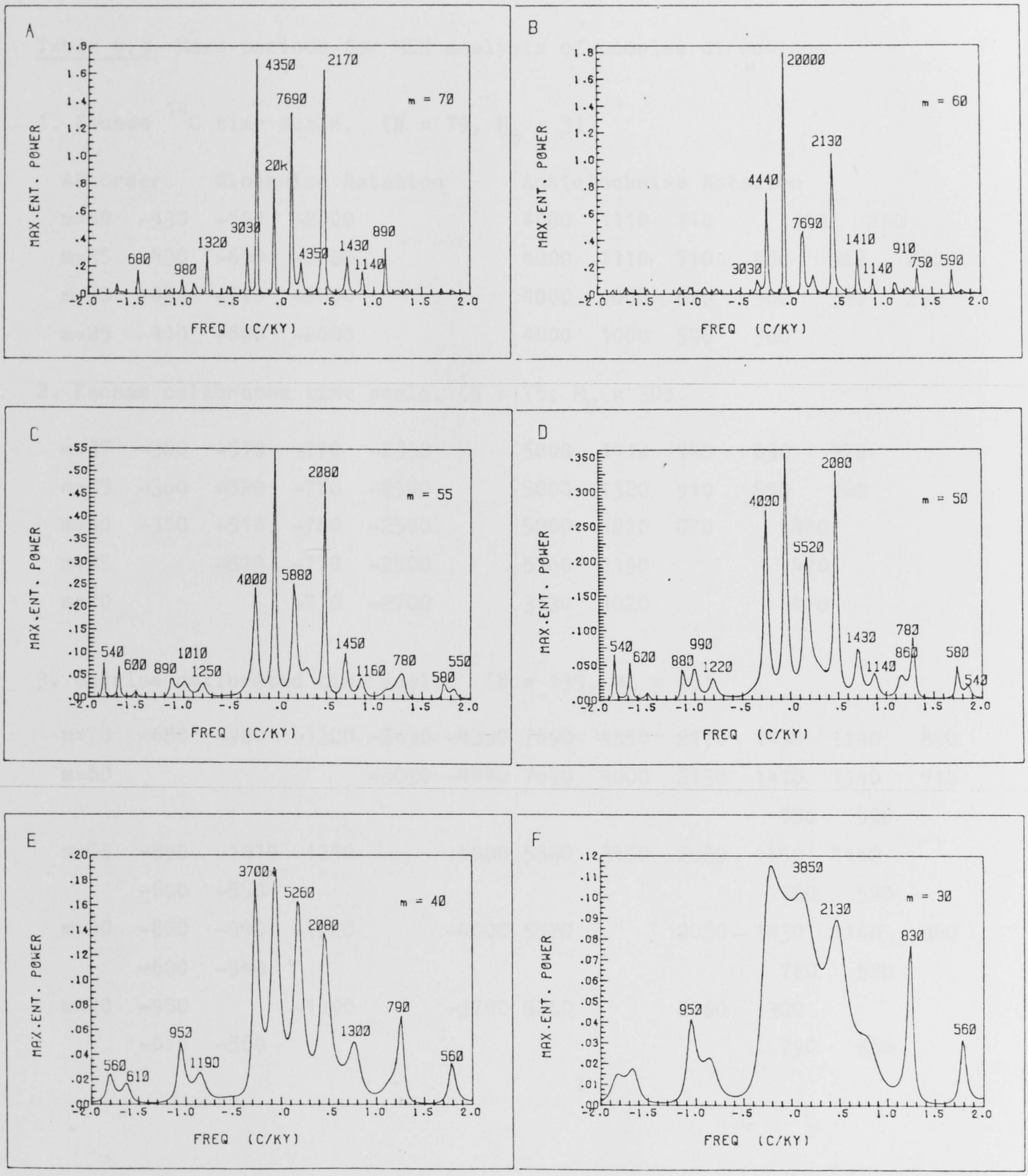

Figure 6.7 Complex MEM spectra for the L. Barrine calibrated series.

Table 6.3 Main periods for MEM analysis of complex directions.

1. Eacham ^{14}C time scale. (N = 79, M_B = 31)

AR order	Clockwise Rotation			Anticlockwise Rotation					
m=40	-430	-690	-2000	4000	1110	710	360	280	
m=35	-430	-690	-2000	4000	1110	710	480	360	280
m=30	-420	-710	-2000	4000	1000	670	360	340	270
m=25	-410	-690	-2000	4000	1000	590	360		

2. Eacham calibrated time scale. (N = 75, M_B = 30)

m=37	-360	-510	-770	-2330	5000	1410	940	630	470	
m=35	-360	-520	-770	-2500	5000	1320	910	590	460	
m=30	-360	-510	-760	-2500	5000	1220	870	460		
m=25		-520	-770	-2500	5560	1190		470		
m=20			-710	-2700	3130	1020		470		

3. Barrine calibrated time scale. (N = 139, M_B = 49)

m=70	-680	-980	-1320	-3030	-4350	7690	4350	2170	1430	1140	890
m=60				-3030	-4440	7690	4000	2130	1410	1140	910
									750	590	
m=55	-890	-1010	-1250		-4000	5880	3450	2080	1450	1160	
	-600	-550							780	580	
m=50	-880	-990	-1220		-4000	5520		2080	1430	1140	860
	-600	-540							780	580	
m=40	-950		-1190		-3700	5260		2080	1300		
	-610	-560							790	560	

balanced in the positive and negative sides of the spectra. In order to test whether these differing results were due to the different record lengths of the 2 sequences complex spectral analysis was repeated on the section of the Barrine record spanning 1 650 to 5 700 years B.P. The results were essentially the same as for the whole record.

This mismatch in the dominant periods of the complex spectra was somewhat dissapointing. It can be attributed to

(1) lack of fidelity in the sediment recording process,

(2) the geomagnetic field motions being only piecewise periodic (at least over the record sampled), and

(3) poor resolution in the time scale.

A comparison of the total geomagnetic field motions recorded in each sequence may be made from Bauer plots (see section 1.1.3). Figure 6.8 shows Bauer plots of the Eacham 60 year block median and Barrine 100 year block median directions after smoothing using a seven point linear filter. The filter characteristics are illustrated in Figure 6.9. Declination and inclination were smoothed independently and directions are centred on the vector mean for each record.

It may be seen (Figure 6.8(a) and (b)) that the anticlockwise motion of the vector between about 5 500 and 4 000 years B.P. is well reflected in both records. The well defined clockwise loop occuring between 3 500 and 2 600B.P. in the Eacham record appears to be much reduced in amplitude and displaced up to the end of the anticlockwise loop in L. Barrine. As has already been stated (section 5.4) it would appear that the resolution of the Eacham record is much better than that of the Barrine and that its geomagnetic variation record is of greater amplitude as a result of its higher sedimentation rate.

The difference in periods for the anticlockwise power bias is also reflected in the Bauer plots. According to the assigned time scales the anticlockwise loop occuring in the Eacham record is covered in several hundreds of years less time than in the Barrine record.

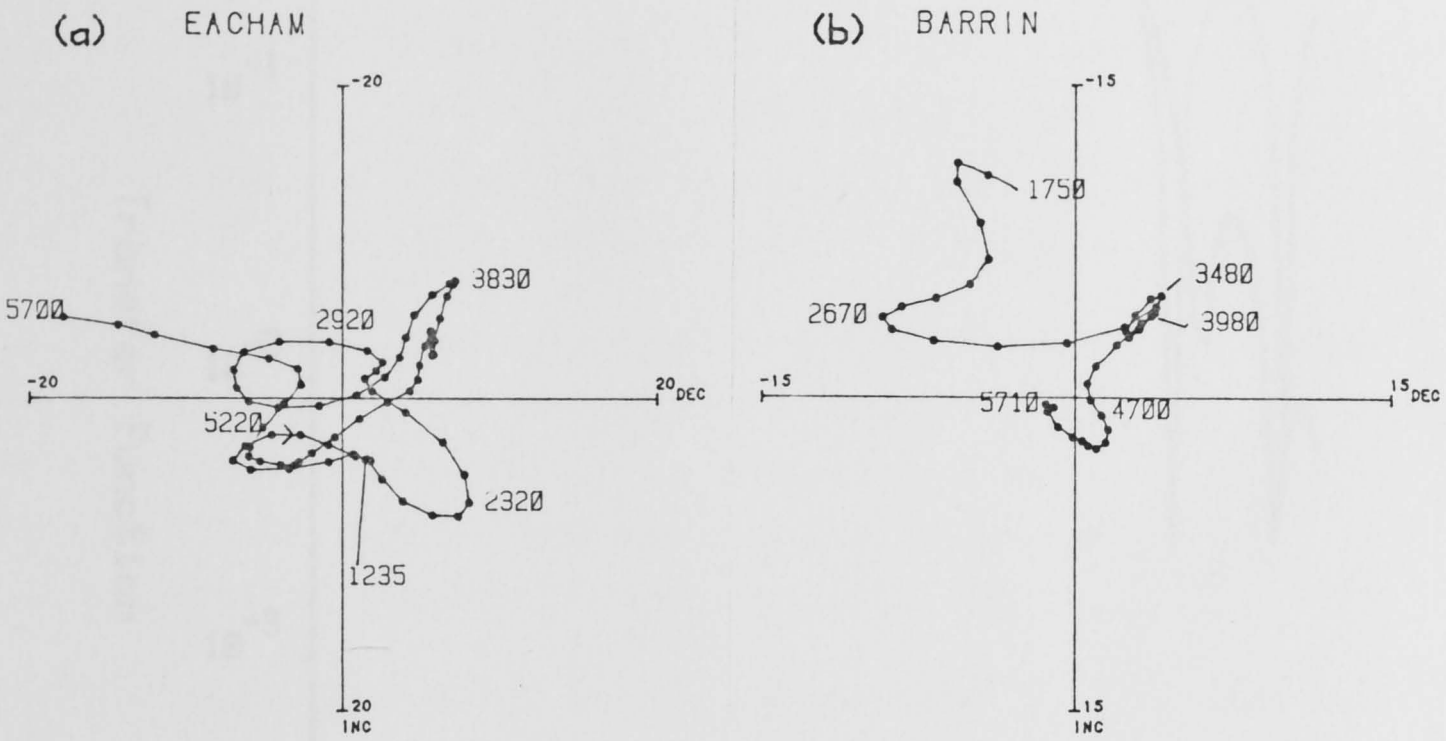

Figure 6.8 Bauer plots centred on the vector means of the data at each site.

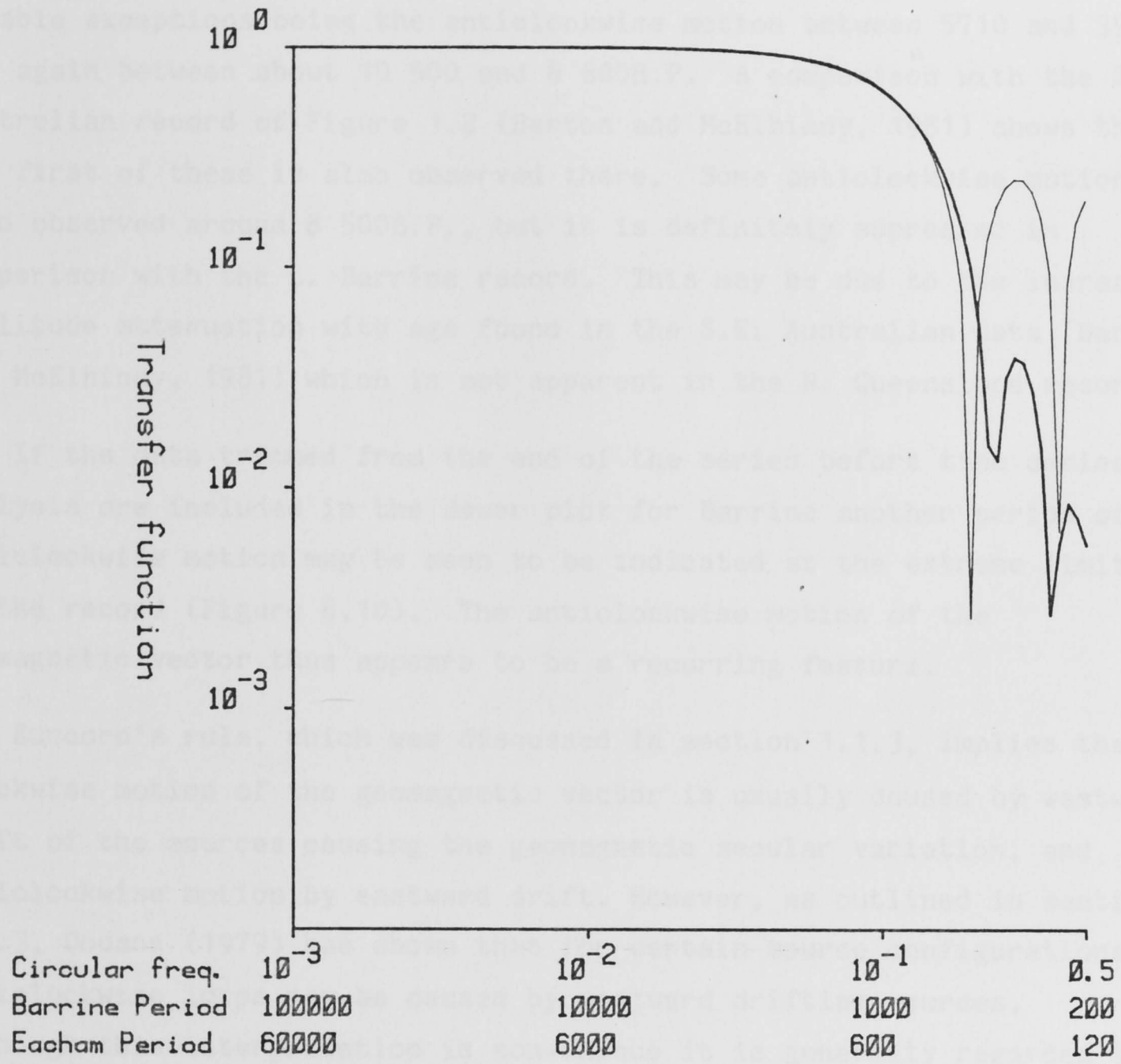

Figure 6.9 Transfer function of the linear filter used on the declination and inclination data to produce the Bauer plots of Figure 6.8 (heavy line). The lighter line shows the characteristics of a 5 point moving average for comparitive purposes.

Throughout the Barrine record most of the motion is clockwise, two notable exceptions being the anticlockwise motion between 5710 and 3980 and again between about 10 500 and 8 800B.P. A comparison with the S.E. Australian record of Figure 1.2 (Barton and McElhinny, 1981) shows that the first of these is also observed there. Some anticlockwise motion is also observed around 8 500B.P., but it is definitely supressed in comparison with the L. Barrine record. This may be due to the increased amplitude attenuation with age found in the S.E. Australian data (Barton and McElhinny, 1981) which is not apparent in the N. Queensland records.

If the data trimmed from the end of the series before time series analysis are included in the Bauer plot for Barrine another period of anticlockwise motion may be seen to be indicated at the extreme limits of the record (Figure 6.10). The anticlockwise motion of the geomagnetic vector thus appears to be a recurring feature.

Runcorn's rule, which was discussed in section 1.1.3, implies that clockwise motion of the geomagnetic vector is usually caused by westward drift of the sources causing the geomagnetic secular variation, and anticlockwise motion by eastward drift. However, as outlined in section 1.1.3, Dodson (1979) has shown that for certain source configurations anticlockwise loops may be caused by westward drifting sources. Although this interpretation is non-unique it is generally regarded as more acceptable than the invocation of eastward drift of sources, which is difficult to reconcile with the core dynamo origin of the field.

In the light of the Queensland data it is worthwhile reconsidering Dodson's (1979) list of the various asymmetries which would be expected to occur in secular variation records if there existed no eastward drift of sources of the geomagnetic field.

(1) The presence of more pronounced anticlockwise loops in the Queensland records than the south-eastern Australian ones is consistent with the expectation of anticlockwise loops seldom being seen at high latitudes (latitude of the Queensland site is $17^{o}15'S$ and of the other lakes is $38^{o}S$).

(2) As in secular variation records from other parts of the world, clockwise loops are more numerous than anticlockwise ones.

(3) Clockwise loops appear on the whole to be larger than anticlockwise ones. This is best illustrated in Figure 6.8(d) between 14 530 and 13 310 years B.P. Estimating the relative sizes of the loops in the other plots is somewhat difficult, but in general the anticlockwise motions tend to enclose less area than the clockwise ones.

(4) Dodson (1979) also predicts that anticlockwise motions would always be accompanied by a decrease in total field intensity while clockwise motion could be accompanied by either an increase or a decrease. The Barrine relative intensity plot of Figure 4.10 was examined between 5 700 and 4 000B.P., 10 500 and 8 800B.P. and 14 200 and 13 200B.P., which are the time spans corresponding to anticlockwise motion in Figure 6.8. A drop in relative intensity occurs at about 5 700B.P. and a rise at about 4 000B.P. However, it does not remain uniformly low throughout this interval. The anticlockwise motion at 10 500B.P. is also accompanied by a drop in field intensity and in this case it remains low until the end of the anticlockwise motion. Between 14 200 and 13 200B.P. the relative intensity decreases, rises sharply and then drops again. It is thus difficult to draw conclusions regarding whether anticlockwise motion is associated with a drop in total field intensity.

The Queensland records may thus be caused by westward drift of the non-dipole sources of the geomagnetic field, despite the anticlockwise motions present in them, if the type of source configurations suggested by Dodson (1979) are involved. The possibility that the anticlockwise contributions to the motion are caused by precession of the dipole axis appears to be ruled out by the comparison of secular variation records from Britain and south-eastern Australia (Barton and McElhinny, 1981).

7 CONCLUSIONS.

The cores examined from the two Queensland crater lakes have provided geomagnetic secular variation records spanning 1 200 to 5 700 years in the case of Lake Eacham and 1 600 to 16 200 in the case of Lake Barrine. The use of two separate sites was intended initially as a means of verifying the accurate recording properties of the lake sediments. However, it is apparent that this also has other advantages in cases where the sedimentation rates in the two lakes are very different. The higher accummulation rate in Lake Eacham has resulted in a record which is less attenuated by the sedimentation process than that from Lake Barrine.

The use of a robust non-linear smoothing technique has made it possible to extract estimates of relative intensity variations over the past 14 000 years. These are in good agreement with south-eastern Australian archaeointensity measurements for the past 7 000 years made by Dr M. Barbetti of Sydney University. This reproducibility of the results is somewhat surprising since in general lake sediments do not appear to provide reliable relative intensity estimates. Possibly the use of an ARM which mimics as closely as possible the actual NRM as a normalizing parameter has been a contributing factor. It now appears worthwhile to use the archaeointensity data to calibrate the North Queensland intensity variations and provide absolute values for the geomagnetic intensity estimates. This will provide a continuous measurement of geomagnetic field intensity at the site over the past 14 000 years. The close match in the Queensland relative intensity records with the south-eastern Australian archaeomagnetic data strongly suggests that the same sources are influencing the secular variation record all over eastern Australia.

Some time series analysis was carried out on the directional data. A comparison of the results from the two sequences was complicated by the poor age control on the Lake Barrine section and the differing lengths of the two records. It is apparent from Bauer plots that the vector often does not move in closed loops and hence that the geomagnetic fluctuations are only piecewise periodic. This and the fact that the periodicities obtained are poorly constrained will tend to hamper the comparison of periodicities from different sites. The

inclusion of the calibrated relative intensity data in a power spectral analysis should provide results of interest as there are at present few other sites where intensity data continuously span periods of thousands of years.

Bauer plots of the motion of the geomagnetic vector indicate that it has been predominantly clockwise. However, two well defined periods of anticlockwise motion are observed between about 5 500 and 4 000B.P. and from 10 500 to 8 800B.P. The sense of motion is predominantly the same over the last 10 000 years as for south-eastern Australian lake sediments studied by Barton and McElhinny (1981), although the second period of anticlockwise motion appears exaggerated in the Queensland record. The vector motions observed are consistent with the secular variation being caused by westward drifting non-dipole sources of the geomagnetic field.

8 REFERENCES

Ables, J. (1972), Maximum entropy spectral analysis; Proc. Symp. on the Collection and Analysis of Astrophysical Data, Nov. 13-15, 1972. Also in Astron. Astrophys. Suppl. Series, 15, 383-393 (1974).

Akaike, H. (1969a), Fitting autoregressive models for prediction; Ann. Inst. Stat. Math., 21, 243-247.

Akaike. H. (1969b), Power spectrum estimation through autoregressive model fitting; Ann. Inst. Stat. Math., 21, 407-419.

Akaike, H. (1970), Statistical predictor identification; Ann. Inst. Stat. Math., 22, 203-217.

Anderson, N. (1974), On the calculation of filter coefficients for maximum entropy spectral analysis; Geophys., 39, 69-72.

As, J.A. and J.D.A. Zijderveld (1958), Magnetic cleaning of rocks in palaeomagnetic research; Geophys. J. Roy. astr. Soc., 1, 308-319.

Banerjee, S.K., J. King and J.Marvin (1981), A rapid method for magnetic granulometry with application to environmental studies; Geophys. Res. Lett., 8, 333-336.

Barbetti, M. (1977), Measurements of recent geomagnetic secular variation in south-eastern Australia and the question of dipole wobble; Earth Planet. Sci. Lett., 36, 207-208.

Barraclough, D.R. (1974), Spherical harmonic analyses of the geomagnetic field for 8 epochs between 1600 and 1910; Geophys. J. Roy. astr. Soc., 36, 497-513.

Barton, C.E. (1978), Magnetic Studies of some Australian Lake Sediments, Ph.D. Thesis (unpubl.), Aust. Nat. Univ.

Barton, C.E. (1982), Spectral analysis of palaeomagnetic time series and the geomagnetic spectrum; Phil. Trans. Roy. Soc. London Ser. A, 306, 203-209.

Barton, C.E. and M.F. Barbetti (1982), Geomagnetic secular variation from recent lake sediments, ancient fireplaces and historical measurements in south-eastern Australia; Earth Planet. Sci. Lett., 59, 375-388.

Barton, C.E. and F.R. Burden (1979), Modifications to the Mackereth

corer; Limnol. Oceanog., 24(5), 977-983.

Barton, C.E. and M.W. McElhinny (1979), Detrital remanent magnetization in five slowly redeposited long cores of sediment; Geophys. Res. Lett., 6, 229-232.

Barton, C.E. and M.W. McElhinny (1981), A 10 000 yr geomagnetic secular variation record from three Australian maars; Geophys. J. Roy. astr. Soc., 67, 465-485.

Barton, C.E. and M.W. McElhinny (1982), Time series analysis of the 10 000 year geomagnetic secular variation record for south-eastern Australia; Geophys. J. Roy. astr. Soc., 68, 709-724.

Barton, C.E., M.W. McElhinny and D.J. Edwards (1980), Laboratory studies of depositional DRM; Geophys. J. Roy. astr. Soc., 61, 355-377.

Bauer, L.A. (1895), On the secular motion of a free magnetic needle II; Rev. Phys., 3, 34-48.

Berryman, J.G. (1978), Choice of operator length for maximum entropy spectral analysis; Geophys., 43, 1384-1391.

Best, J.G. (1960), Some Cainozoic basaltic volcanoes in North Queensland; Bur. Min. Resour. Aust. Rec. 1960/78 (unpubl.).

Bingham, C., M.D. Godfrey and J.W. Tukey (1967), Modern techniques of power spectrum estimation; I.E.E.E. Trans. Audio and Electroacoust., AU15, 56-66.

Bloomfield, P. (1976), Fourier Analysis of Time Series: an Introduction, Wiley, New York.

Bullard, E.D., C. Freedman, H. Gellman and J. Nixon (1950), The westward drift of the earth's magnetic field; Phil. Trans. Roy. Soc. London Ser. A, 243, 67-92.

Burg, J.P. (1967), Maximum entropy spectral analysis; Proc. of the 37th meeting of the S.E.G.

Burg, J.P. (1968), A new analysis technique for time series data; presented at the NATO Advanced Study Institute on Signal Processing with Emphasis on Underwater Acoustics, Aug. 12-23, 1968; also in Modern Spectrum Analysis, D.G. Childers (ed.), I.E.E.E. Press, N.Y., pp42-48.

Cain, J.C. (1975), Structure and secular change of the geomagnetic

field; Rev. Geophys. Space Phys., 13, 203-205.

Champion, D.E. (1980), Holocene Geomagnetic Secular Variation in the Western United States: Implications for the Global Geomagnetic Field, Ph.D. Thesis (unpubl.), Cal. Inst. Tech.

Clark, R.M. (1975), A calibration curve for radiocarbon dates; Antiquity, 49, 251-266.

Clark, R.M. (1977), Non-parametric estimation of a smooth regression function; J. Roy. Stat. Soc. B, 39, 107-113.

Clark, R.M. and R. Thompson (1978), An objective method for smoothing palaeomagnetic data; Geophys. J. Roy. astr. Soc., 52, 205-213.

Clegg, J.A., M. Almond and P.H.S. Stubbs (1954), The remanent magnetism of some sedimentary rocks in Britain; Phil. Mag., 45, 583-598.

Cooley, J.W. and J.W. Tukey (1965), An algorithm for the machine calculation of complex Fourier series; Math. Comp., 19, 297-301.

Cox, A. and R.R. Doell (1964), Long period variations of the geomagnetic field; Bull. Seism. Soc. Am., 54, 2243-2270.

Creer, K.M. (1974), Geomagnetic secular variations for the interval 7 000 to 25 000 years B.P. as recorded in a core of sediment from station 1474 of the Black Sea cruise of "Atlantis II"; Earth Planet. Sci. Lett., 23, 34-42.

Creer, K.M., T.E. Hogg, Z. Malkowski, J.E. Mojski, E. Krol-Niedziolka, P.W. Readman and P. Tucholka (1979), Palaeomagnetism of Holocene lake sediments from north Poland; Geophys. J. Roy. astr. Soc., 59, 287-313.

Creer, K.M., T.E. Hogg, P.W. Readman and C. Reynaud (1980), Palaeomagnetic secular variation curves extending back to 13 400 yr B.P. from two cores from Lac de Joux, Switzerland; J. Geophys., 48, 139-147.

Creer, K.M., P.W. Readman and S. Papamarinopoulus (1981), Geomagnetic secular variation in Greece through the last 6 000 years obtained from lake sediment studies; Geophys. J. Roy. astr. Soc., 66, 193-219.

Currie, R.G. (1968), Geomagnetic spectrum of internal origin and lower mantle conductivity; J. Geophys. Res., 73, 2779.

Currie, R.G. (1973), Pacific region anomaly in the geomagnetic spectrum at about 60 years; S. African J. Sci., 69, 379-383.

Damon, P.E., A. Long and E.I. Wallick (1972), Dendrochronological calibration of the ^{14}C time scale; Proc. 8th Int. Conf. on Radiocarbon Dating, Lower Hutt City, 1, 45-49.

Dankers, P.H. (1978), Magnetic Properties of Dispersed Natural Iron Oxides of Known Grain Size, Ph.D. Thesis (unpubl.), Univ. Utrecht.

Davis, M.B. (1969), Climatic changes in southern Connecticut recorded by pollen deposition at Rogers Lake; Ecology, 50, 409-422.

Day, R., M.D. Fuller and V.A. Schmidt (1977), Hysteresis properties of titanomagnetites: grain size and composition dependence; Phys. Earth Planet. Int., 13, 260-266.

Denham, C.R. (1975), Spectral analysis of palaeomagnetic time series; J. Geophys. Res., 80, 1897-1901.

Denham, C.R. (1981), Numerical correlation of recent palaeomagnetic records in two Lake Tahoe cores; Earth Planet. Sci. Lett., 54, 48-52.

Dodson, R.E. (1979), Counterclockwise precession of the geomagnetic field vector and westward drift of the non-dipole field; J. Geophys. Res., 84, 637-644.

Dodson, R.E., M.D. Fuller and W.F. Kean (1977), Palaeomagnetic records of secular variation from Lake Michigan sediment cores; Earth Planet. Sci. Lett., 34, 387-395.

Dodson, R.E., M.D. Fuller and W. Pilant (1974), On the measurement of the remanent magnetism of long cores; Geophys. Res. Lett., 1, 185-188.

Douglas, I. (1965), Physical limnology of two North Queensland crater lakes; Aust. Soc. Limnol. Newsl., 4(1).

Evans, M.E. (1969), Precambrian Palaeomagnetism of Australia and Africa, Ph.D. Thesis (unpubl.), Aust. Nat. Univ.

Gentleman, W.M. and G. Sande (1966), Fast Fourier transforms - for fun and profit; Appl. Statist., 14, 48-69.

Goree, W.S. and M.D. Fuller (1976), Magnetometers using RF driven SQUIDs and their applications in rock magnetism and palaeomagnetism; Rev.

Geophys. Space Phys., 14, 591-608.

Granar, L. (1958), Magnetic measurements on Swedish varved sediments; Ark. Geofys., 3, 1-40.

Griffiths, D.H. (1955), Remanent magnetism of varved clays from Sweden; Mon. Not. Roy. astr. Soc. Geophys. Suppl., 7, 103-114.

Gutowski, P.R., E.A. Robinson and S. Treitel (1978), Spectral estimation: fact or fiction; I.E.E.E. Trans. Geosci. Electron., GE16, 80-84.

Hamano, Y. (1980), An experiment on the post-depositional remanent magnetization in artificial and natural sediments; Earth Planet. Sci. Lett., 51, 221-232.

Harrison, C.G.A. (1966), The palaeomagnetism of deep sea sediments; J. Geophys. Res., 71, 3033-3043.

Henshaw, P.C. and R.T. Merrill (1980), Magnetic and chemical changes in marine sediments; Rev. Geophys. Space Phys., 18, 483-504.

Hillhouse, J.W. (1977), A method for removal of rotational remanent magnetization acquired during alternating field demagnetization; Geophys. J. Roy. astr. Soc., 50, 29-34.

Irving, E. (1964), Paleomagnetism and its Application to Geological and Geophysical Problems, Wiley.

Irving, E. and A. Major (1964), Post-depositional remanent magnetization in a synthetic sediment; Sedimentology, 3, 135-143.

Jardine, F. (1925), The drainage of the Atherton Tableland; Rept. Gt. Barrier Reef Comm., 1, 141-147.

Johnson, E.A., T. Murphy and O.W. Torreson (1948), Prehistory of the Earth's magnetic field; Terr. Magn. Atm. Electr. 53, 349.

Johnson, H.P., H. Kinoshita and R.T. Merrill (1975), Rock magnetism and paleomagnetism of some North Pacific deep-sea sediments; Geol. Soc. Am. Bull., 86, 412.

Kawai, N., K. Hirooka and S. Sasajima (1965), Counterclockwise rotation of the geomagnetic dipole axis revealed in the archaeosecular variations; Proc. Japan Acad., 41, 398-403.

Kawai, N. and K. Hirooka (1967), Wobbling motion of the geomagnetic dipole in historic time during these 2 000 years; J. Geomag.

Geoelectr., 19, 217-227.

Kendall, R.L. (1969), An ecological history of the L. Victoria basin; Ecol. Monog., 39, 121-176.

Kent, D.V. (1973), Post depositional remanent magnetization in deep sea sediments; Nature, 246, 32-34.

Kershaw, A.P. (1973), Late Quaternary Vegetation of the Atherton Tableland, North-East Queensland, Australia, Ph.D. Thesis (unpubl.), Aust. Nat. Univ.

Kershaw, A.P. (1974), A long continuous pollen sequence from north-eastern Australia; Nature, 251, 222-223.

de Keyser, F. (1972), Innisfail, Queensland 1:250,000 Geological series, Bur. Min. Resour. Explan. Notes SE/55-6.

de Keyser, F. and K.G. Lucas (1968), Geology of the Hodgkinson and Laura Basins, North Queensland; Bull. Bur. Min. Resour. Geol. Geophys. Aust., 84.

King, R.F. (1955), The remanent magnetism of artificially deposited sediments; Mon. Not. Roy. astr. Soc. Geophys. Suppl., 7, 115-134.

King, J.W., S.K. Banerjee, J. Marvin and N. Holschuh (1981), A critical evaluation of a method: the NRM/ARM ratio of lake sediments as an estimate of relative geomagnetic field intensity; E.O.S., 62, 272.

King, J.W., S.K. Banerjee, J. Marvin and O. Ozdemir (1982), A comparison of different magnetic methods for determining relative grain size of magnetite in natural materials: some results from lake sediments; Earth Planet. Sci. Lett., 59, 404-419.

Koenigsberger, K. (1938), Natural residual magnetism of eruptive rocks, part I and II; Terr. Magn. Atm. Elec., 43, 119-127 and 299-300.

Levi, S. and S.K. Bannerjee, (1976), On the possibility of obtaining relative palaeointensities from lake sediments; Earth Planet. Sci. Lett., 29, 219-226.

Løvlie, R., (1974), Postdepositional remanent magnetization in a redeposited deep sea sediment; Earth Planet. Sci. Lett., 21, 315-320.

Løvlie, R., (1976), The intensity pattern of post-depositional remanence acquired in some marine sediments deposited during a reversal of

the external magnetic field; Earth Planet. Sci. Lett., 30, 209-214.

Lund, S.P. and S.K. Banerjee (1979), Palaeosecular variations from lake sediments; Rev. Geophys. Space Phys., 17, 244-249.

Mackereth, F.J.H. (1958), A portable core sampler for lake deposits; Limnol. Oceanog., 3,181-191.

Mackereth, F.J.H. (1971), On the variation in direction of the horizontal component of remanent magnetization in lake sediments; Earth Planet. Sci. Lett., 12, 332-338.

McElhinny, M.W. (1966), An improved method for demagnetizing rocks in alternating magnetic fields; Geophys. J. Roy. astr. Soc., 10, 369-374.

McElhinny, M.W. (1973), Palaeomagnetism and Plate Tectonics, Cambridge Univ. Press, Cambridge.

McElhinny, M.W. and R.T. Merrill (1975), Geomagnetic secular variation over the past 5 m.y.; Rev. Geophys. Space Phys., 13, 687-708.

McElhinny, M.W. and W.E. Senanayake (1982), Variations in the geomagnetic dipole I: the past 50 000 years; J. Geomag. Geoelectr., 34, 39-51.

McFadden, P.L. (1982), Comment on 'Numerical correlation of recent palaeomagnetic records in two L. Tahoe cores' by C.R. Denham; Earth Planet. Sci. Lett., in press.

McNeil, D.R. (1977), Interactive Data Analysis, Wiley, N.Y.

Merrill, R.T. and M.W. McElhinny (1983), The Earth's Magnetic Field: its History, Origin and Planetary Perspective, Academic Press.

Molyneux, L. (1971), A complete result magnetometer for measuring the remanent magnetization of rocks; Geophys. J. Roy. astr. Soc., 24, 429-433.

Molyneux. L., R. Thompson, F. Oldfield and M.E. McCallan (1972), Rapid measurement of the remanent magnetization of long cores of sediment; Nature, 237, 42-43.

Nakajima, T. and N. Kawai (1973), Secular variation in the recent 60 000 years found from the Lake Biwa sediments; Rock Magnet. Paleogeophys. (Publ. Rock Magnet. Palaeogeophys. Res. Group, Japan), 34-38.

Nesbit, J.D. (1966), Variation of the ratio intensity to susceptibility in red sandstones; Nature 210, 618.

Oeschger, H., J. Houtermans, H. Loosli and M. Wahlen (1970), The constancy of cosmic radiation from isotope studies in meteorites and on the Earth; In XII Nobel Symposium Volume, Radiocarbon Variations and Absolute Chronology, I.U. Olsson (ed.), Wiley N.Y. pp471-496.

Opdyke, N.D. and K.W. Henry (1969), A test of the dipole hypothesis; Earth Planet. Sci. Lett., 6, 138-151.

Özdemir, Ö. and S. K. Banerjee (1982), A preliminary magnetic study of soil samples in west-central Minnesota; Earth Planet. Sci. Lett. 59, 393-403.

Polach, H. and J. Chappell (1979), Radioisotope dating with accelerators, its potential for Australian Quaternary and environmental research; Atomic Energy in Australia, 22 (3 and 4), 3-12.

Ralph, E.K., H.N Michael and M.C. Han (1973), Radiocarbon dates and reality; MASCA Newsl., 9(1), 1-20.

Runcorn, S.K. (1959), On the theory of geomagnetic secular variation; Ann. de Géophys., 15, 87-92.

Rymer, L. and J. Neale (1979), Freeze coring as a method of collecting unconsolidated lake sediments; Aust. J. Ecology, 6, 123-126.

Senanayake, W.E. (1981), Geomagnetic Field Intensity in the Geological Past, Ph.D. Thesis (unpubl.), Aust. Nat. Univ., pp 129-141.

Skiles, D.D. (1970), A method of inferring the direction of drift of the geomagnetic field from palaeomagnetic data; J. Geomag. Geoelectr., 22, 441-462.

Smith, G. and R.T. Merrill (1980), The origin of rotational remanent magnetization; Geophys. J. Roy. astr. Soc., 61, 329-336.

Stephenson, A. (1980), Rotational remanent magnetization and the torque exerted on a rotating rock in an alternating magnetic field; Geophys. J. Roy. astr. Soc., 62, 113-132.

Stober, J.C. and R. Thompson (1977), Palaeomagnetic secular variation studies of Finnish lake sediment and the carriers of remanence;

Earth Planet. Sci. Lett., 37, 139-149.

Suess, H.E. (1970), Bristlecone-pine calibraton of the radiocarbon time scale 5 200 BC to the present; In XII Nobel Symposium Volume, Radiocarbon Variations and Absolute Chronology, I.U. Olsson (ed.), Wiley, N.Y. pp303-309.

Suter, M. R. Balzer, G. Bonani, Ch Stoller, W. Wölfli, J. Beer, H. Oeschger and B. Stauffer (1981a), Proc. Symp. Acc. Mass. Spectr., Argonne, May 11-13, 1981, p87.

Suter, M. R. Balzer, G. Bonani, W. Wölfli, J. Beer, H. Oeschger and B. Stauffer (1981b), I.E.E.E. Trans. on Nucl. Sci., NS28, 1475.

Switsur, R. (1973), The radiocarbon calendar recalibrated; Antiquity, 47, 131.

Thellier, E. and Thellier, O. (1959), Sur l'intensité du champ magnétique terrestre dans le passé historique et géologique; Ann. Géophys. 15, 258-376.

Thompson, R. (1975), Long period European geomagnetic secular variation confirmed; Geophys. J. Roy. astr. Soc., 43, 847-859.

Thompson, R. and K. Kelts (1974), Holocene sediments and magnetic stratigraphy from Lakes Zug and Zurich, Switzerland; Sedimentology, 21, 577-596.

Thompson, R. and G.M. Turner (1979), British geomagnetic master curve 10 000 - 0 years BP for dating European sediments; Geophys. Res. Lett., 6, 249-250.

Thompson, R., J. Bloemendal, J.A Dearing, F. Oldfield, T.A. Rummery, J.C. Stober and G.M. Turner (1980), Environmental applications of magnetic measurements; Science, 207, 481-486.

Timms, B.V. (1976), Morphology of Lakes Barrine, Eacham and Euramoo, Atherton Tableland, North Queensland; Proc. Roy. Soc. Qld, 87, 81-84.

Tucker, P. (1979), Selective postdepositional realignment in a synthetic sediment; Phys. Earth Planet. Int., 20, 11-14.

Tucker, P. (1980a), A grain mobility model of post depositional realignment; Geophys. J. Roy. astr. Soc., 63, 149-163.

Tucker, P. (1980b), Stirred remanent magnetization: a laboratory

analogue of postdepositional realignment; Geophys., 48, 153-157.

Tucker, P. (1981), Palaeointensities from sediments: normalization by laboratory redepositions; Earth Planet. Sci. Lett., 56, 398-404.

Tukey, J.W. (1977), Exploratory Data Analysis, Addison-Wesley, Reading, Mass.

Turner, G.M. and R. Thompson (1981), Lake sediment record of the geomagnetic secular variation in Britain during Holocene times; Geophys. J. Roy. astr. Soc., 65, 703-725.

Ulrych, T.J. and T.N. Bishop (1975), Maximum entropy spectral analysis and autoregressive decomposition; Rev. Geophys. Space Phys., 13, 183-200.

Velleman, P.F. (1980), Definition and comparison of robust nonlinear data smoothing algorithms; J. Amer. Stat. Ass., 75, 609-615.

Verosub, K. L. (1977), Depositional and postdepositional processes in the magnetization of sediments; Rev. Geophys. Space Phys., 15, 129-143.

Walker, G. (1931), On periodicity in series of related terms; Proc. Roy. Soc. London Ser. A, 131, 518-532.

Wilson, R.L. (1970), Permanent aspects of the earth's non-dipole magnetic field over upper Tertiary times; Geophys. J. Roy. astr. Soc., 19, 417.

Wilson, R.L. and R. Lomax (1972), Magnetic remanence related to slow rotation of ferromagnetic material in alternating magnetic fields; Geophys. J. Roy. astr. Soc., 30, 295-303.

Wilson, R.L. and M.W. McElhinny (1974), Investigation of the large scale palaeomagnetic field over the past 25 million years; eastward shift of the Icelandic spreading ridge; Geophys. J. Roy. astr. Soc., 39, 571.

Wölfli, W., G. Bonani, M. Suter, R. Balzer, M. Nessi, Ch. Stoller, J. Beer, H. Oeschger and M. Andrée (1983), Radioisotope dating with the ETHZ-EN tandem accelerator; Radiocarbon, in press.

Yukutake, T. (1967), The westward drift of the earth's magnetic field in historic times; J. Geomag. Geoelectr., 19, 103.

Yukutake, T. (1973), Fluctuations in the Earth's rate of rotation

related to changes in the geomagnetic dipole field; J. Geomag. Geoelectr., 25, 195-212.

Yukutake, T. and H. Tachinaka (1969), Separation of the earth's magnetic field into drifting and standing parts; Bull. Earthquake Res. Inst., Tokyo Univ., 47, 65.

Yule, G.U. (1927), On a method of investigating periodicities in disturbed series, with special reference to Wolfer's sunspot numbers; Phil. Trans. Roy. Soc. London Ser. A, 226, 267-298.

The following should also be included in the above reference list.

Creer,K.M. (1959), A.C. magnetization of unstable Triassic Keuper Marls from S.W. England; Geophys. J. Roy. astr. Soc., 2, 261.

Hamming, R.W. (1977), Digital Filters, Prentice Hall, Englewood Cliffs, N.J.

McFadden, P.L. (1981), A theoretical investigation of the effect of individual grain anisotropy in alternating field demagnetization; Geophys. J. Roy. astr. Soc., 67, 35-51.

McNish, A.G. and E.A. Johnson (1938), Magnetization of unmetamorphosed varves and marine sediments; Terr. Magn. Atmos. Electr., 43, 401-407.